Supplementary Information

Matsuda-Heck arylation of itaconates: a versatile approach to heterocycles from a renewable resource

*Andreas Krause, Eric Sperlich and Bernd Schmidt**

Universitaet Potsdam, Institut fuer Chemie, Karl-Liebknecht-Strasse 24-25, D- 14476 Potsdam-Golm, Germany

bernd.schmidt@uni-potsdam.de

Contents:

A General Methods

All reactions were carried out in dry reaction vessels and under an atmosphere of dry nitrogen using standard Schlenk technique. All solvents were purified by standard procedures. NMR spectra were obtained using Bruker Avance-300 and Bruker Neo-400 instruments at 300 or 400 MHz (for ^{1}H-NMR-spectroscopy) in $CDCl_3$ with C*H*Cl_3 (δ = 7.26 ppm) as a calibrant. Coupling constants are given in Hertz (Hz). $^{13}C\{^{1}H\}$ NMR spectra were recorded at 75 or 100 MHz in $CDCl_3$ with $CDCl_3$ (δ = 77.1 ppm) as a calibrant. Whenever the solubility of the sample was insufficient in $CDCl_3$, it was replaced by either acetone-d_6 (acetone-d_5 as a calibrant for ^{1}H NMR spectroscopy, δ = 2.05 ppm; acetone-d_6 as a calibrant for $^{13}C\{^{1}H\}$ NMR spectroscopy, δ = 29.9 ppm) or DMSO-d_6 (DMSO-d_5 as a calibrant for ^{1}H NMR spectroscopy, δ = 2.50 ppm; DMSO-d_6 as a calibrant for $^{13}C\{^{1}H\}$ NMR spectroscopy, δ = 39.5 ppm). IR spectra were recorded as ATR-FTIR spectra using a Perkin-Elmer UART TWO FT-IR-spectrometer. Wavenumbers ($\tilde{\nu}$) are given in cm^{-1}. The peak intensities are defined as strong (s), medium (m), or weak (w). Low- and high-resolution mass spectra were obtained by EI-TOF or ESI-TOF using a Waters Micromass Manchester instrument. Melting points were measured using a SMP-10 instrument of Bibby Scientific (Stuart). All starting materials were purchased from commercial sources or synthesized following published procedures. References are provided at the appropriate position.

B Syntheses of compounds 3a-c

General procedure for the β-selective esterification of itaconic acid (1). To a solution of itaconic acid (**1**, 10.00 g, 77.0 mmol) in acetonitrile (50 mL) was added the appropriate alkanol (92 mmol, 1.2 equiv.). *para*-Toluene sulfonic acid-mono hydrate (0.73 g, 3.8 mmol, 5 mol-%) was added and the solution was heated at 82 °C for 16 h. The mixture was cooled to ambient

temperature, the resulting precipitate was filtered off and the solution was evaporated. The residue was purified by column chromatography on silica, using hexanes-MTBE mixtures of increasing polarity as eluent.

4-Ethoxy-2-methylene-4-oxobutanoic acid (3a).[1] Following the general procedure, itaconic acid (6.00 g, 46.1 mmol) was converted to **3a** (6.25 g, 39.5 mmol, 86%): colourless viscous liquid; ^{1}H NMR (400 MHz, $CDCl_3$) δ 10.78 (s, 1H), 6.45 (s, 1H), 5.82 (s, 1H), 4.15 (q, J = 7.1 Hz, 2H), 3.32 (s, 2H), 1.24 (t, J = 7.1 Hz, 3H); ^{13}C{^{1}H} NMR (101 MHz, $CDCl_3$) δ 171.7, 170.7, 133.5, 130.8, 61.2, 37.4, 14.2; IR (ATR) ν 2986 (s), 1724 (s), 1697 (s), 1633 (s), 1442 (m), 1398 (m), 1370 (m), 1314 (s), 1195 (s), 1152 (s), 1095 (w), 1027 (m), 946 (m), 822 (w), 737 (w); HRMS (ESI) calcd for $C_7H_{11}O_4$ [M+H$^+$] 159.0657, found 159.0662.

4-Isopropoxy-2-methylene-4-oxobutanoic acid (3b).[2] Following the general procedure, itaconic acid (10.0 g, 77.0 mmol) was converted to **3b** (9.50 g, 55.2 mmol, 72%): colourless, waxy solid; ^{1}H NMR (300 MHz, acetone-d_6) δ 6.25 (s, 1H), 5.77 (s, 1H), 4.95 (sept., J = 6.3 Hz, 1H), 3.29 (s, 2H), 1.19 (d, J = 6.3 Hz, 6H); ^{13}C{^{1}H} NMR (75 MHz, acetone-d_6) δ 170.5, 167.6, 135.8, 128.2, 68.3, 38.4, 21.9, 21.9; IR (ATR) ν 2985 (s), 2939 (m), 2628 (w), 1724 (s), 1696 (s), 1633 (s), 1429 (w), 1310 (s), 1206 (m), 1164 (m), 1103 (m), 969 (w), 927 (w), 763 (w); HRMS (ESI) calcd for $C_8H_{13}O_4$ [M+H$^+$] 173.0814, found 173.0826.

4-Butoxy-2-methylene-2-oxobutanoic acid (3c).[3] Following the general procedure, itaconic acid (5.00 g, 38.0 mmol) was converted to **3c** (4.50 g, 24.2 mmol, 63%). Colourless oil; ^{1}H NMR (400 MHz, $CDCl_3$) δ 10.11 (s, 1H), 6.43 (s, 1H), 5.80 (s, 1H), 4.09 (t, J = 6.6 Hz, 2H), 3.32 (s, 2H), 1.57 (m, 2H), 1.34 (m, 2H), 0.90 (t, J = 7.3 Hz, 3H); ^{13}C{^{1}H} NMR (101 MHz, $CDCl_3$) δ 171.4, 170.7, 133.4, 130.6, 64.9, 37.3, 30.5, 19.0, 13.6; IR (ATR) ν 2961 (s), 2875 (m), 1697 (s), 1634

(m), 1430 (w), 1394 (w), 1286 (m), 1148 (s), 956 (w), 824 (w); HRMS (EI) calcd for $C_9H_{15}O_4$ [M+H$^+$] 187.0970, found 187.0982.

C Arene diazonium salts 4

General procedure for the synthesis of arene diazonium salts 4a-p. A solution of the appropriate aniline (5.0 mmol) was dissolved in THF and cooled to 0 °C. An aq. solution of HBF_4 (48 wt-%, 4.58 g, 25.0 mmol) was added, the mixture was stirred at 0 °C for 5 min., and *tert*-butyl nitrite (0.62 g, 6.0 mmol) was added dropwise. Stirring was continued at 0 °C for 0.5 h, and the reaction mixture was poured into ice-cold diethyl ether. The arene diazonium salts (**Table SI-1**) precipitated as colourless solids and were isolated by filtration.

Table SI-1. Arene diazonium salts used in this study and references for their synthesis.

4a[4]		**4h**[5]	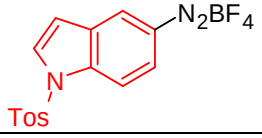	**4o**[6]	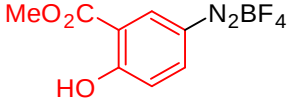
4b[7]	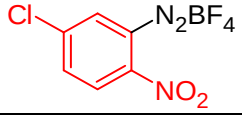	**4i**[8]	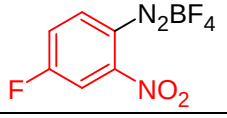	**4p**[9]	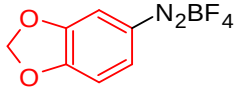
4c[4]	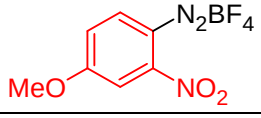	**4j**[10]	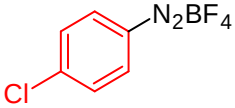		
4d[11]		**4k**[12]	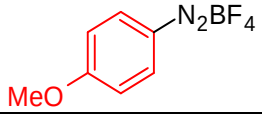		
4e[13]	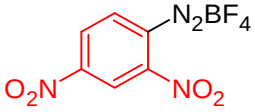	**4l**[14]	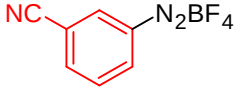		
4f[15]	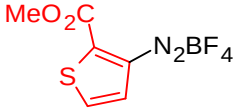	**4m**[16]	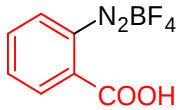		
4g[17]	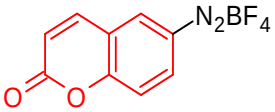	**4n**[9]	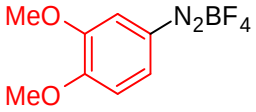		

D Crystal structure analyses of 6bk and 9aa

1 General details of X-ray structure analysis

Crystalline samples of the compounds **6bk** and **9aa** were analyzed under an optical microscope with polarizing filter. Crystals of compound **9aa** are shown in **Figure SI-1**. Single crystals suitable for single crystal structure analysis were separated by oil and measured on a Stadivari diffractometer (Stoe) with a Genix microfocus tube. The measurement was performed at 210 K with Mo-Kα radiation (λ = 0.71073 Å). The data were corrected for absorption as well as for Lorentz and polarization effects using the program X-Area.[18] The structure was solved by direct methods and refined against F^2 on all data by full-matrix least-squares using the SHELX suite of programs.[19, 20] The crystal structure was visualized with Diamond 4.[21] The data (**6bk**: CCCD 2060196; **9aa**: CCDC 2064789) can be obtained free of charge from The Cambridge Crystallographic Data Centre, http://www.ccdc.cam.ac.uk.

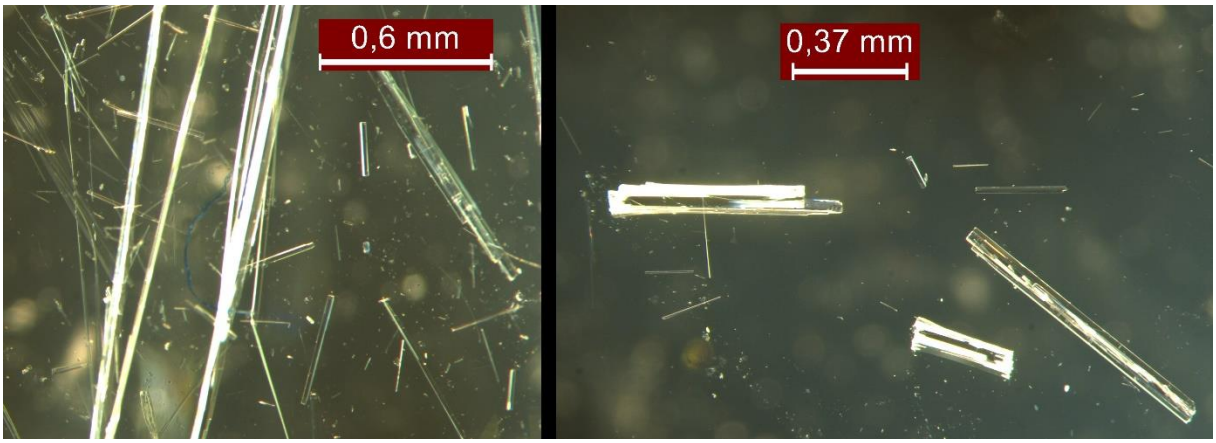

Figure SI-1. Light microscope images of the needle-shaped crystals of compound **9aa**.

2 Crystallographic Data

Table SI-2. Crystal data and details of structure refinement for **6bk** and **9aa**.

	6bk	**9aa**
Empirical formula	$C_{15}H_{18}O_5$	$C_{12}H_{10}BrNO_3$
M [g mol^{-1}]	278.29	296.12
T [K]	210	210
λ [Å]	0.71073 (Mo $K\alpha$)	0.71073 (Mo $K\alpha$)
Crystal system	Monoclinic	Monoclinic
Space group	$I2/a$	$C2/c$
Unit cell dimensions		
a [Å]	29.6153(12)	23.452(5)
b [Å]	4.86890(10)	4.5449(9)
c [Å]	20.5000(9)	22.939(5)
α [°]	90	90
β [°]	104.698(3)	111.31 (3)
γ [°]	90	90
V [Å^3]	2859.25(18)	2277.8(9)
Z	8	8
ρ_{calc} [g cm^{-3}]	1.293	1.727
μ [mm^{-1}]	0.097	3.61
F(000)	1184	1184
Crystal description	colorless, prism	colorless, needle
Crystal size [mm^3]	0.90 x 0.30 x 0.25	0.45 × 0.20 × 0.05
θ_{min} / θ_{max} [°]	2.78 – 33.43	3.5 – 31.1°
Index ranges	$-41 \le h \le 41$	$-29 \le h \le 29$
	$-6 \le k \le 6$	$-5 \le k \le 5$
	$-28 \le l \le 28$	$-28 \le l \le 28$
Reflection collected	74300	12003
Independent reflection	4156	2363
R_{int}	0.0391	0.050
Reflections I>2σ(I)	3151	2363
Parameter	216	155
R_1/wR_2 [I>2σ(I)]	0.0415/0.1129	0.0382/0.0869
R_1/wR_2 [all data]	0.0564/0.1204	0.0630/0.0983
min./max. $\Delta\rho$ [10^{-6} e pm^{-3}]	0.37/-0.287	0.45/ −0.39
GooF	1.07	1.04

3 Crystal structure and intermolecular interactions:

Compound ***6bk***. **Figure SI-2** shows the molecular structure of the compound in ellipsoid representation with atomic labels. All non-hydrogen atoms were refined anisotropically, all hydrogen atoms bound to C atoms were placed on calculated positions and refined using a riding model. The *iso*-propyl group C13 to C14 is disordered on two crystallographic layers (A and B), the two layers are shown in color in **Figure SI-3**. The occupancy of the main layer A is 68% and the occupancy of the second layer B is 38%.

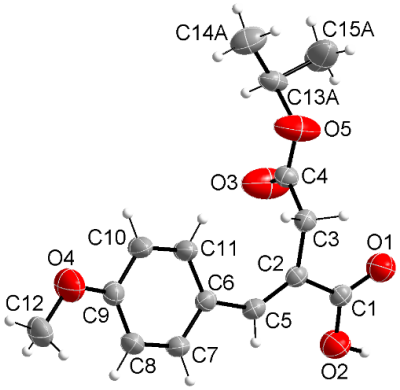

Figure SI-2. Molecular structure of **6bk** with atomic labels. Displacement ellipsoids are shown at the 50% probability level.

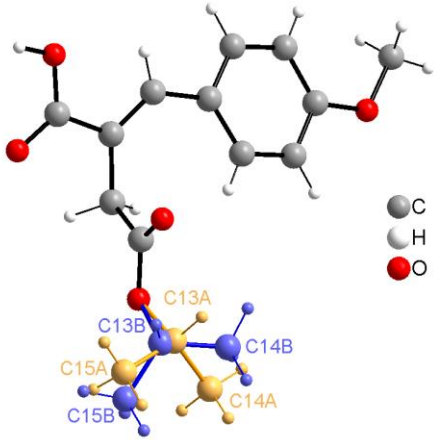

Figure SI-3. Disorder of the *iso*-propyl group, with occupation of the main crystallographic layer A, shown in orange, of 68% and the second crystallographic layer B, shown in blue, of 32%.

In the solid state, the molecules arrange themselves to form dimers due to hydrogen bonds (see **Figure SI-4**). This results in π-bond cooperativity between the two carboxylic acid groups, and the two symmetry-equivalent hydrogen bonds are relatively strong with a donor-acceptor distance of 2.66 Å and are within the expected range for such cyclic hydrogen bond dimers. The position of the acidic hydrogen atom H2 was taken from the differential electron density map and the H···O distance (H-acceptor distance) of 1.749 Å is relatively large, for O-H···O hydrogen bonds. The reason for this is due to the repulsive interaction of the two H2 atoms of both hydrogen bonds (see Figure SI-4, black dashed lines). A shorter H···O distance would lead to a larger H···H repulsion and is therefore not formed.[22]

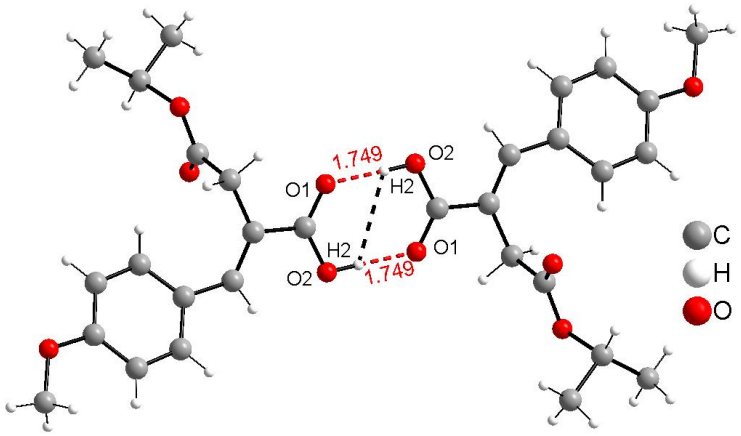

Figure SI-4. Hydrogen bonding (red dashed lines) between the molecules forming dimers of **6bk** and short repulsive H-H contacts (black dashed lines).

In addition to hydrogen bonds, parallel-displaced stacking interactions and lone-pair π interactions are formed between the molecules (see **Figure SI-5**). The centers of the aromatic rings of neighboring molecules arrange parallel to each other at a distance of 4.869 Å, suggesting an attractive interaction.[23] In addition, the O4 atoms arrange themselves exactly under the aromatic center of the neighboring molecule at a distance of 3.595 Å, suggesting an attractive interaction of oxygen with the π system of the aromatic in the form of lone-pair π interactions.[24] These two

interactions, which have the effect of strengthening each other, lead to a stacking of the molecules in the direction of the crystallographic b axis.

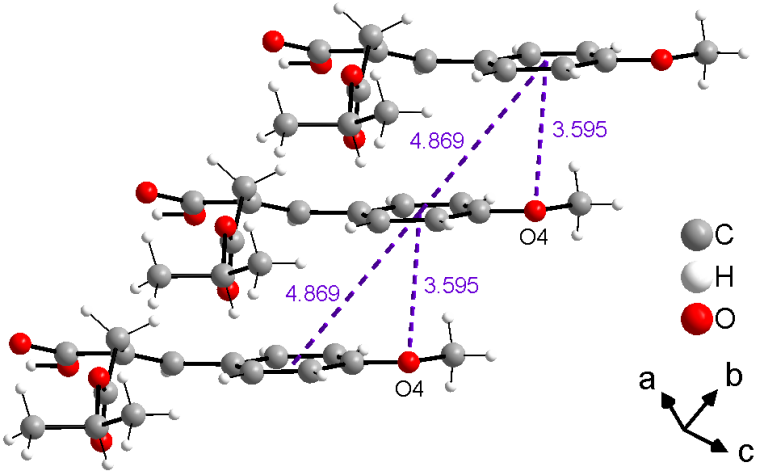

Figure SI-5. Parallel displaced stacking interactions and lone pair-π interactions (purple dotted lines) between the molecules result in stacking of the molecules along the crystallographic b axis.

There is also another interesting structural feature (see **Figure SI-6**). The C1 atoms and the O1 atoms of neighboring molecules arrange themselves at a distance of 3.201 Å, which is significantly smaller than the sum of the van der Waals radii of both atoms ($\sum r_{CO}$ = 3.32 Å).[25] The resulting COC angles (**Figure SI-6**, α) are 89°, suggesting a strong, directional electrostatic interaction between partially negative O atoms and the partially positive C atoms.[26] For such electrostatic interactions between two dipolar functional groups, three frequently occurring geometries have been described so far, of which type 2, i.e. the anti-parallel arrangement is found in **6bk**.[27] .[9] The interaction between two carbonyl groups can be energetically so strong that it even competes with hydrogen bonds.[28]

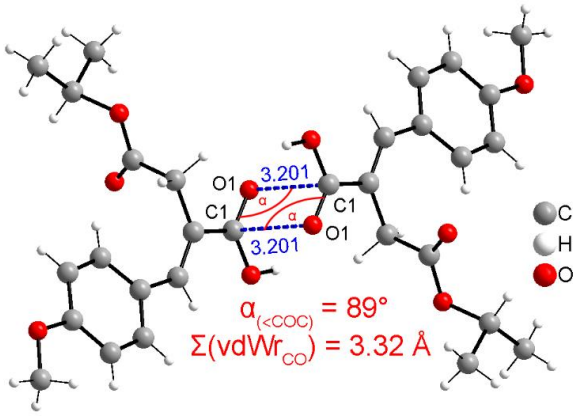

Figure SI-6. Short contacts between the O1 and the C1 of neighboring molecules (blue dotted lines) and COC angles (α) of 89° indicate electrostatic interactions.

The interactions described above, namely hydrogen bonds, parallel-shifted stacking interactions, lone-pair π interactions and electrostatic CO interactions, result in the formation of a one-dimensional network of molecules in the solid state (see **Figure SI-7**). There is stacking of the units in the b direction by aromatic interactions (purple lines), formation of dimers by hydrogen bonds (red lines), and crosslinking of these dimers by electrostatic CO interactions (blue lines). This leads to one-dimensional cross-linking along the crystallographic b axis.

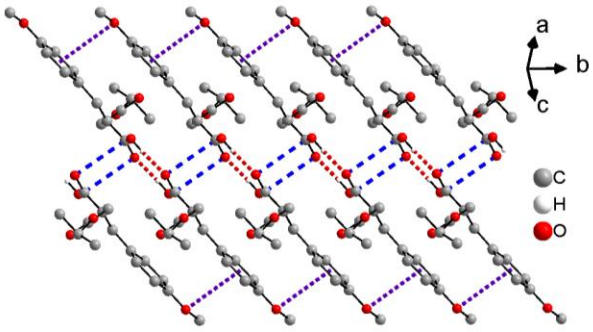

Figure SI-7. The combination of hydrogen bonding, lone pair-π interactions, and electrostatic interactions leads to one-dimensional networking of the molecules along the crystallographic b axis.

These one-dimensional molecular chains can be seen very well in the packing image looking in the direction of the crystallographic b axis (**Figure SI-8**). In the image shown, nine such one-dimensional molecular arrangements are depicted, for a better overview, the non-acidic hydrogens have been omitted.

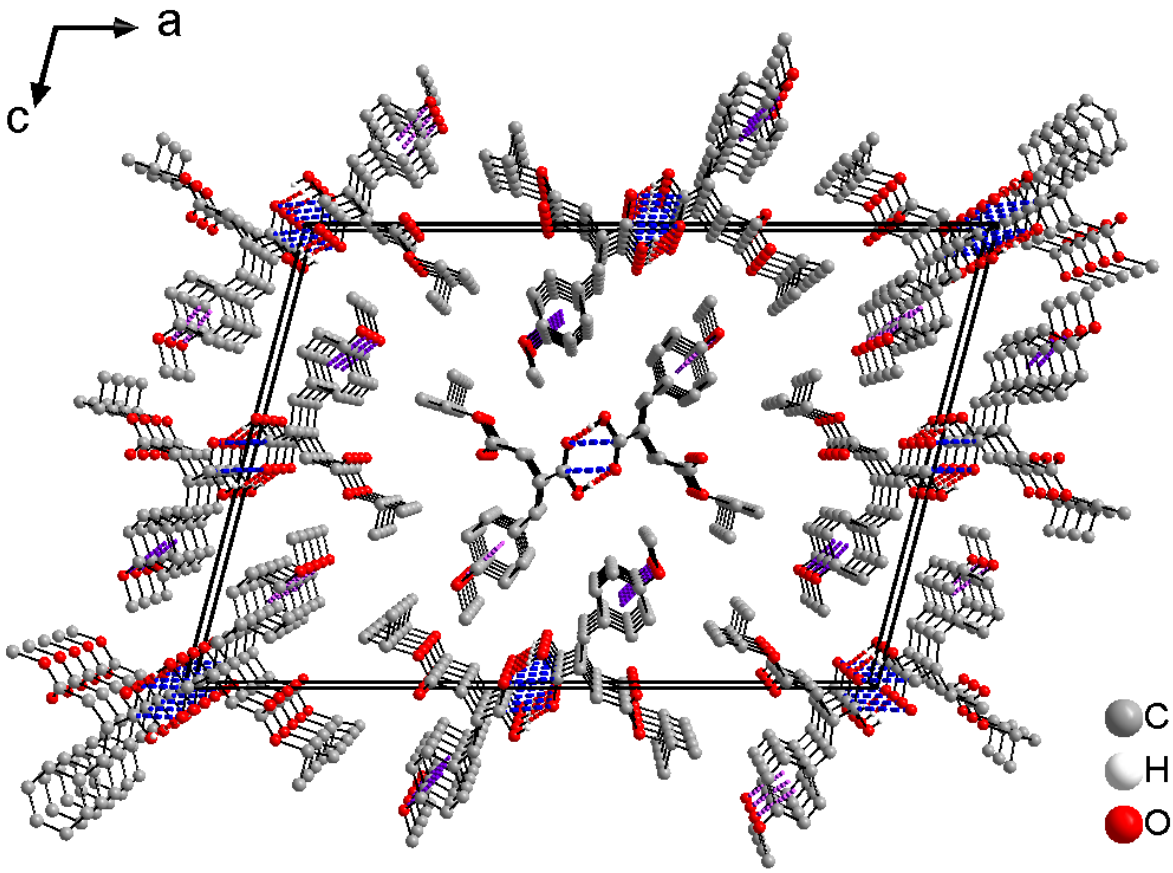

Figure SI-8. The cell view of the compound with view along the crystallographic b axis shows different chains of intermolecular cross-linked molecules
(non-acid hydrogen atoms were omitted).

*Compound **9aa***. **Figure SI-9** shows the molecular structure of **9aa** with atomic label and ellipsoid view. All non-hydrogen atoms were refined anisotropically, all hydrogen atoms were placed on calculated positions and refined using a riding model.

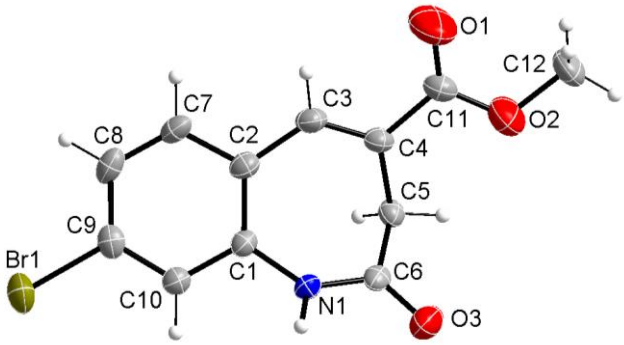

Figure SI-9. Molecular structure of AM-X3 with atomic labels. Displacement ellipsoids are shown at the 50% probability level.

As in **6bk**, cyclic hydrogen bonds are formed between two molecules in **9aa** (**Figure SI-10**). In each molecule, the N-H group serves as the proton donor and the carbonyl oxygen O3 as the proton acceptor. This results in hydrogen-bridged molecular dimers. The N···O distance is 2.91 Å, which is as large as the distance in compounds known from literature.[29]

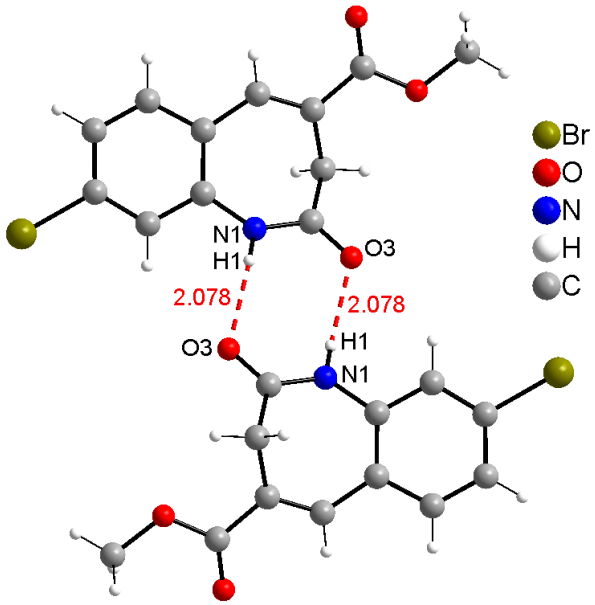

Figure SI-10. Hydrogen bonding (red dashed lines) between the molecules forming dimers of **9aa**.

In the solid state of **9aa**, the molecules also arrange themselves in such a way that parallel displaced stacking interactions are formed (**Figure SI-11**).[23] The distance between the aromatic centers of

neighboring molecules is 4.545 Å, which is shorter than in **6bk**. The reason for this may be the possibility of better overlap of the relatively planar molecules of **9aa**. In addition, the weaker parallel-displaced stacking interactions in **6bk**, can be explained by the fact that the weakening leads to the strengthening of the lone-pair π interaction, resulting in a larger total interaction energy.

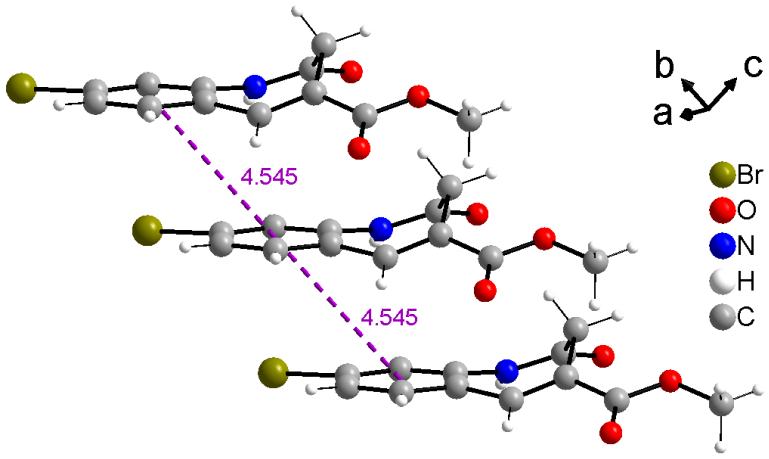

Figure SI-11. Parallel displaced stacking interactions (purple dotted lines) between the molecules result in stacking of the molecules along the crystallographic b axis.

The combination of hydrogen bonds and parallel-displaced stacking interactions leads to the one-dimensional interconnection of the molecules of **9aa** (**Figure SI-12**). Two molecules always form hydrogen bonded dimers and each of these dimers has a total of four parallel-displaced stacking interactions, resulting in a molecular chain along the crystallographic b axis.

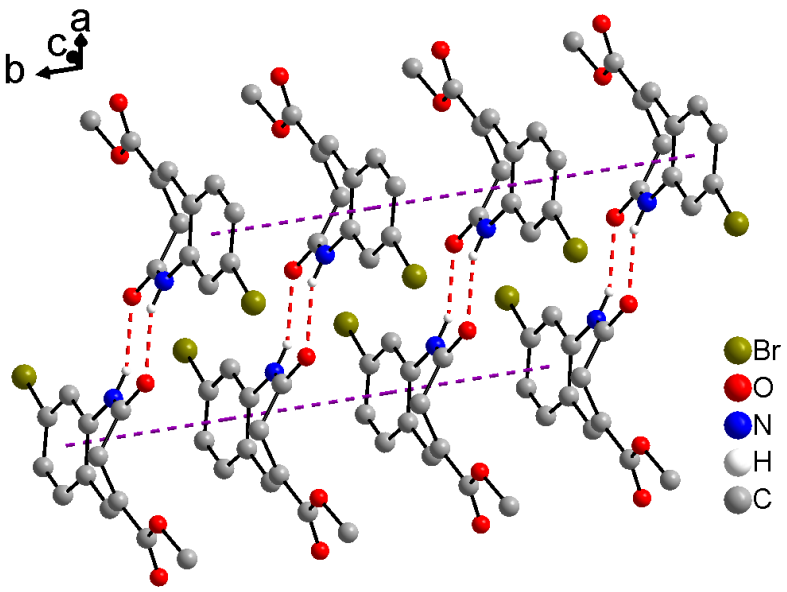

Figure SI-12. The combination of hydrogen bonding and stacking interactions leads to one-dimensional networking of the molecules along the crystallographic b axis.

Hydrogen bonds and stacking interactions are well studied and represent typical interactions between such molecules. Since no further such typical interactions occur, the question is how the molecular chains, shown in **Figure SI-12**, arrange themselves with respect to each other and whether this is only done by forming the densest possible packing or whether further intermolecular interactions influence the arrangement. In fact, it can be assumed that these intermolecular chains (**Figure SI-12**) are further extended by interactions between the electronegative bromine atoms of one molecule of **9aa** and the electropositive regions of the methyl ester carbon (C12) of a neighboring molecule. **Figure SI-13** shows the described interaction.

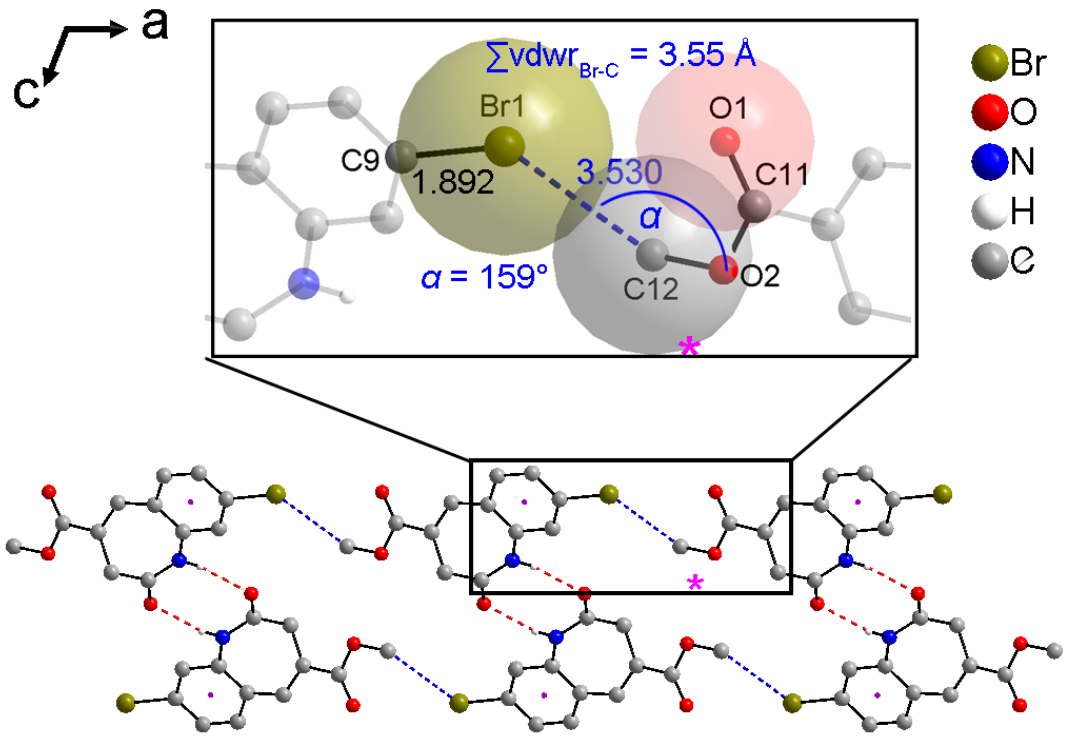

Figure SI-13. Arrangement of molecular chains in the ac plane and potential weak tetrel bridges (shown as blue dashed lines).

There are a few reasons to assume that the arrangement of molecules along the b axis occurs with the formation of so-called tetrel bridges. Tetrel bridges are σ-hole interactions whose σ-hole donor respectively electron acceptor is a 4th main group element.[30, 31] First of all, the distance between Br1 and the C12 atom is very small, it is even slightly smaller than the sum of the Van der Waals radii of both elements which is 3.55 Å.[25] In addition, the orientation of the methyl group is toward bromine, although there is a large cavity between the molecules. Denser packing would be possible by repositioning C12 in the c axis direction (the possible position is shown with * in **Figure SI-13**). Classically, σ-hole interactions result in *R*-donor-acceptor angles α close to 180°, but in the structure of AM-X3 this angle α is only 159°. The deviation can be explained by the destructive interaction of atoms C12 and O1. If the angle α were close to 180°, then the electron shells of C12 and O1 would strongly overlap, which is energetically not favorable. For this reason, the angle for

the tetrel bridge is 159°. As with hydrogen bonds, the formation of σ-hole interactions also leads to a weakening of the covalent bonds of the atoms involved. This is also seen in the C-Br bond which is slightly enlarged at 1.89 Å compared to literature known C_{sp2}-Br bonds.[32] In summary, there is evidence that tetrel bridges are formed between molecules. These are in direct competition with destructive electrostatic C12-O1 interactions, and therefore the ideal distance and angle between atoms cannot be achieved. As a result, these interactions are very weak.

Figure SI-14 shows the cell of **9aa** with viewing direction along the crystallographic b direction. The molecules associate through hydrogen bonds to form dimers, these stack in the direction of the crystallographic b axis. In the crystallographic a direction, these molecular chains interact to form tetrel bridges.

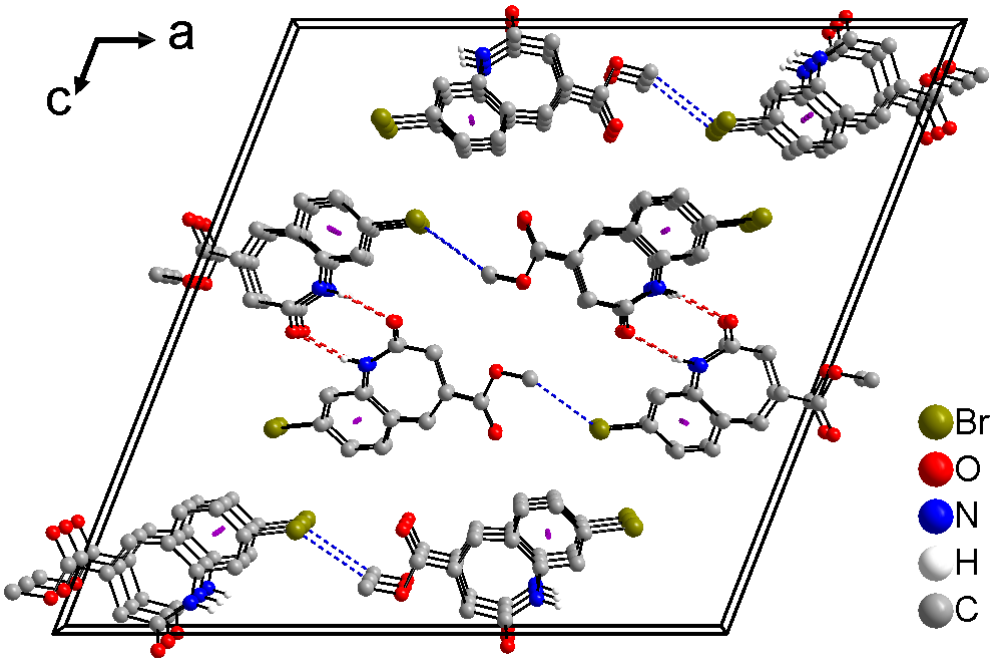

Figure SI-14. Cell view of **9aa** looking along the crystallographic b axis. Hydrogen bonds are shown as red dashed lines, stacking interactions as purple dashed lines, and tetrel bonds as blue dashed lines (non-acidic hydrogen atoms have been omitted).

The resulting intermolecular layers are stacked in the direction of the crystallographic c axis. In the direction of c, the layers are arranged alternately in two different orientations A and B (see **Figure SI-15**).

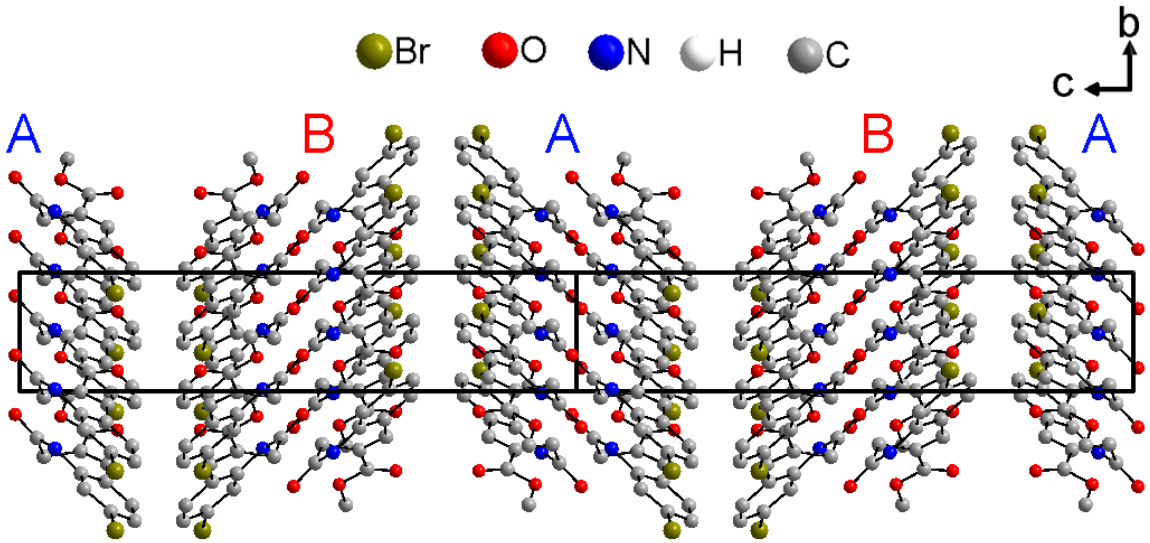

Figure SI-15. Illustration of two unit cells with viewing direction along the crystallographic a axis. Along the c axis, an alternating arrangement of layers A and B is obtained (hydrogen atoms have been omitted).

E References

1. P. Gopinath, S. Nilaya and K. M. Muraleedharan, *Org. Lett.*, 2011, **13**, 1932-1935.
2. A. J. Lampkins, Y. Li, A. Al Abbas, K. A. Abboud, I. Ghiviriga and R. K. Castellano, *Chem. Eur. J.*, 2008, **14**, 1452-1463.
3. S. Pérocheau Arnaud, E. Andreou, L. V. G. Pereira Köster and T. Robert, *ACS Sustainable Chem. Eng.*, 2020, **8**, 1583-1590.
4. J. T. Kuethe and K. G. Childers, *Adv. Synth. Catal.*, 2008, **350**, 1577-1586.
5. B. Schmidt, F. Wolf and H. Brunner, *Eur. J. Org. Chem.*, 2016, 2972-2982.
6. B. Schmidt, F. Hölter, R. Berger and S. Jessel, *Adv. Synth. Catal.*, 2010, **352**, 2463-2473.
7. D. J. Adams, A. Goddard, J. H. Clark and D. J. Macquarrie, *Chem. Commun.*, 2000, 987-988.
8. M. Protiva, J. Jílek, I. Červená, J. Pomykáček, V. Bártl, A. Dlabač, M. Valchář, J. Metyšová, J. Holubek and E. Svátek, *Collect. Czech. Chem. Commun.*, 1986, **51**, 2598-2616.
9. N. H. Nguyen, C. Cougnon and F. Gohier, *J. Org. Chem.*, 2009, **74**, 3955-3957.
10. A. Prechter and M. R. Heinrich, *Synthesis*, 2011, 1515-1525.
11. M. R. Heinrich, O. Blank, D. Ullrich and M. Kirschstein, *J. Org. Chem.*, 2007, **72**, 9609-9616.

12. B. Schmidt, R. Berger and F. Hölter, *Org. Biomol. Chem.*, 2010, **8**, 1406-1414.
13. S. K. Fehler, G. Pratsch, C. Östreicher, M. C. D. Fürst, M. Pischetsrieder and M. R. Heinrich, *Tetrahedron*, 2016, **72**, 7888-7893.
14. M. O. Akram, P. S. Shinde, C. C. Chintawar and N. T. Patil, *Org. Biomol. Chem.*, 2018, **16**, 2865-2869.
15. X. Wang, B. Jiang, C. Du, X. Ren, Z. Duan and H. Wang, *New J. Chem.*, 2019, **43**, 16411-16420.
16. M. P. Doyle and W. J. Bryker, *J. Org. Chem.*, 1979, **44**, 1572-1574.
17. W. Erb, A. Hellal, M. Albini, J. Rouden and J. Blanchet, *Chem. Eur. J.*, 2014, **20**, 6608-6612.
18. STOE & Cie GmbH, X-Area. Software package for collecting single-crystal data on STOE area-detector diffractometers, for image processing, for the correction and scaling of reflection intensities and for outlier rejection. STOE & Cie GmbH, Darmstadt, Germany, 2018.
19. G. Sheldrick, *Acta Cryst. A*, 2008, **A64**, 112-122.
20. G. Sheldrick, *Acta Cryst. A*, 2015, **A71**, 3-8.
21. K. Brandenburg and H. Putz. Crystal Impact Diamond. Diamond - Crystal and Molecular Structure Visualization. Bonn, Germany, 2020.
22. T. Steiner, *Angew. Chem., Int. Ed.*, 2002, **41**, 48-76.
23. C. Janiak, *J. Chem. Soc., Dalton Trans.*, 2000, 3885-3896.
24. T. J. Mooibroek, P. Gamez and J. Reedijk, *CrystEngComm*, 2008, **10**, 1501-1515.
25. A. Bondi, *J. Phys. Chem.*, 1964, **68**, 441-451.
26. R. Bishop, *CrystEngComm*, 2015, **17**, 7448-7460.
27. K. Manoj, R. G. Gonnade, M. M. Bhadbhade and M. S. Shashidhar, *Acta Cryst. C*, 2007, **C63**, o555-o558.
28. F. H. Allen, C. A. Baalham, J. P. M. Lommerse and P. R. Raithby, *Acta Cryst. B*, 1998, **B54**, 320-329.
29. A. Johansson, P. Kollman, S. Rothenberg and J. McKelvey, *J. Am. Chem. Soc.*, 1974, **96**, 3794-3800.
30. A. Bauzá, T. J. Mooibroek and A. Frontera, *Angew. Chem. Int. Ed.*, 2013, **52**, 12317-12321.
31. A. Bauzá, T. J. Mooibroek and A. Frontera, *Chem. Rec.*, 2016, **16**, 473-487.
32. F. H. Allen, O. Kennard, D. G. Watson, L. Brammer, A. G. Orpen and R. Taylor, *J. Chem. Soc., Perkin Trans. 2*, 1987, S1-S19.

F Copies of NMR-spectra

^{1}H NMR (400 MHz, $CDCl_3$) of **3a**

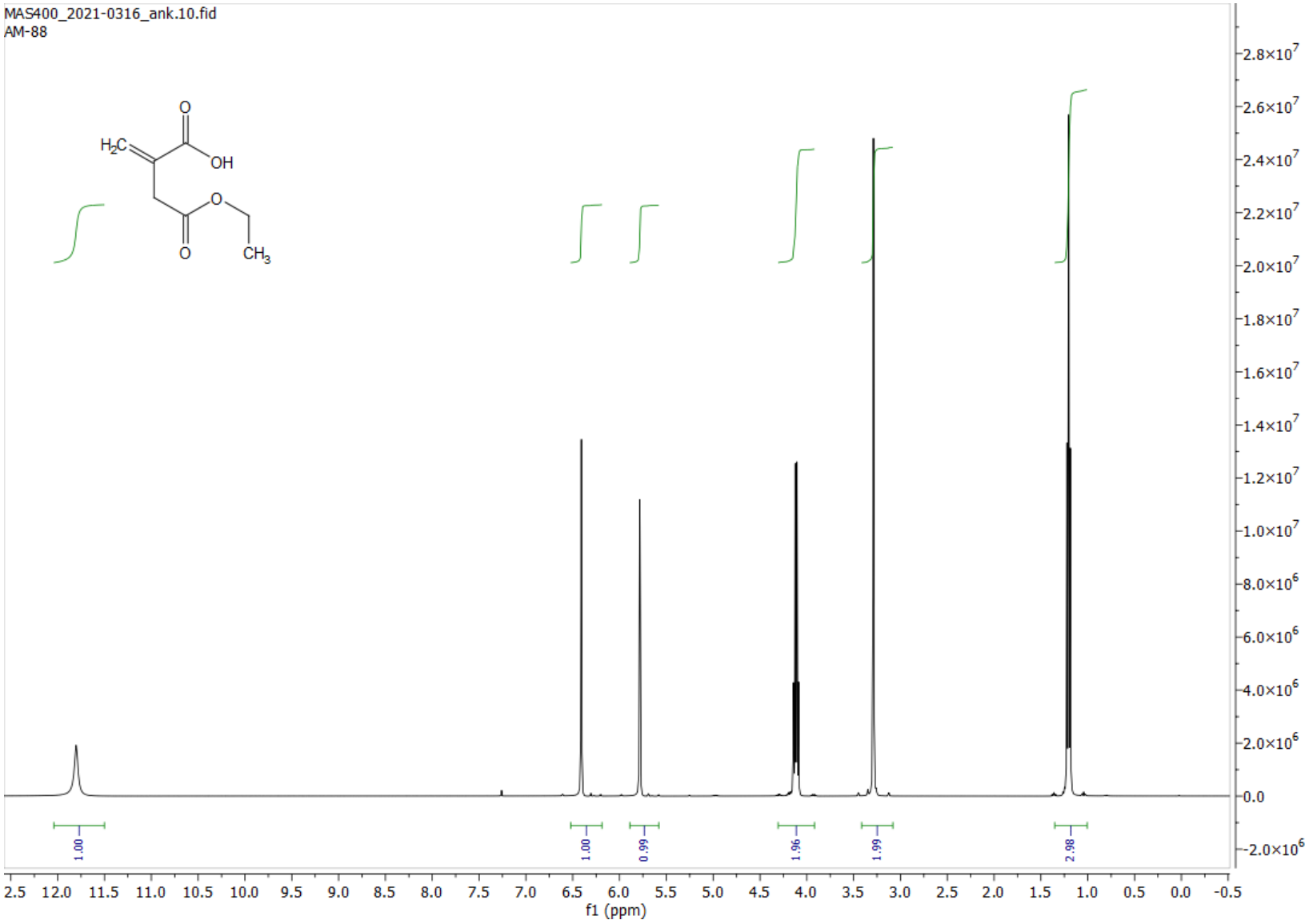

$^{13}C\{^{1}H\}$ NMR (101 MHz, $CDCl_3$) of **3a**

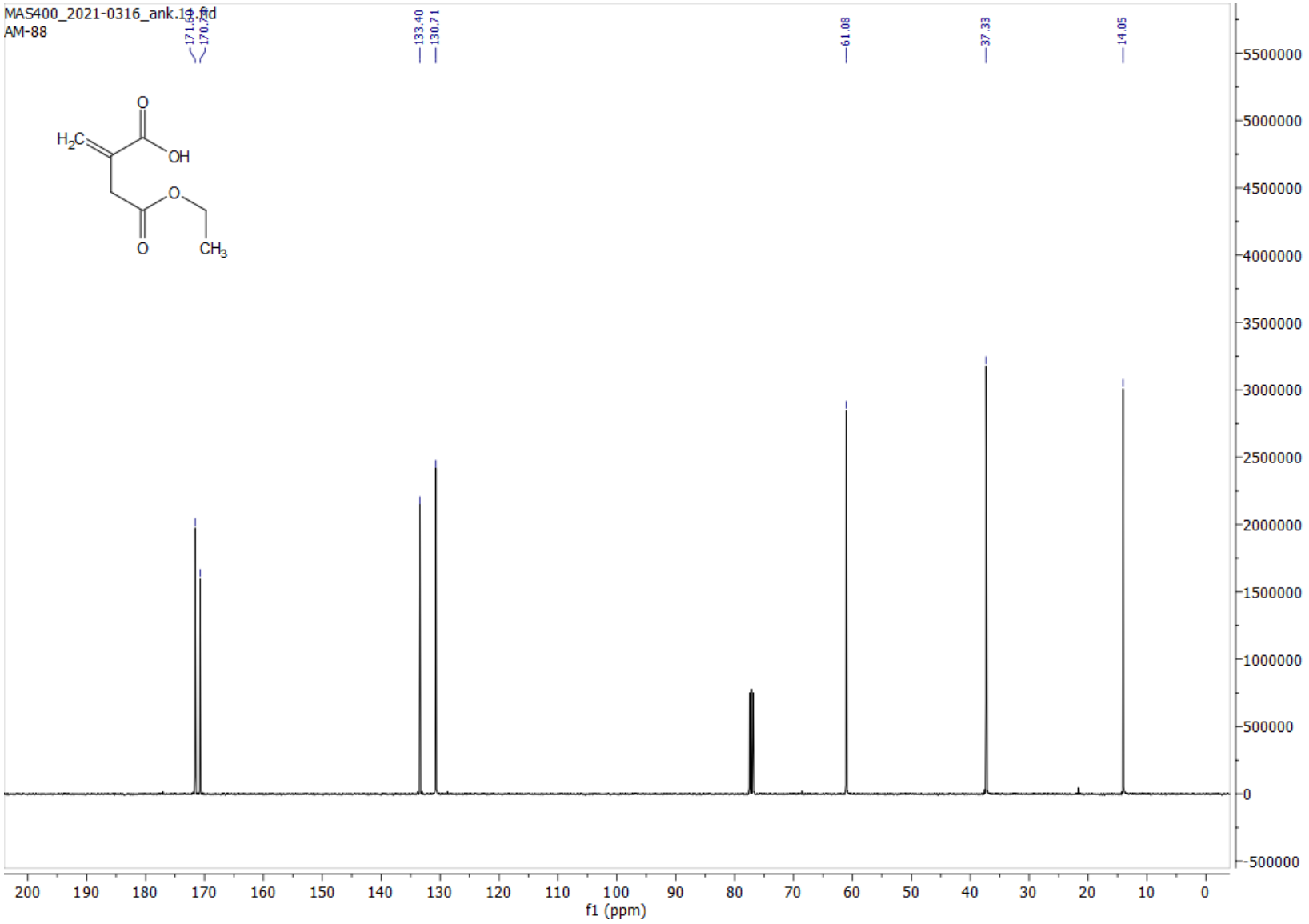

^{1}H NMR (300 MHz, acetone-d_6) of **3b**

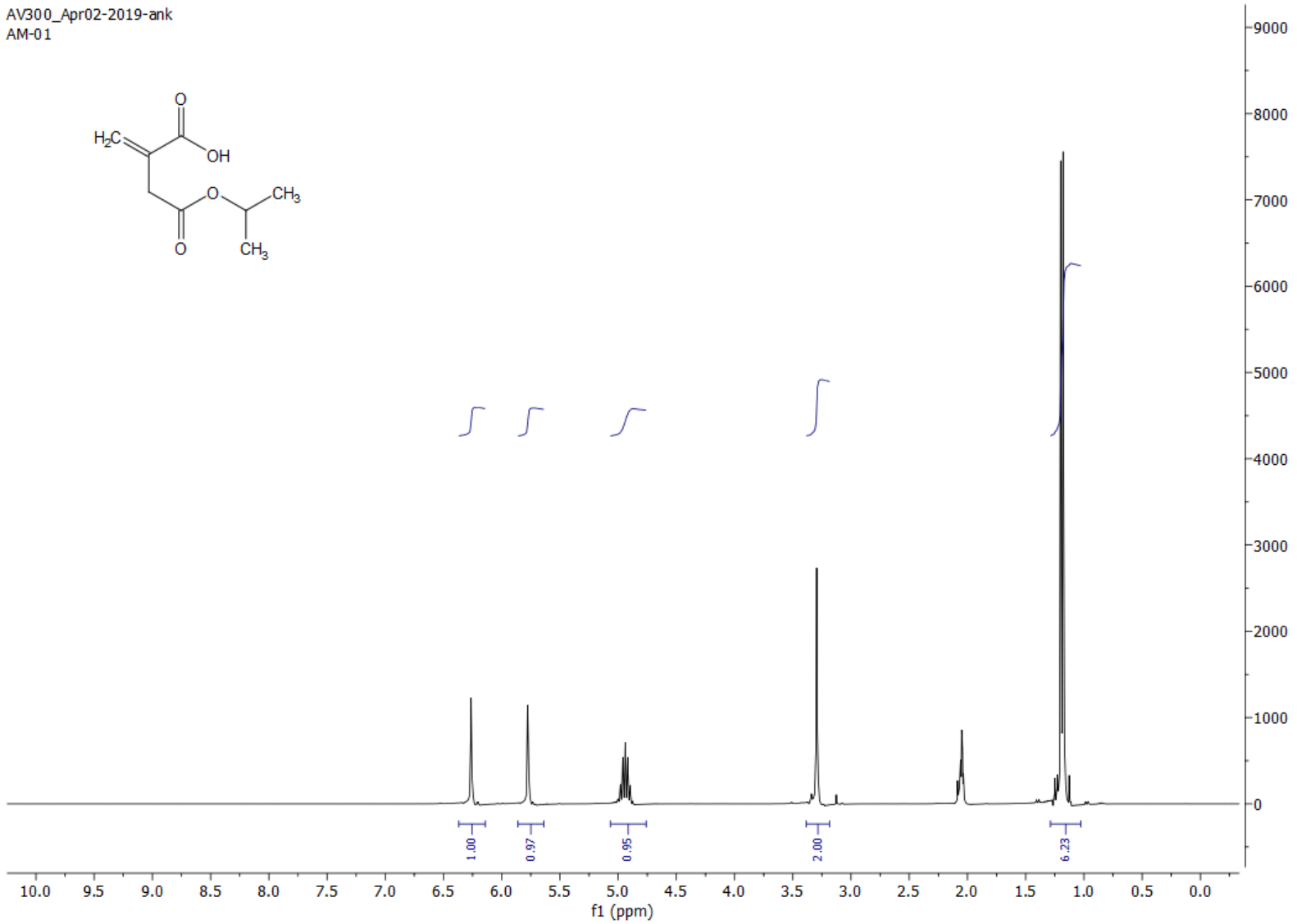

$^{13}C\{^{1}H\}$ NMR (75 MHz, acetone-d_6) of **3b**

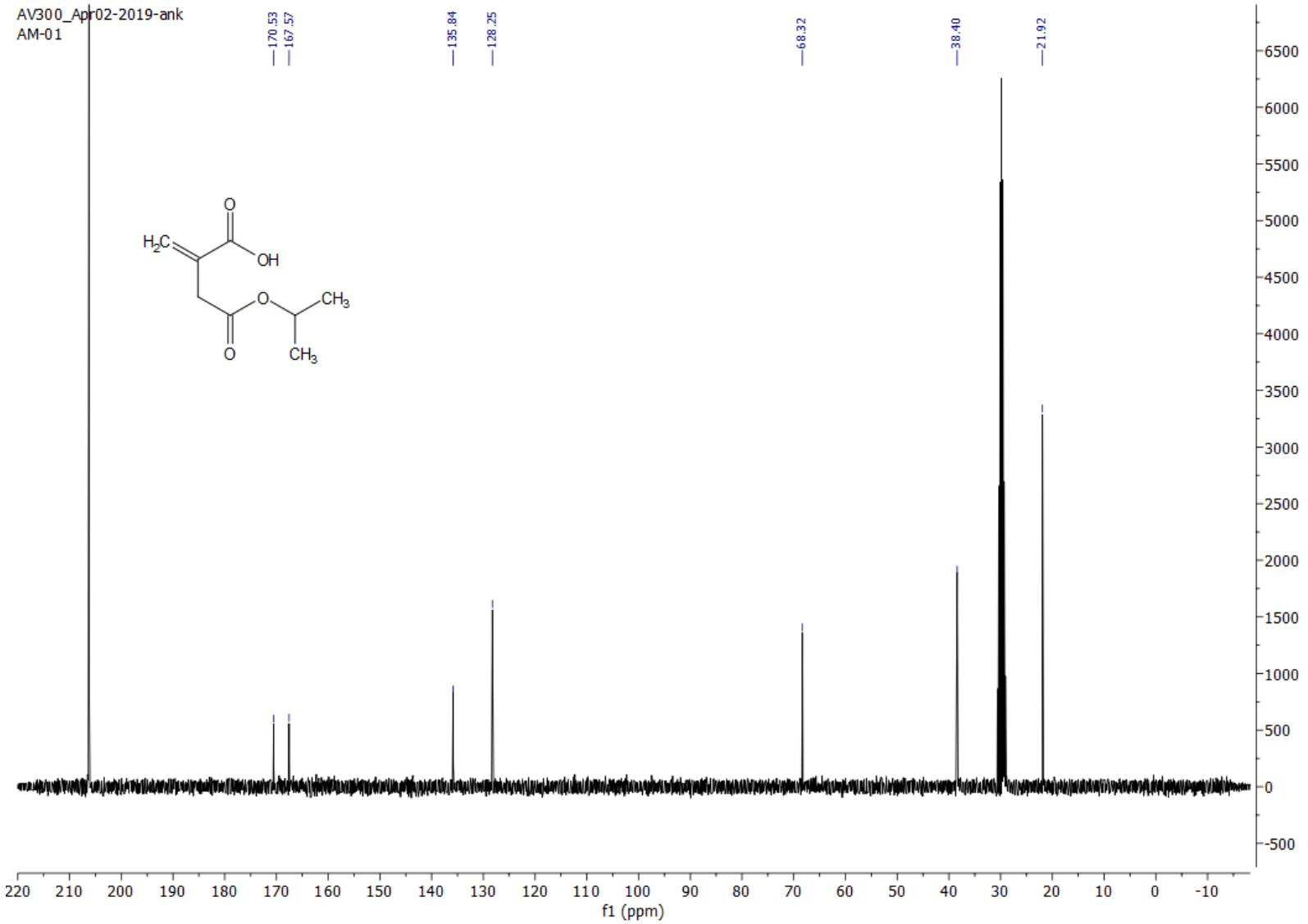

HSQC (300/75 MHz, acetone-d_6) of **3b**

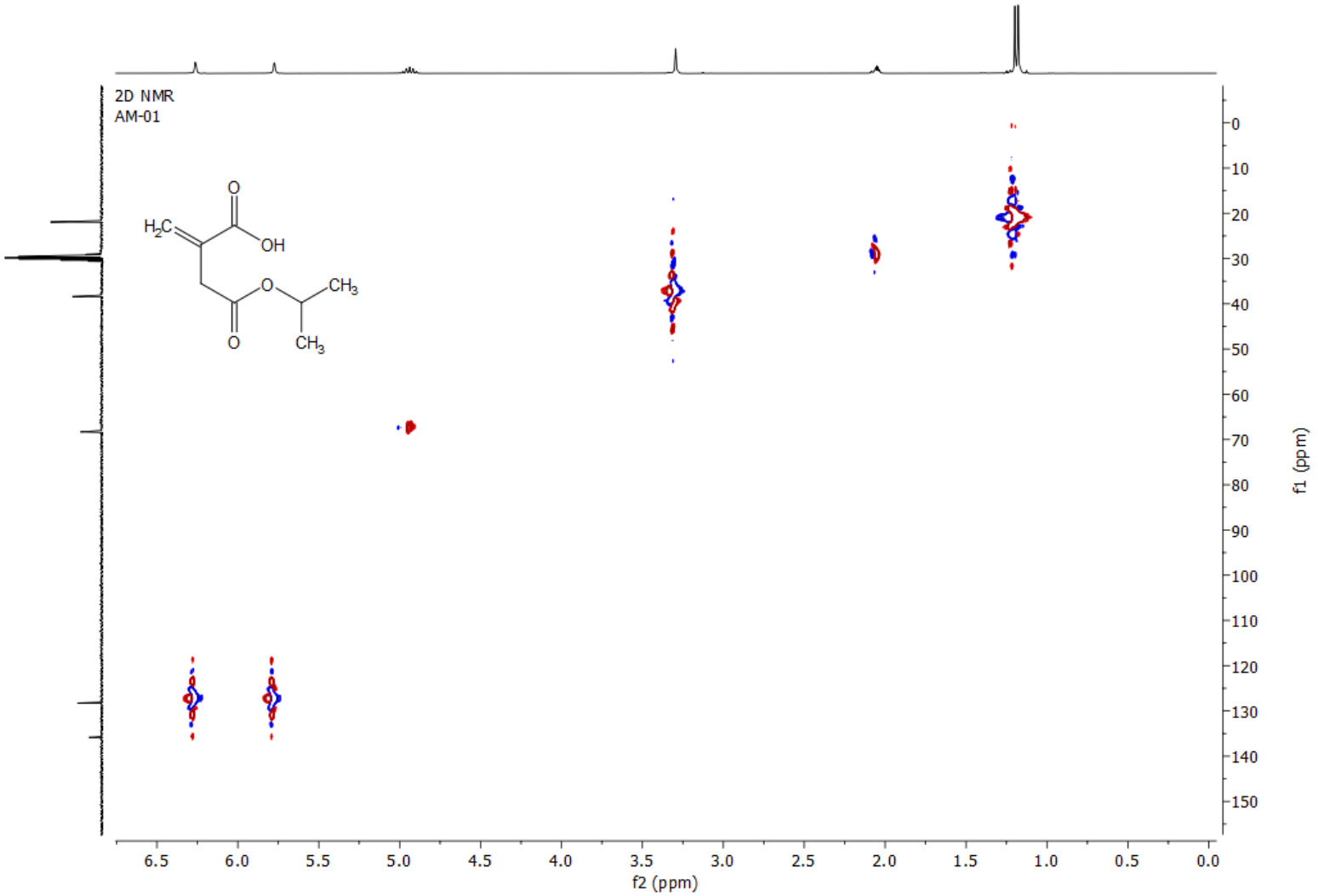

HMBC (300/75 MHz, acetone-d_6) of **3b**

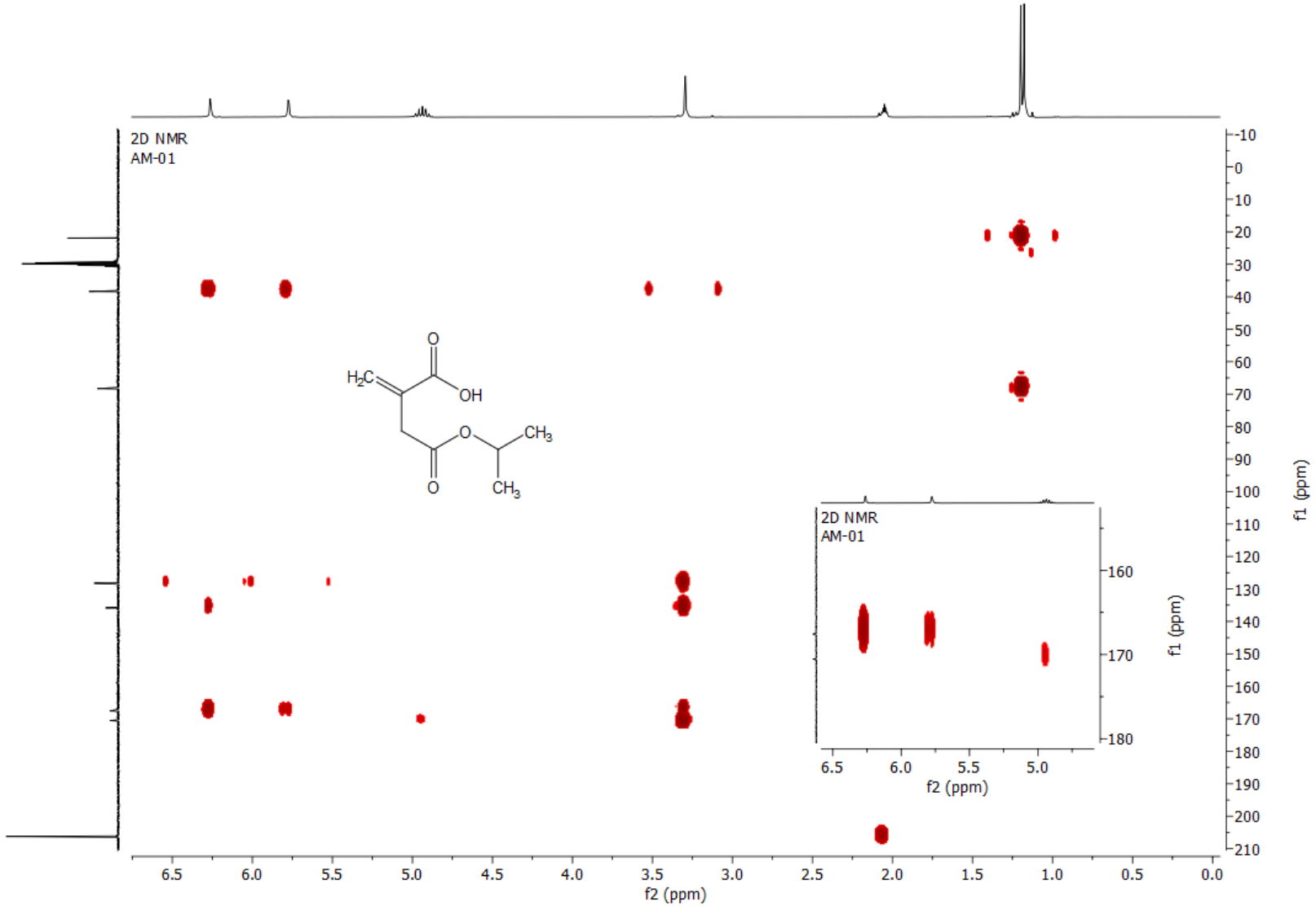

^{1}H NMR (400 MHz, $CDCl_3$) of **3c**

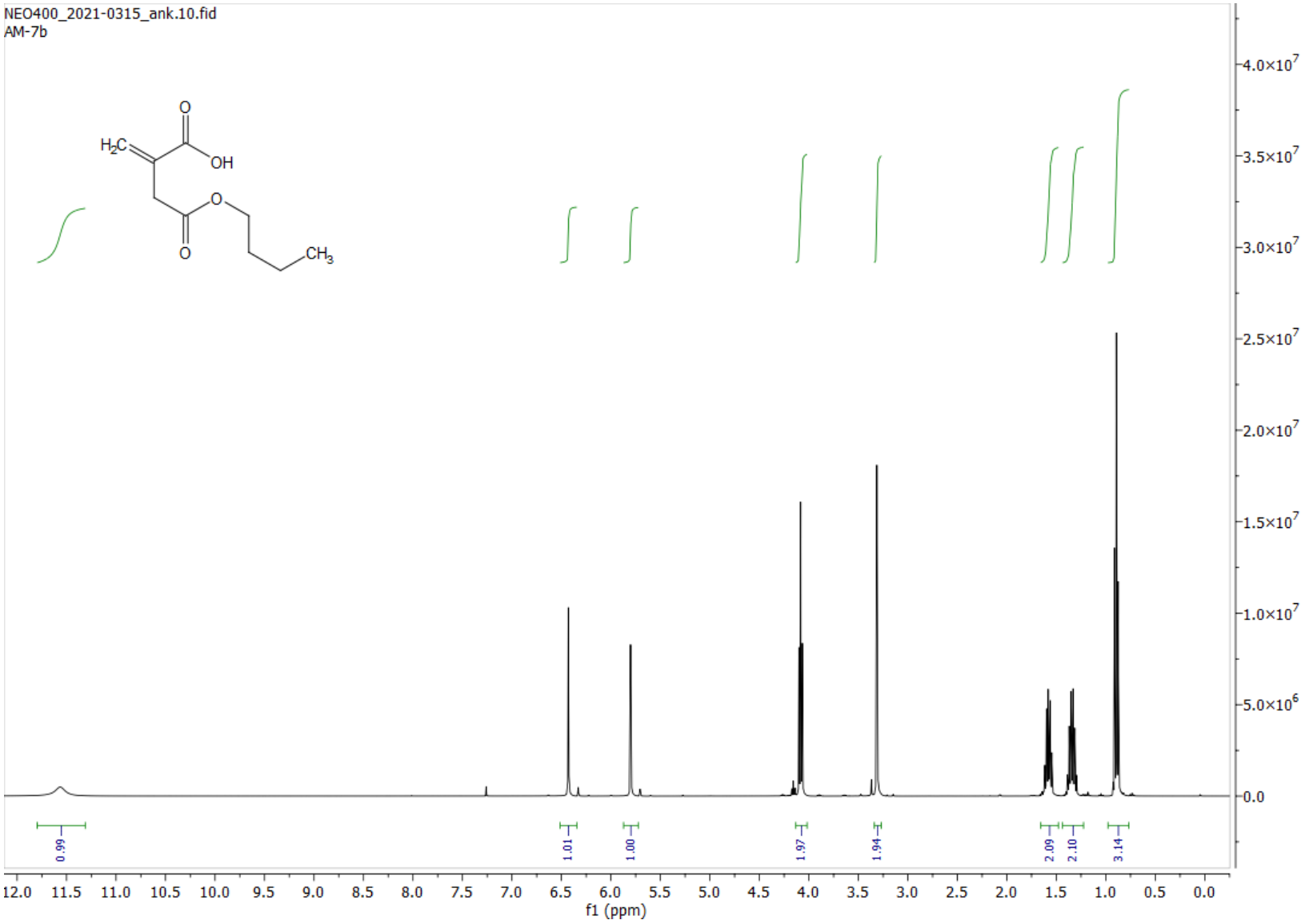

$^{13}C\{^{1}H\}$ NMR (101 MHz, $CDCl_3$) of **3c**

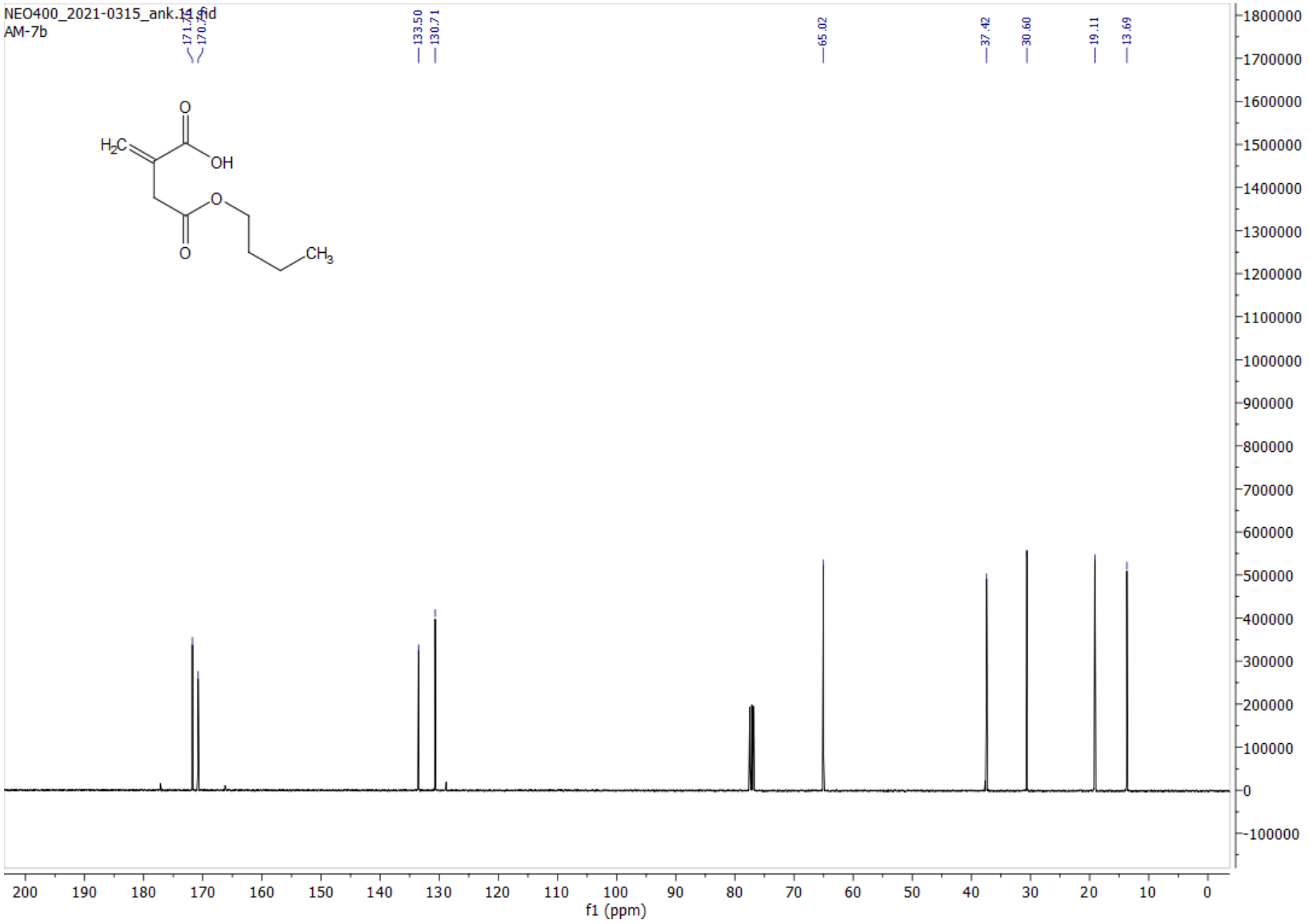

^{1}H NMR (400 MHz, $CDCl_3$) of **5aa**

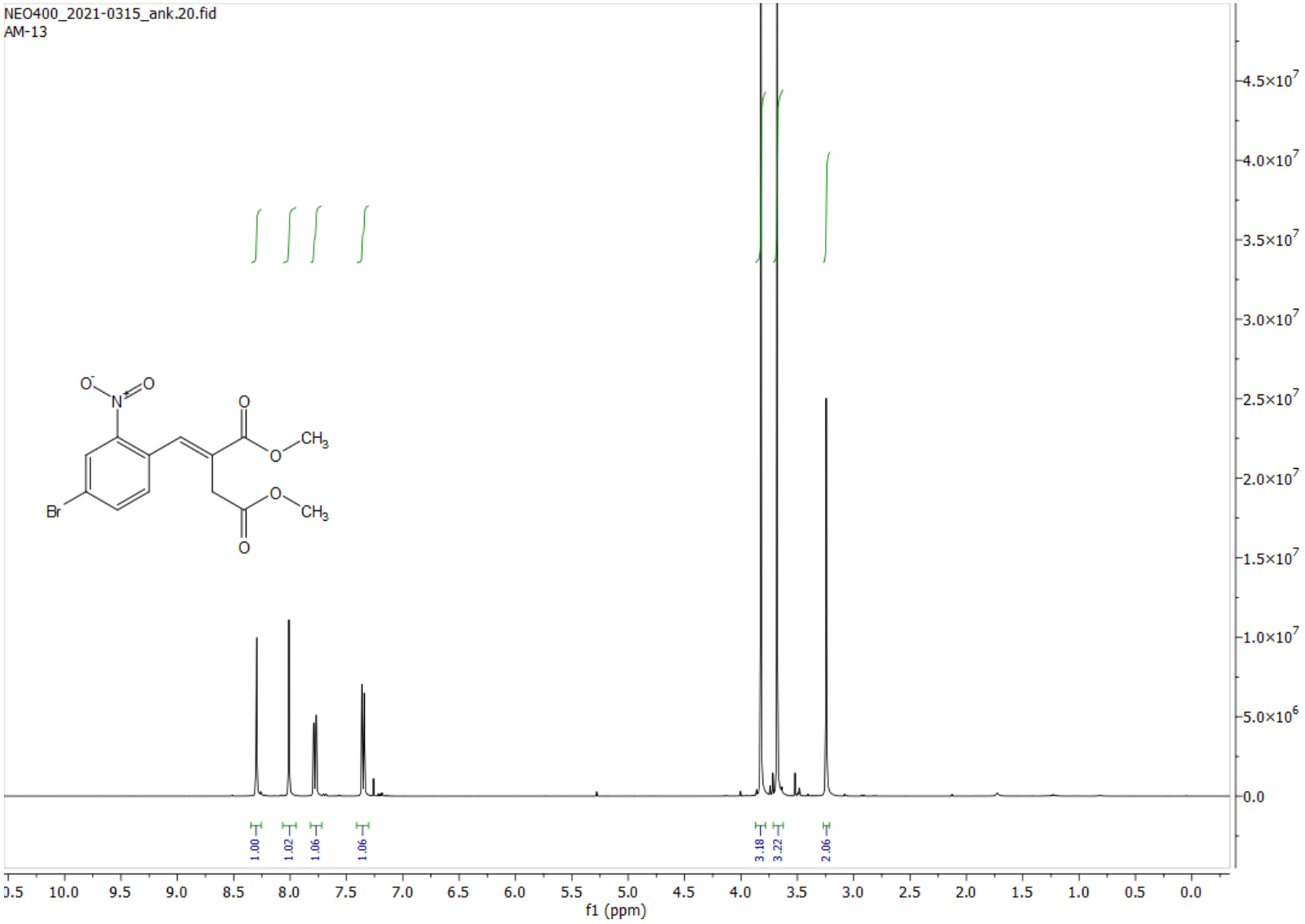

$^{13}C\{^{1}H\}$ NMR (101 MHz, $CDCl_3$) of **5aa**

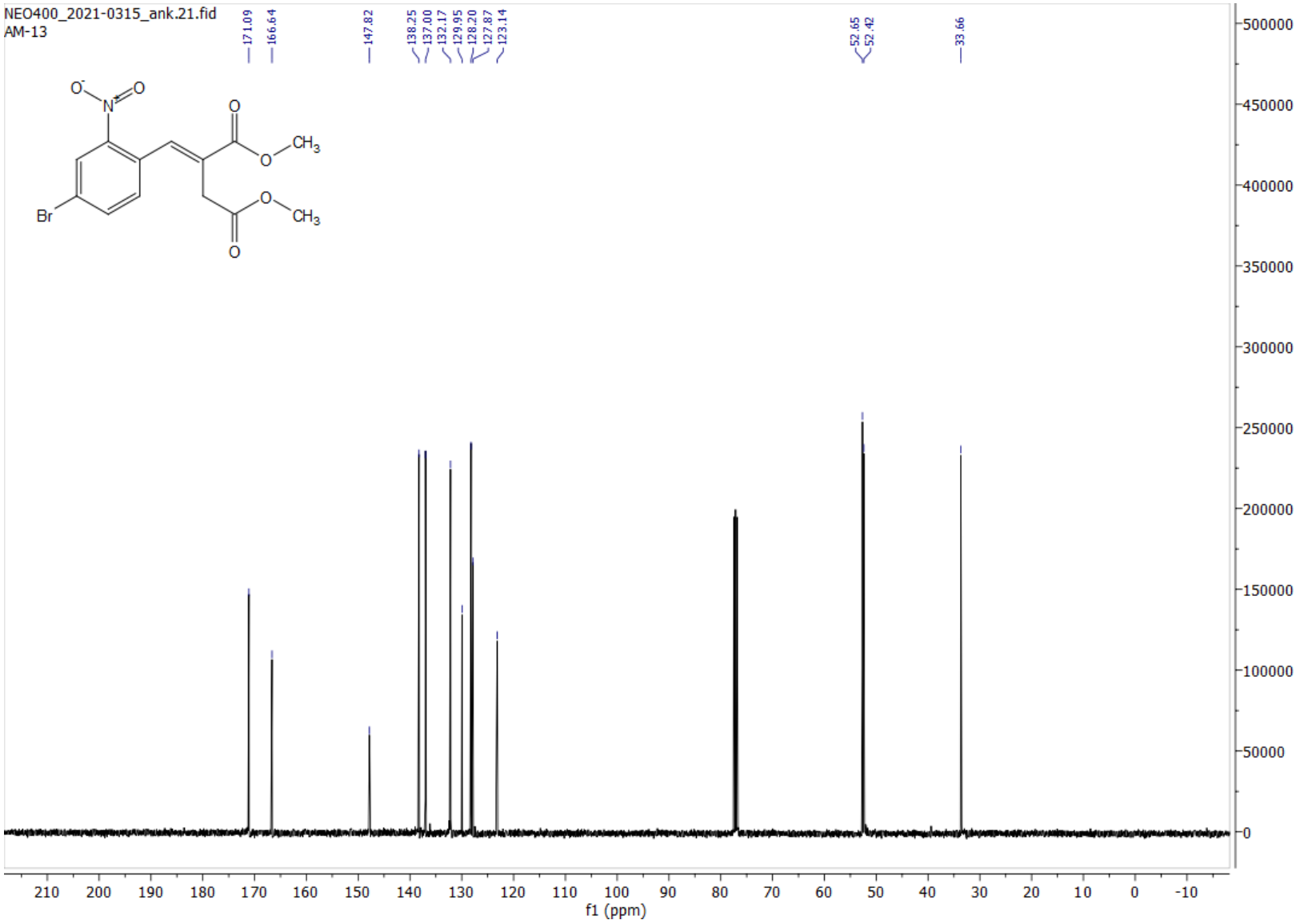

^{1}H NMR (400 MHz, $CDCl_3$) of **5ba**

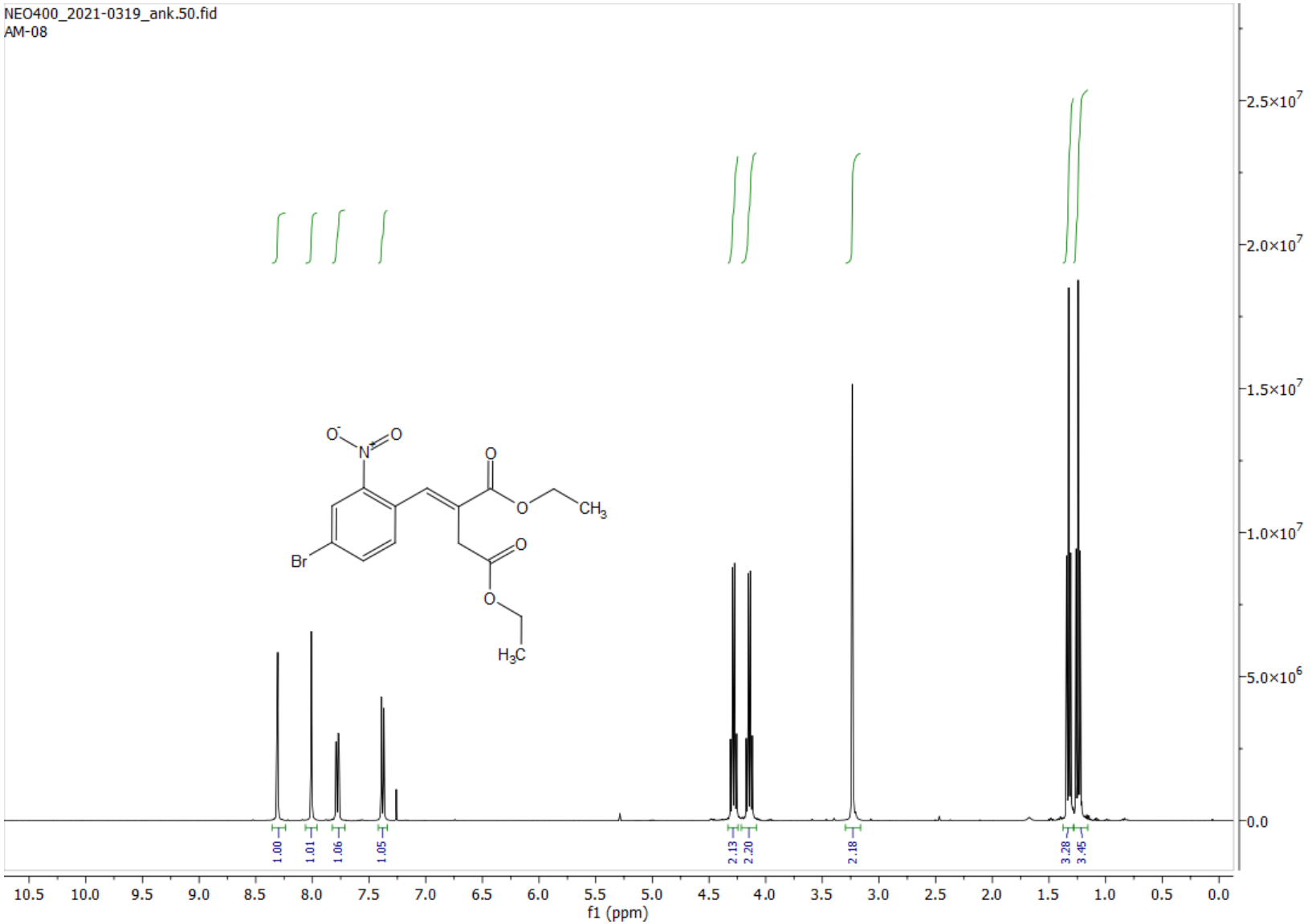

$^{13}C\{^{1}H\}$ NMR (101 MHz, $CDCl_3$) of **5ba**

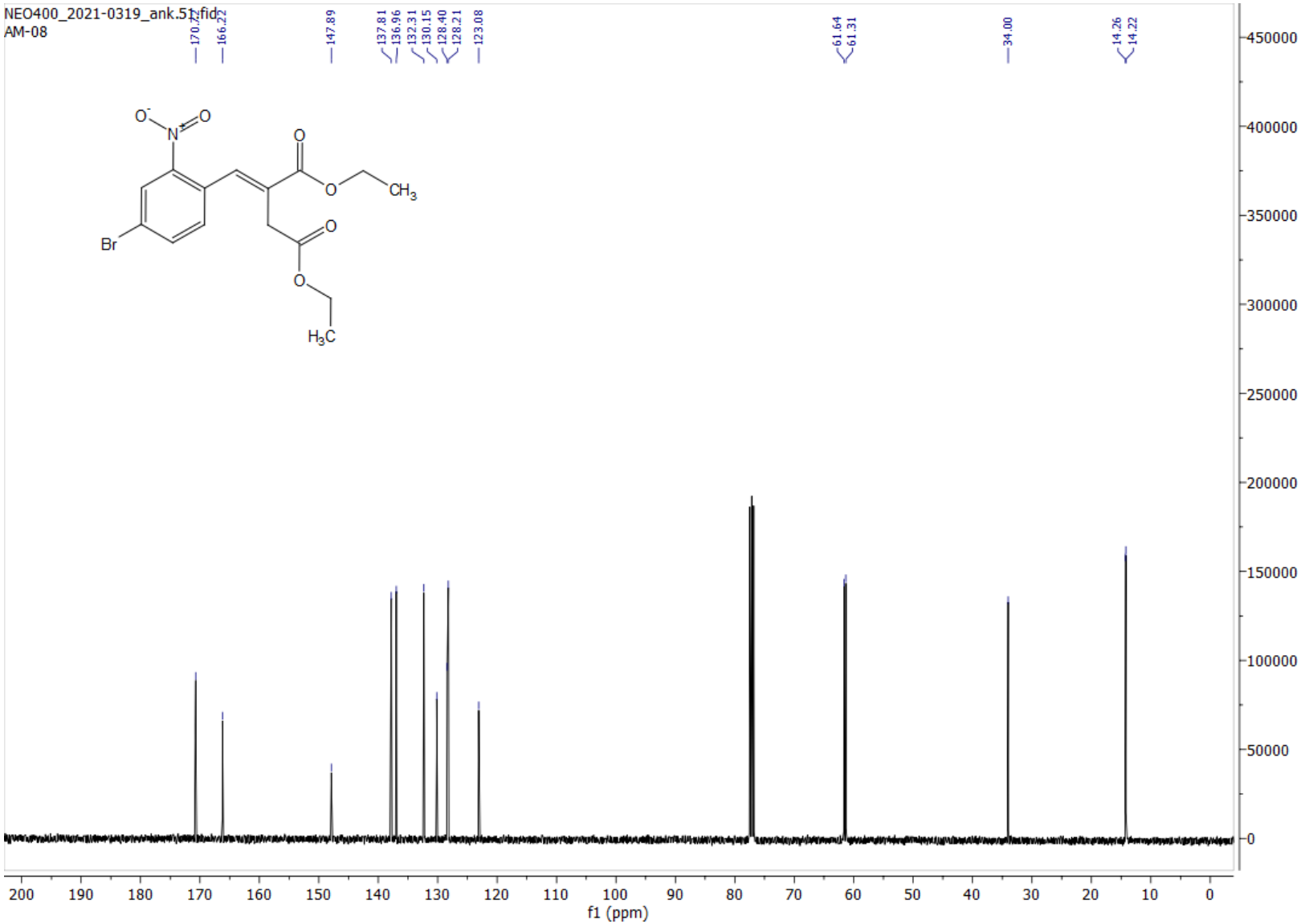

^{1}H NMR (300 MHz, $CDCl_3$) of **5ab**

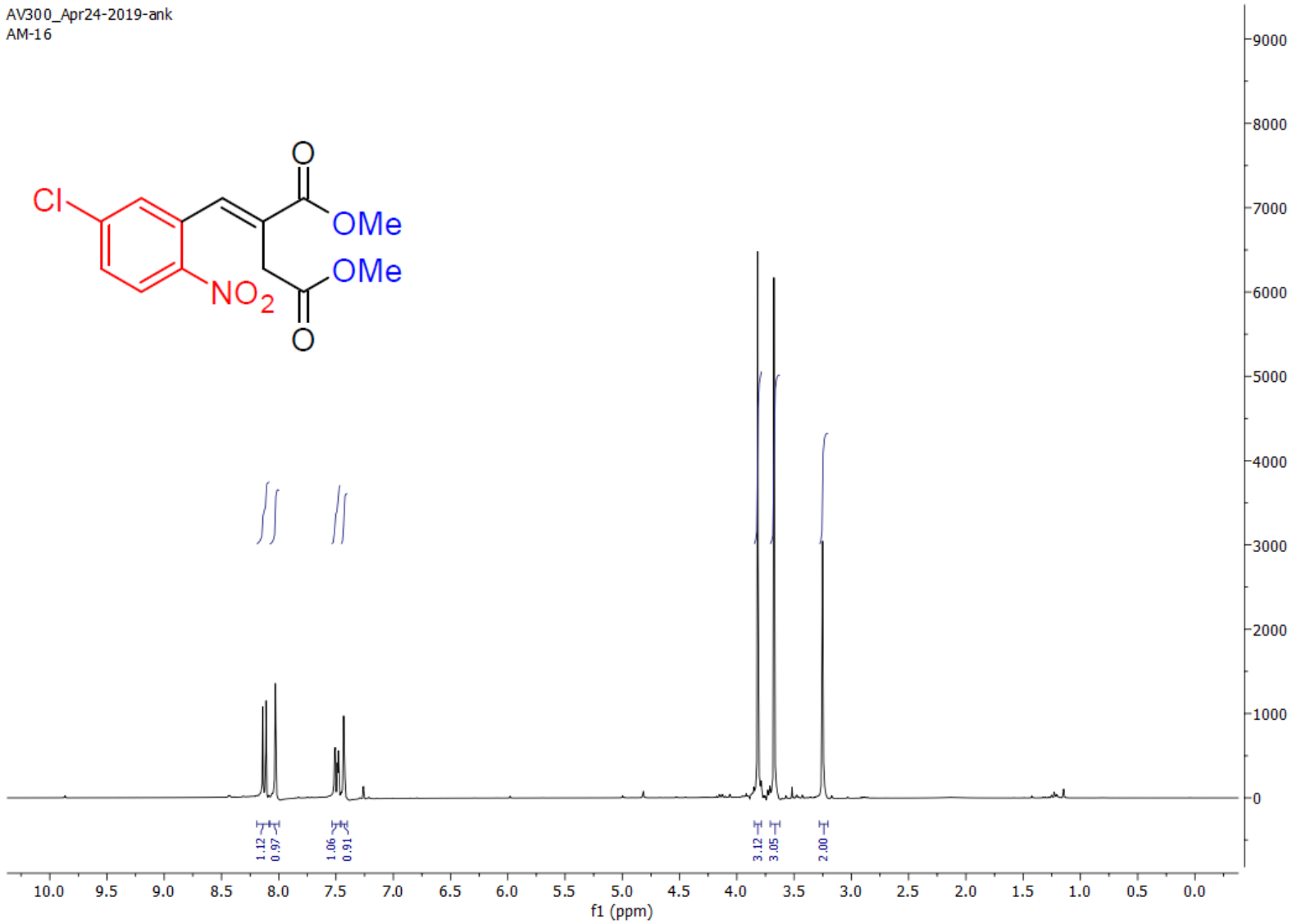

$^{13}C\{^{1}H\}$ NMR (75 MHz, $CDCl_3$) of **5ab**

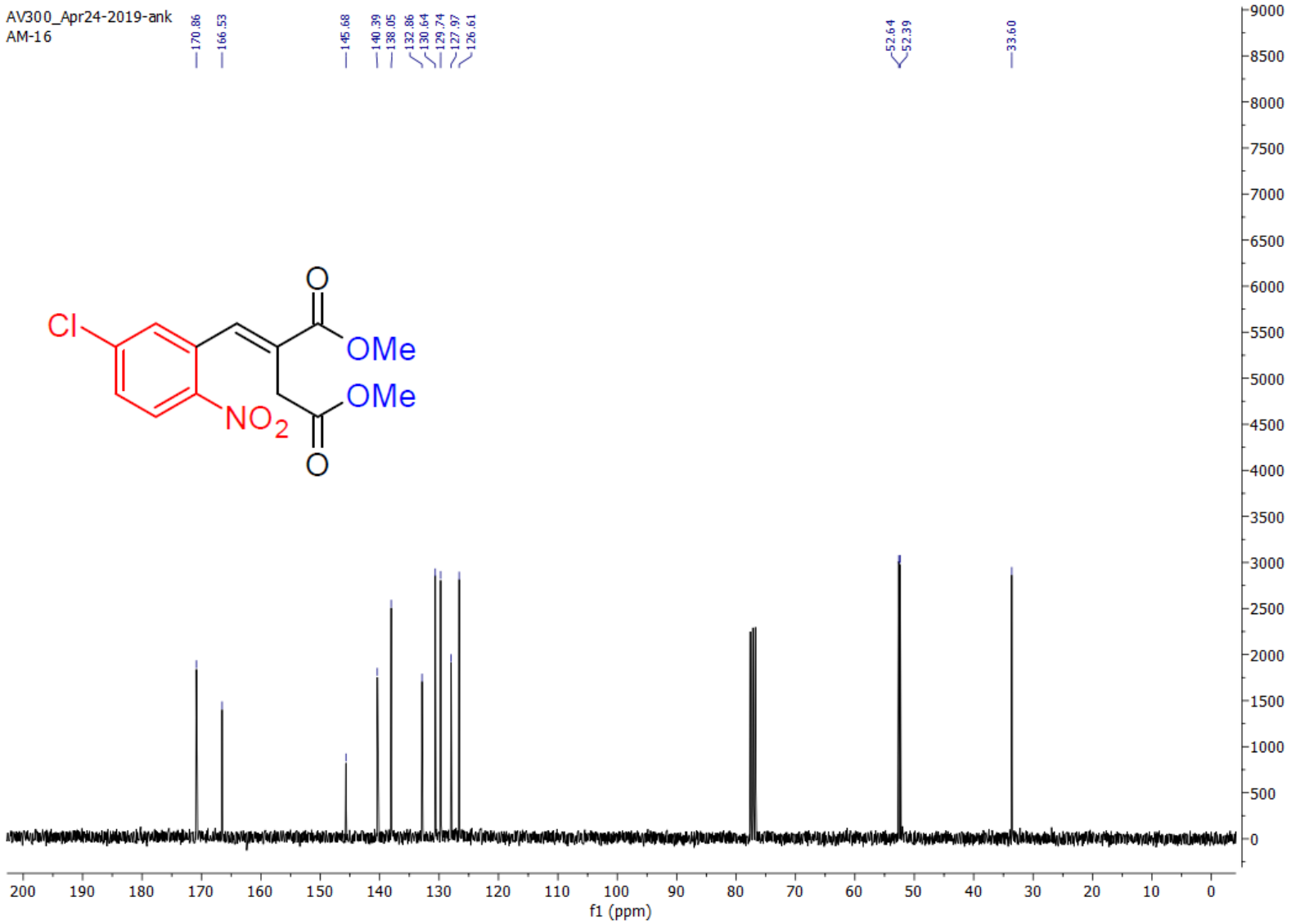

^{1}H NMR (400 MHz, $CDCl_3$) of **5bb**

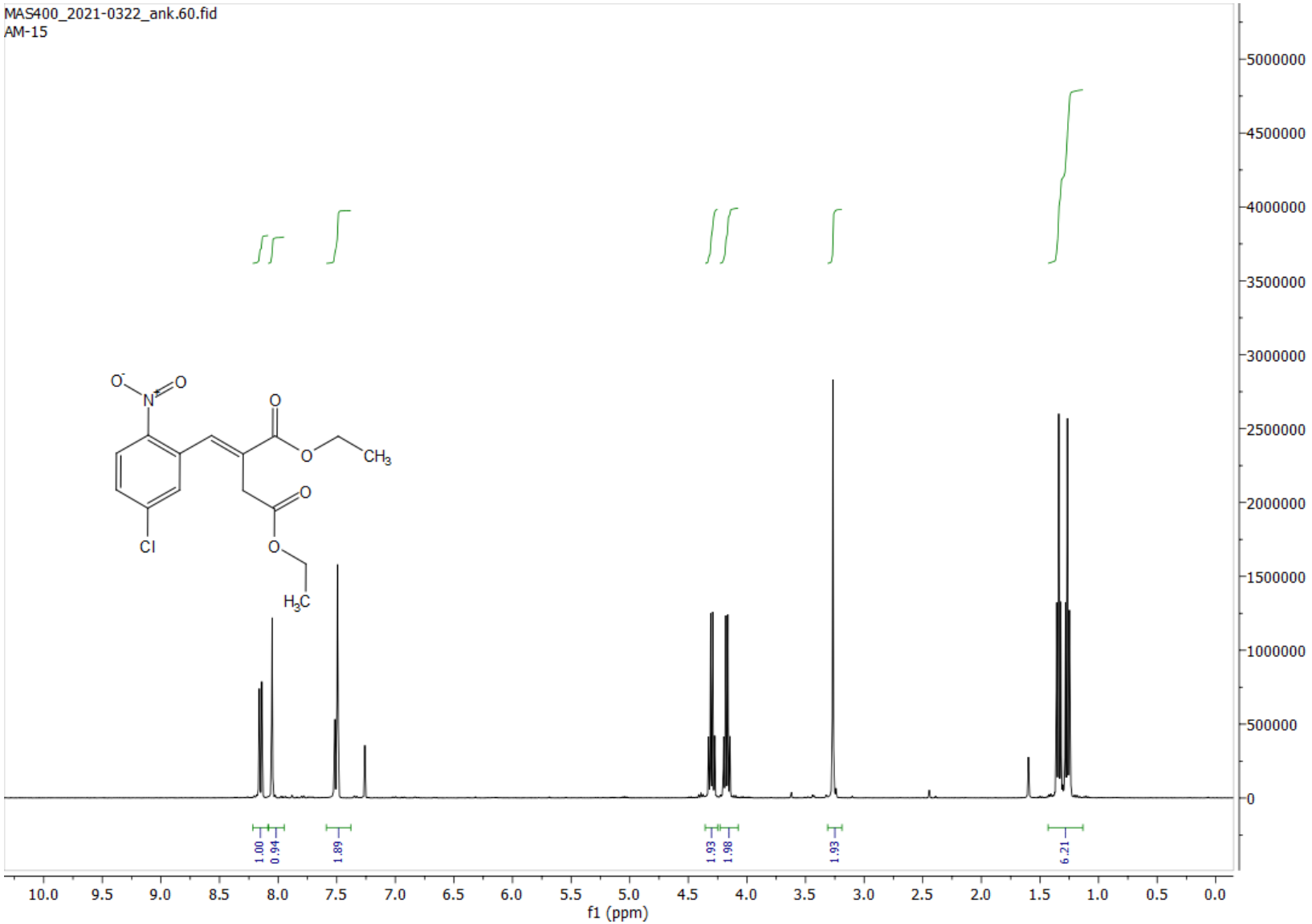

$^{13}C\{^{1}H\}$ NMR (101 MHz, $CDCl_3$) of **5bb**

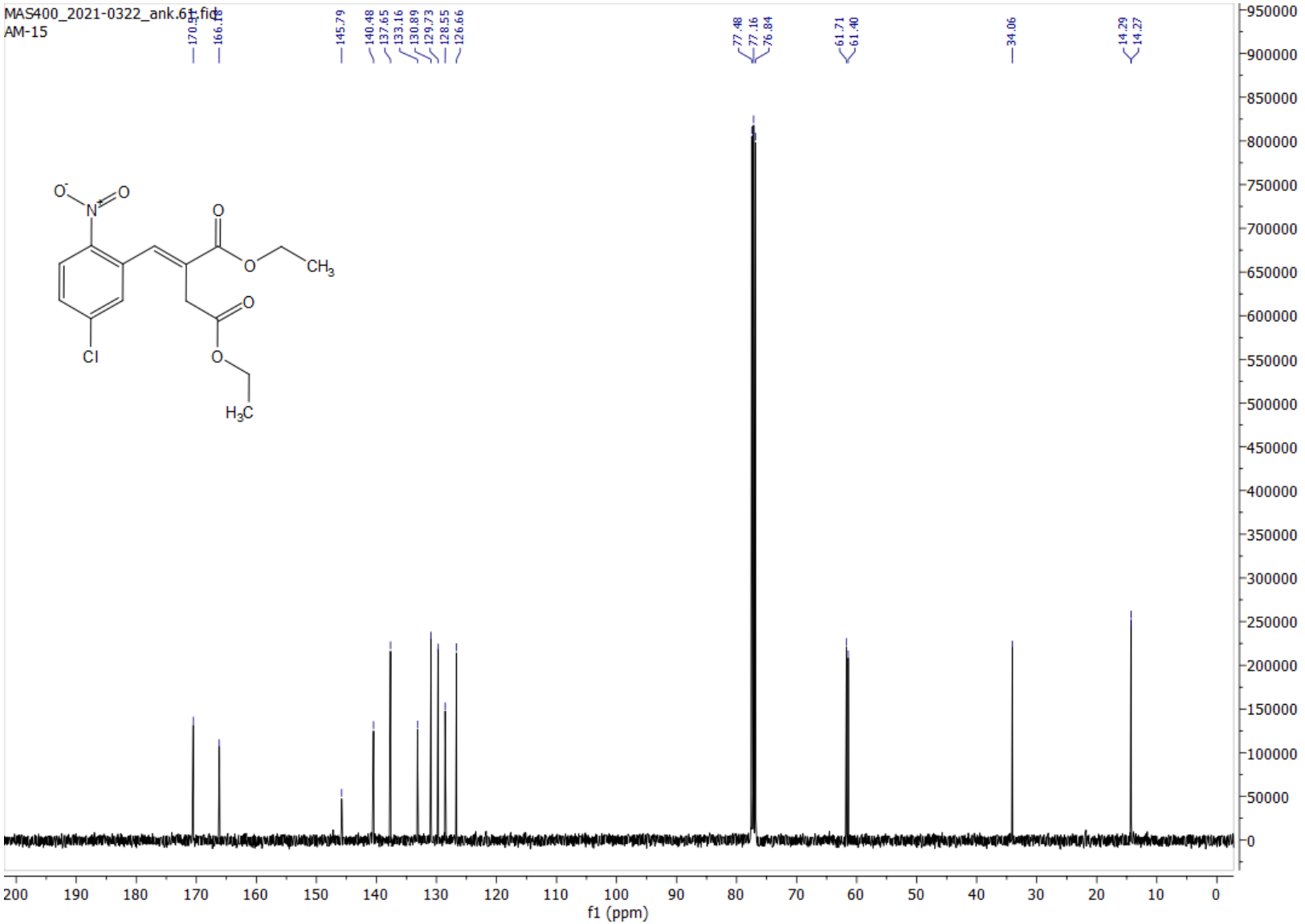

^{1}H NMR (400 MHz, $CDCl_3$) of **5ac**

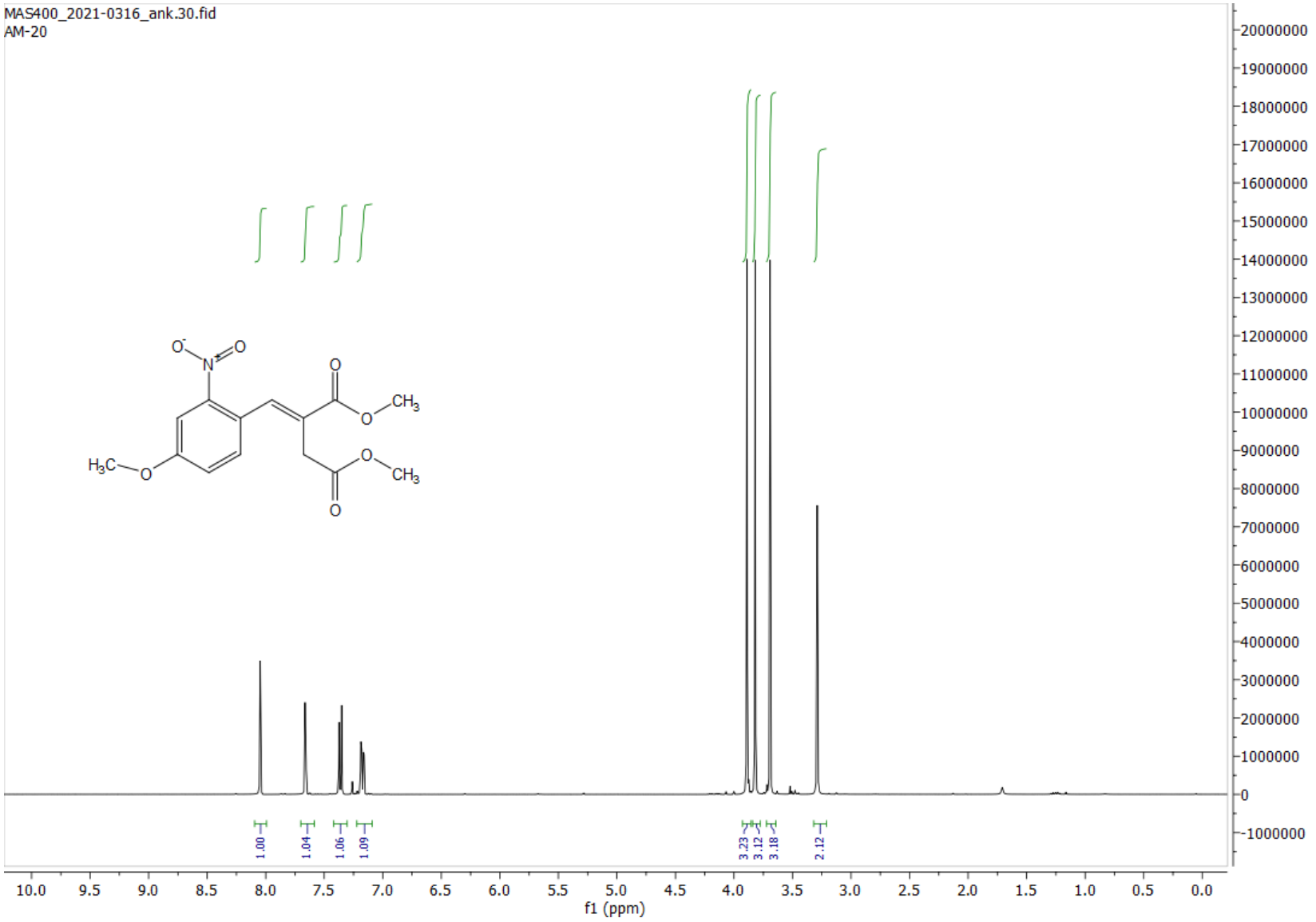

$^{13}C\{^{1}H\}$ NMR (101 MHz, $CDCl_3$) of **5ac**

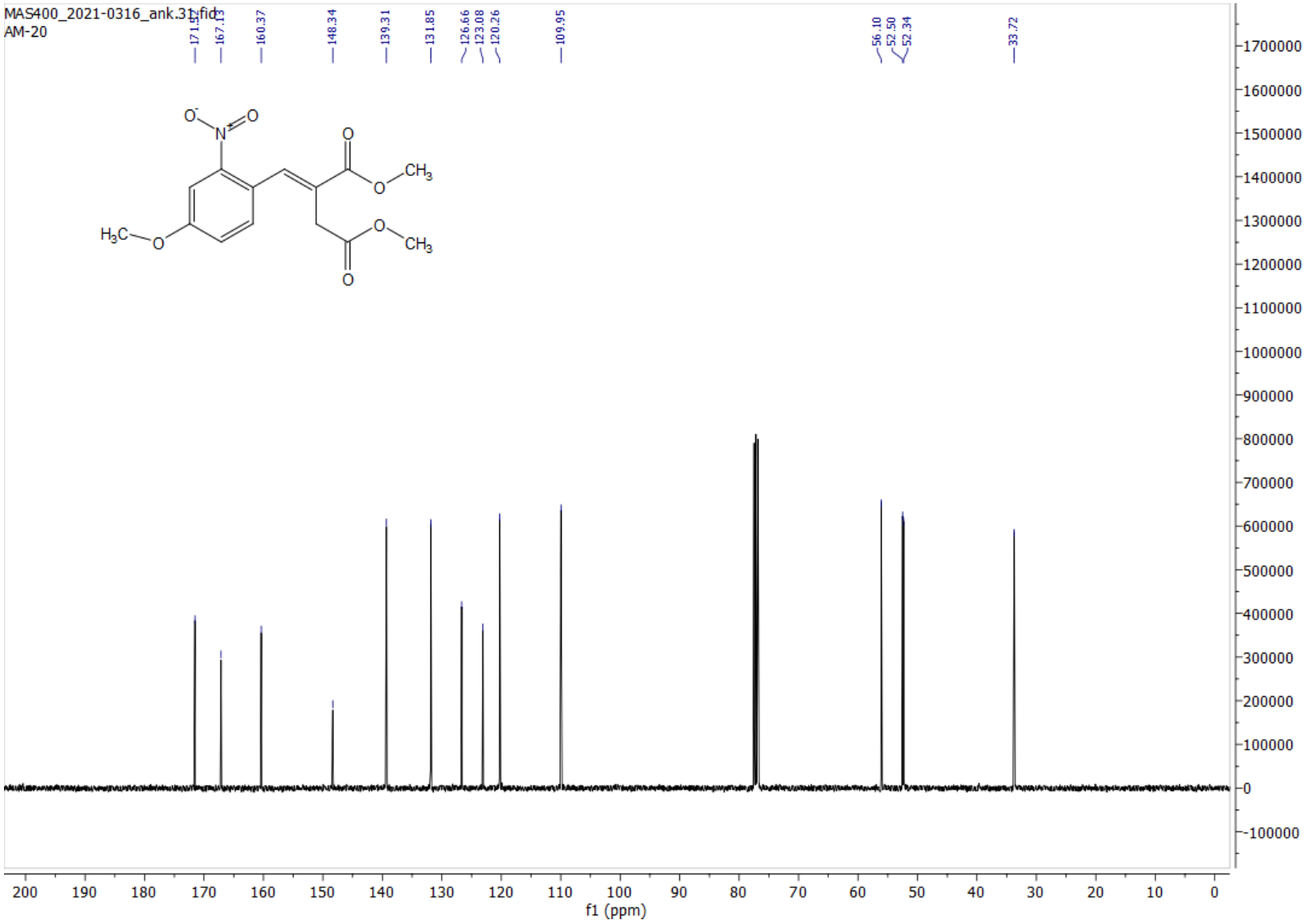

^{1}H NMR (400 MHz, $CDCl_3$) of **5bc**

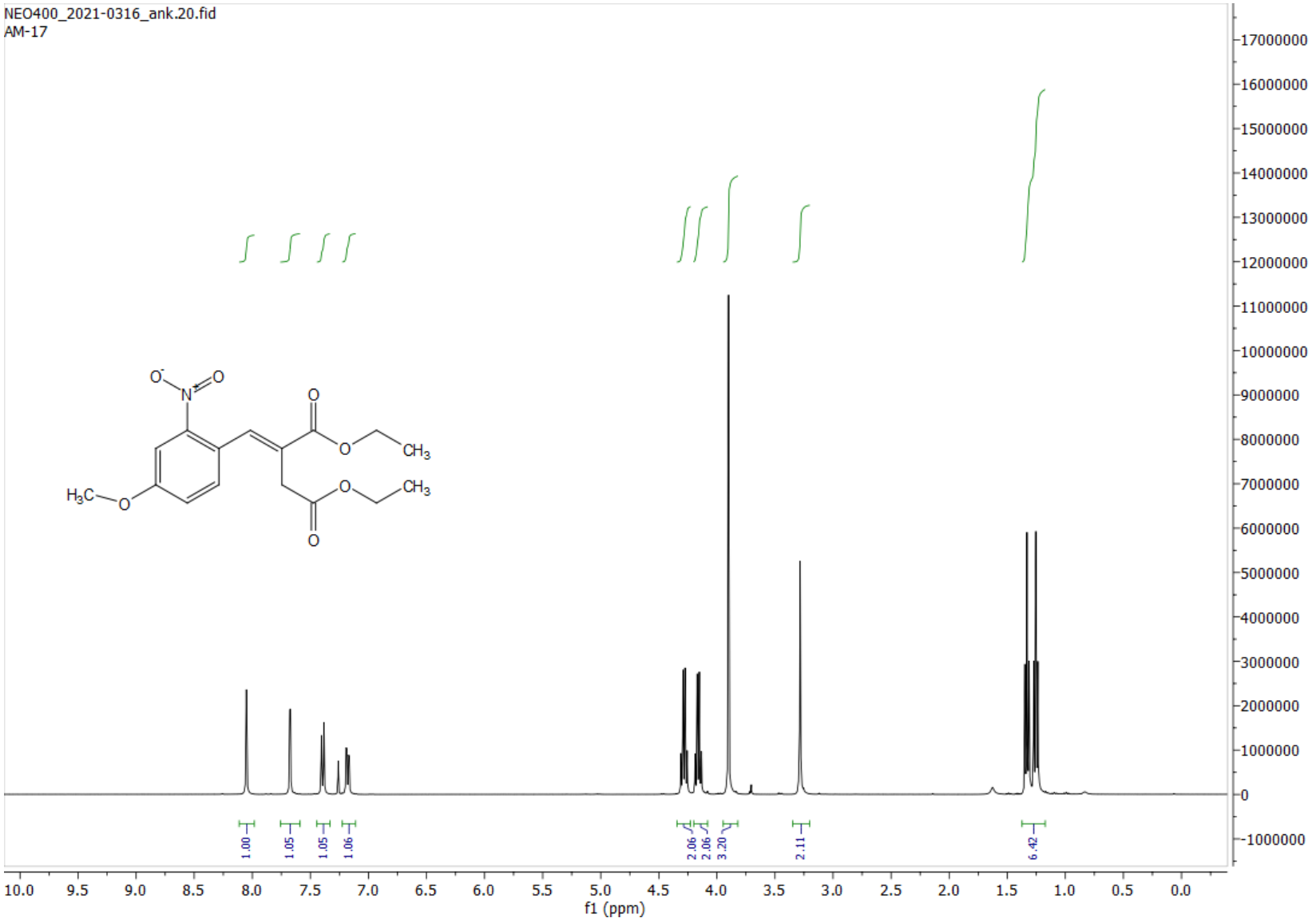

$^{13}C\{^{1}H\}$ NMR (101 MHz, $CDCl_3$) of **5bc**

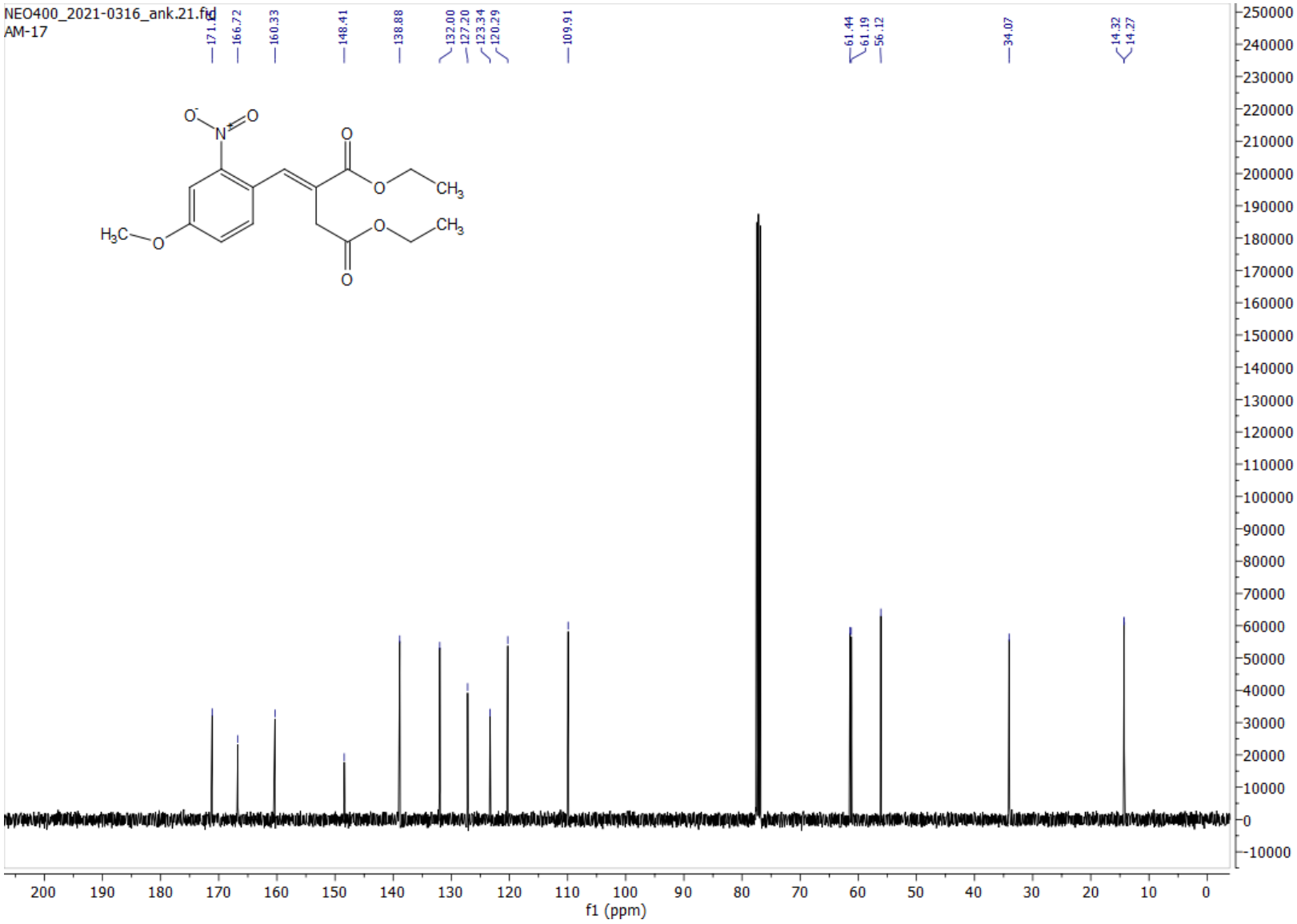

^{1}H NMR (400 MHz, $CDCl_3$) of **5bd**

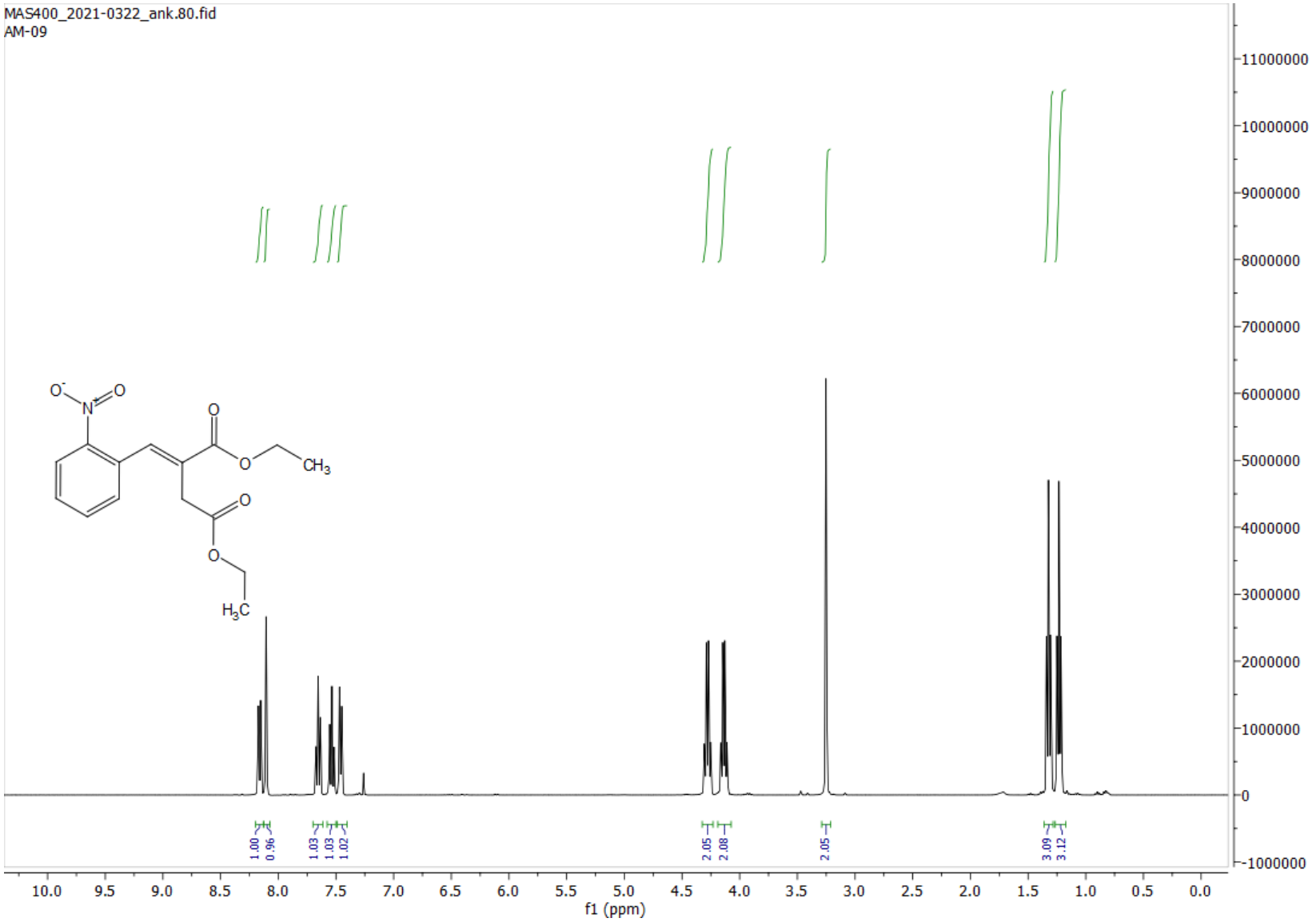

$^{13}C\{^{1}H\}$ NMR (101 MHz, $CDCl_3$) of **5bd**

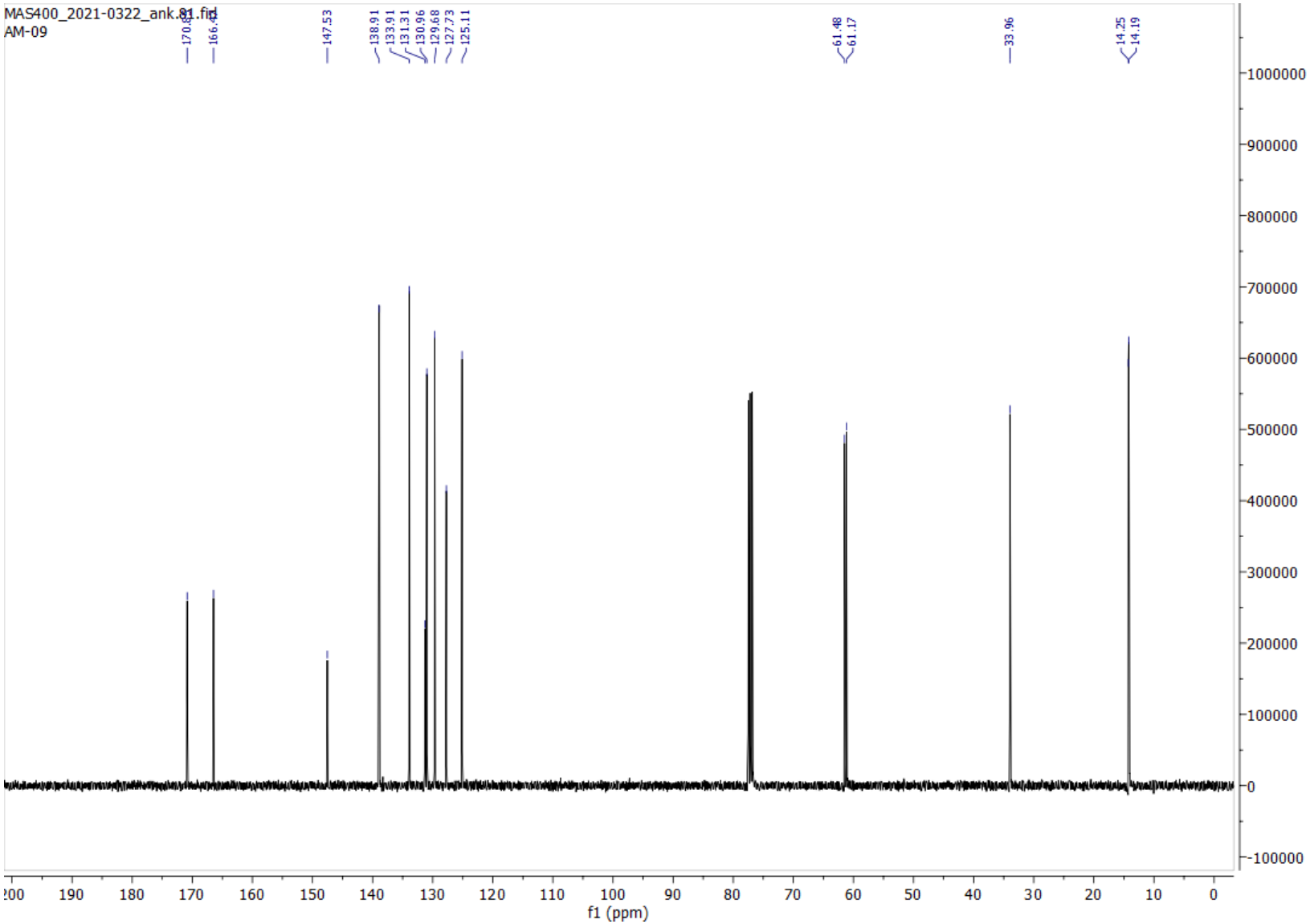

^{1}H NMR (300 MHz, $CDCl_3$) of **5cd**

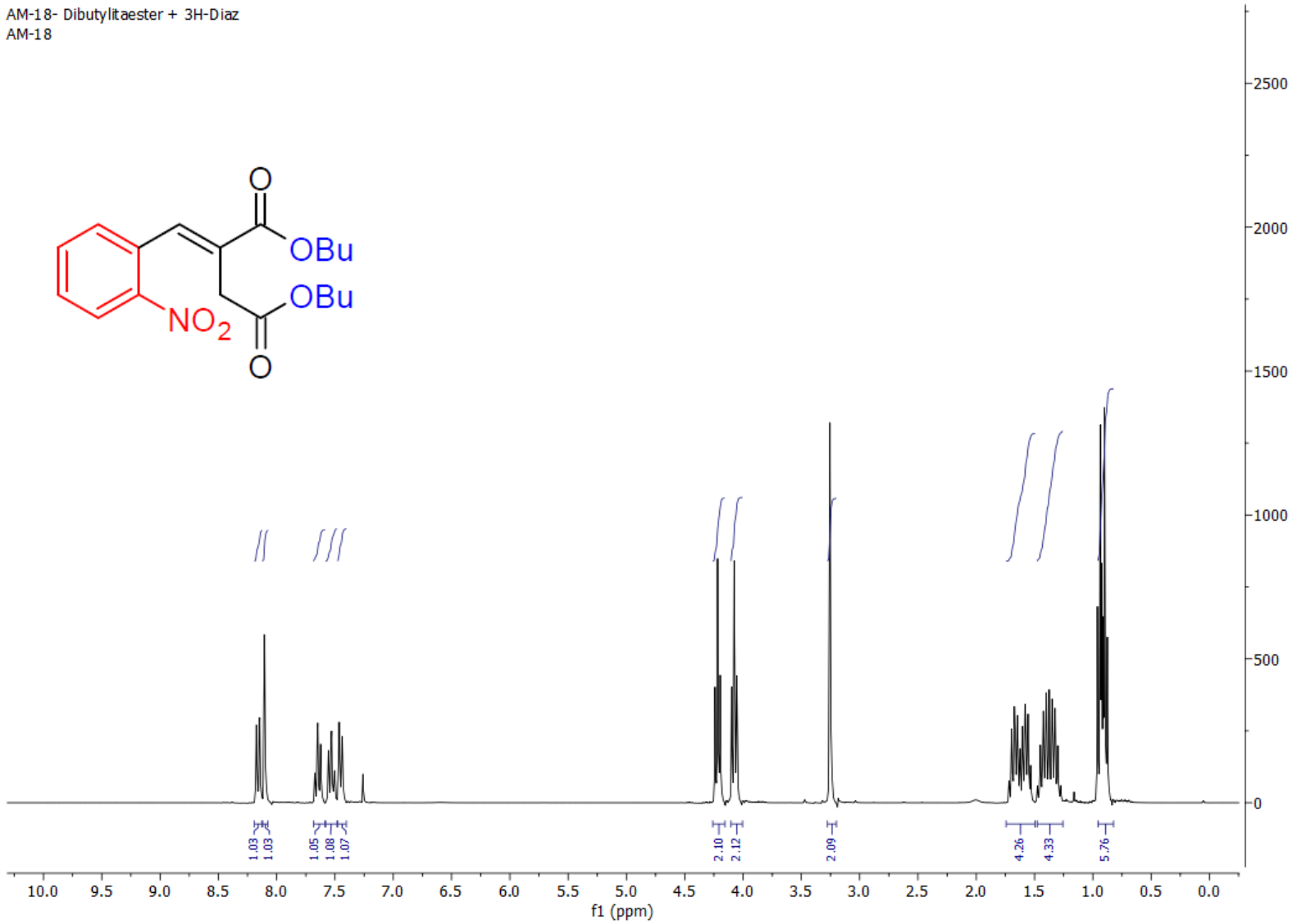

$^{13}C\{^{1}H\}$ NMR (75 MHz, $CDCl_3$) of **5cd**

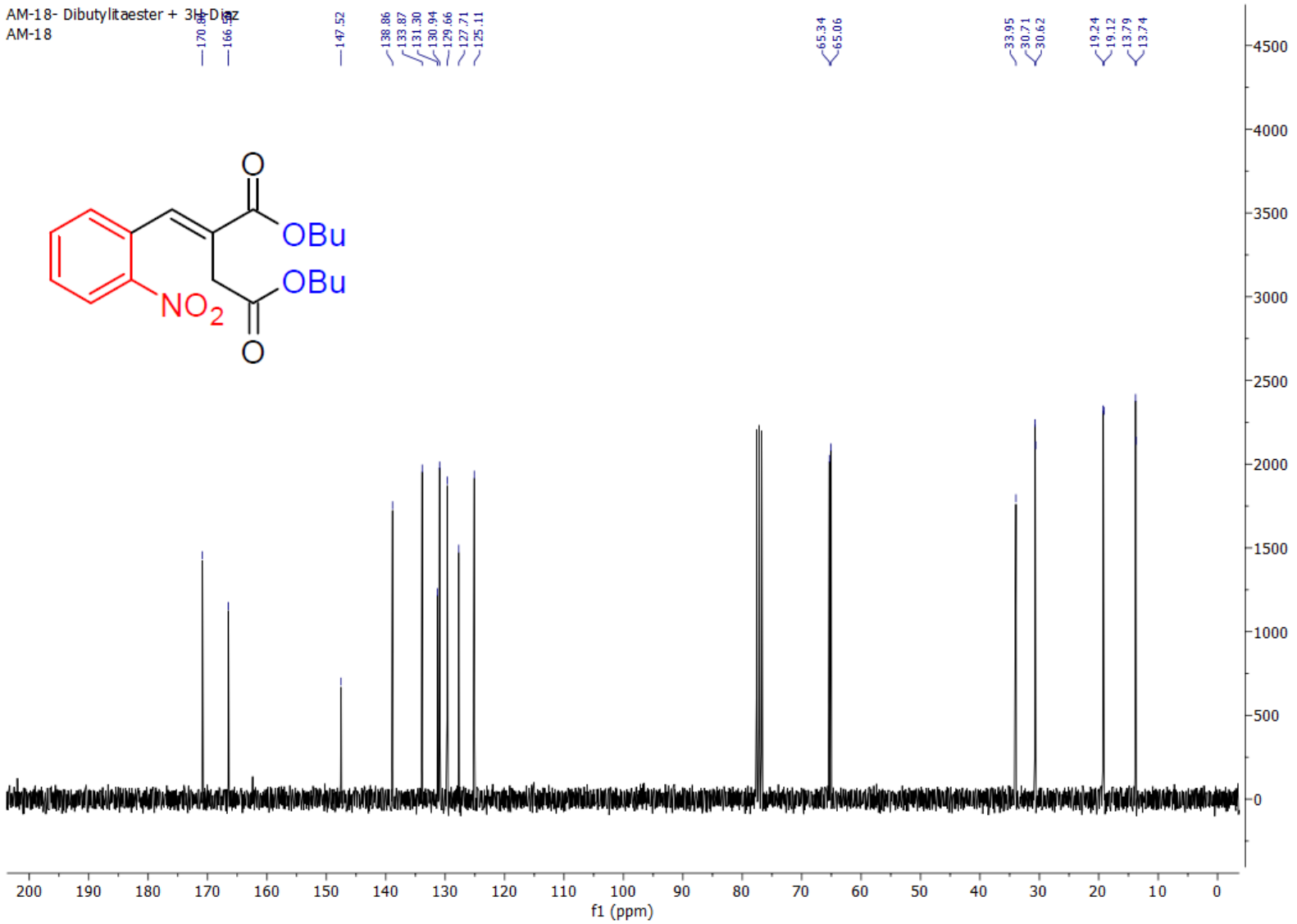

^{1}H NMR (400 MHz, $CDCl_3$) of **5ae**

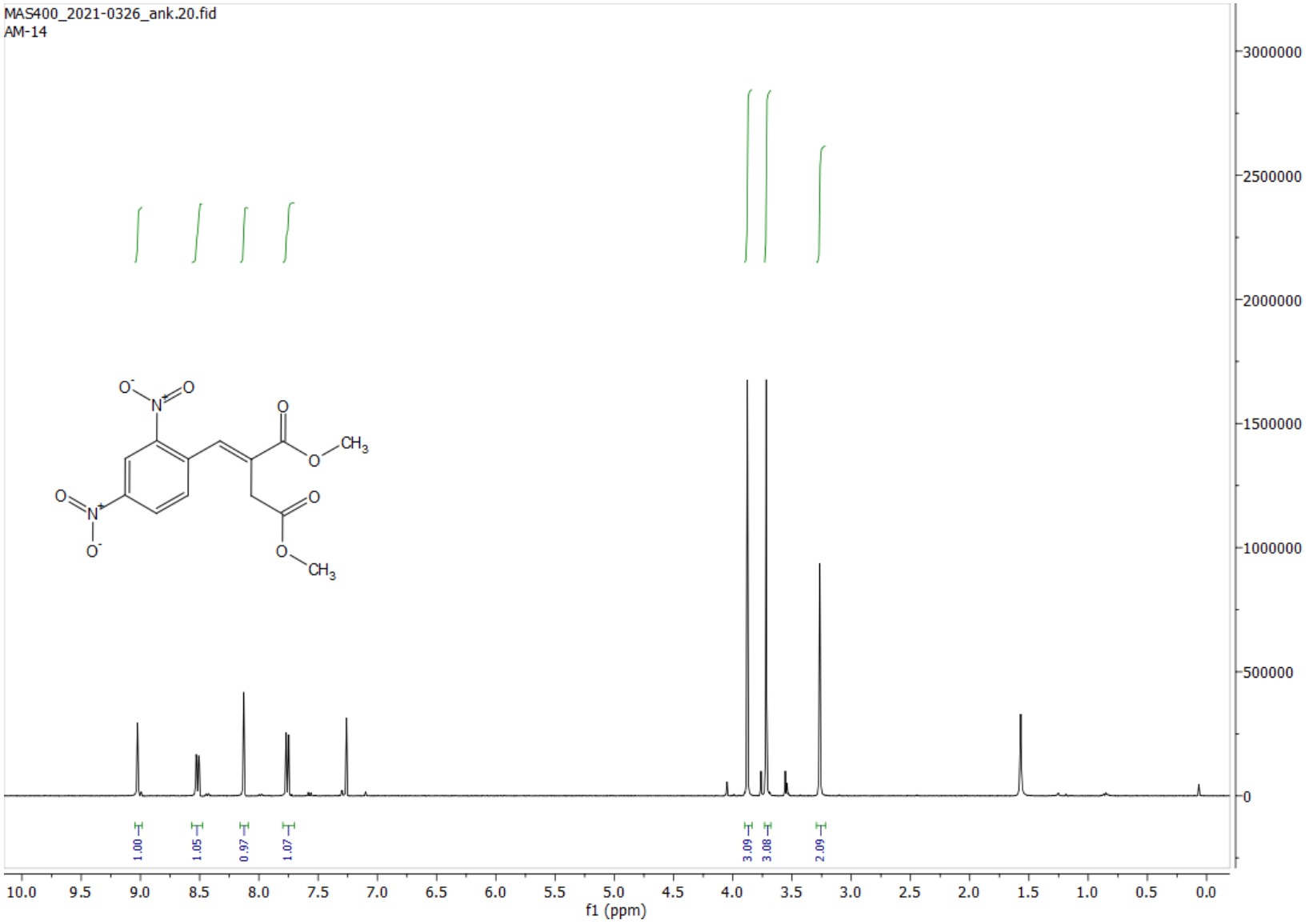

$^{13}C\{^{1}H\}$ NMR (101 MHz, $CDCl_3$) of **5ae**

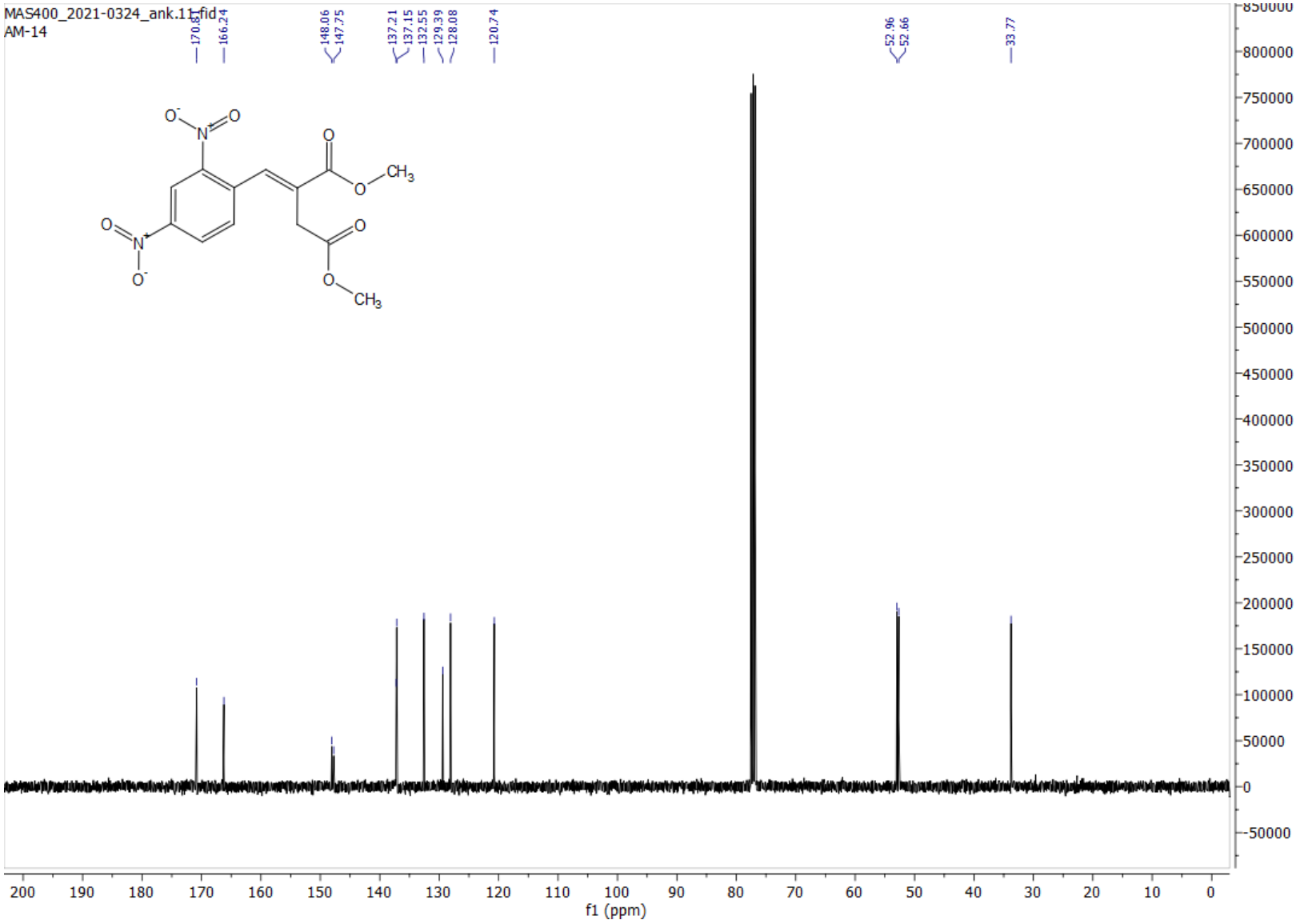

^{1}H NMR (300 MHz, CD_2Cl_2) of **5ce**

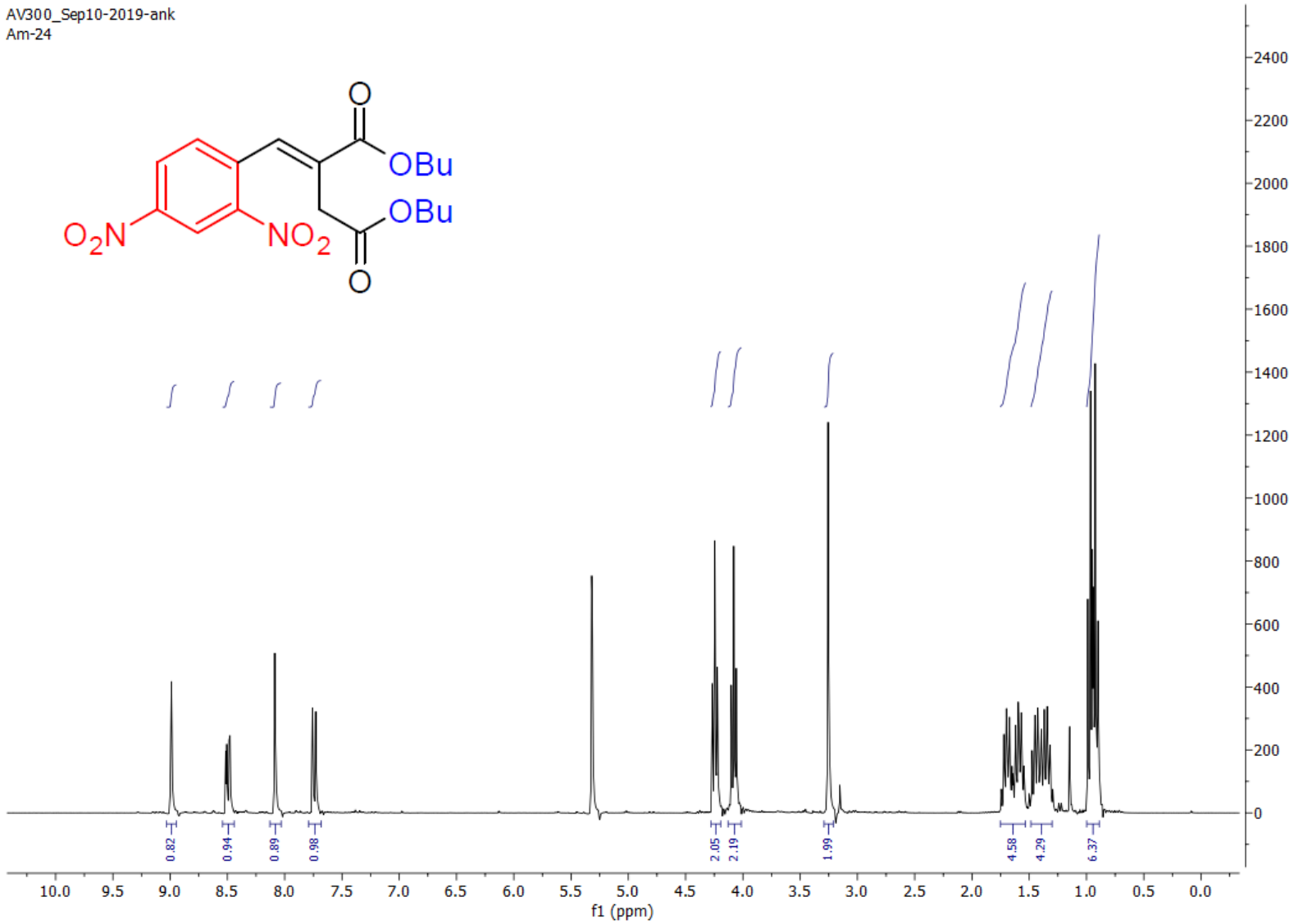

$^{13}C\{^{1}H\}$ NMR (75 MHz, CD_2Cl_2) of **5ce**

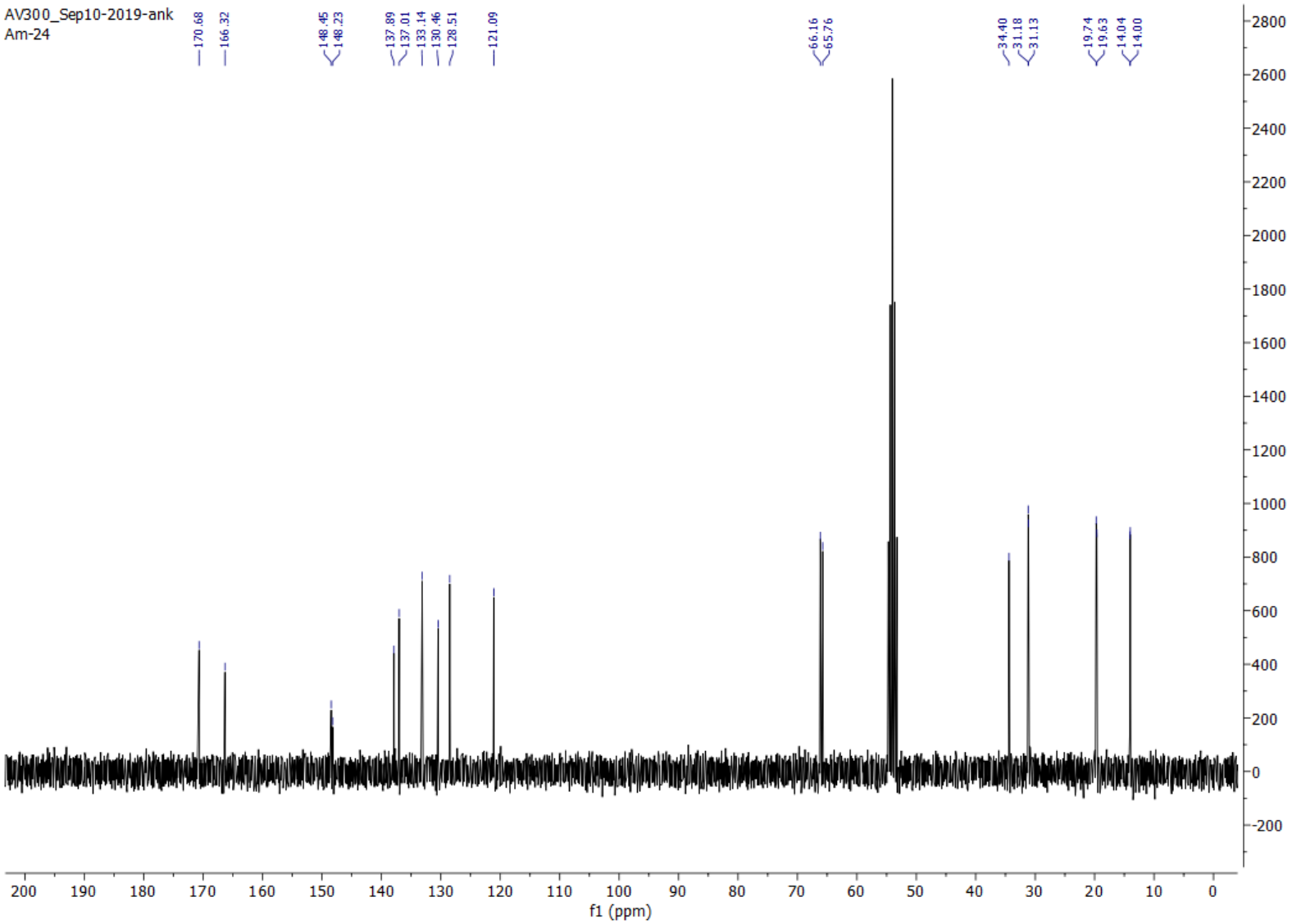

^{1}H NMR (300 MHz, $CDCl_3$) of **5bf**

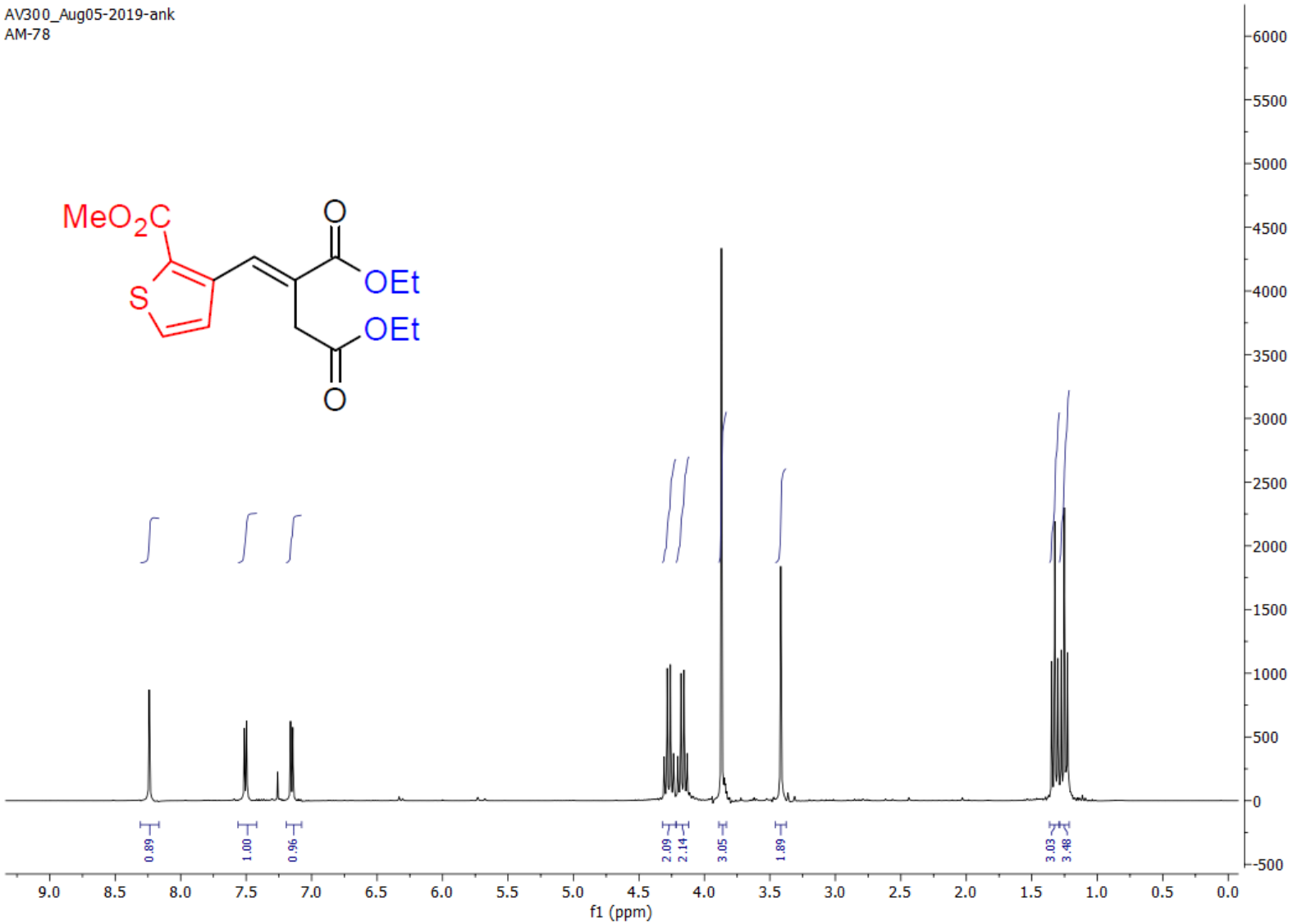

$^{13}C\{^{1}H\}$ NMR (75 MHz, $CDCl_3$) of **5bf**

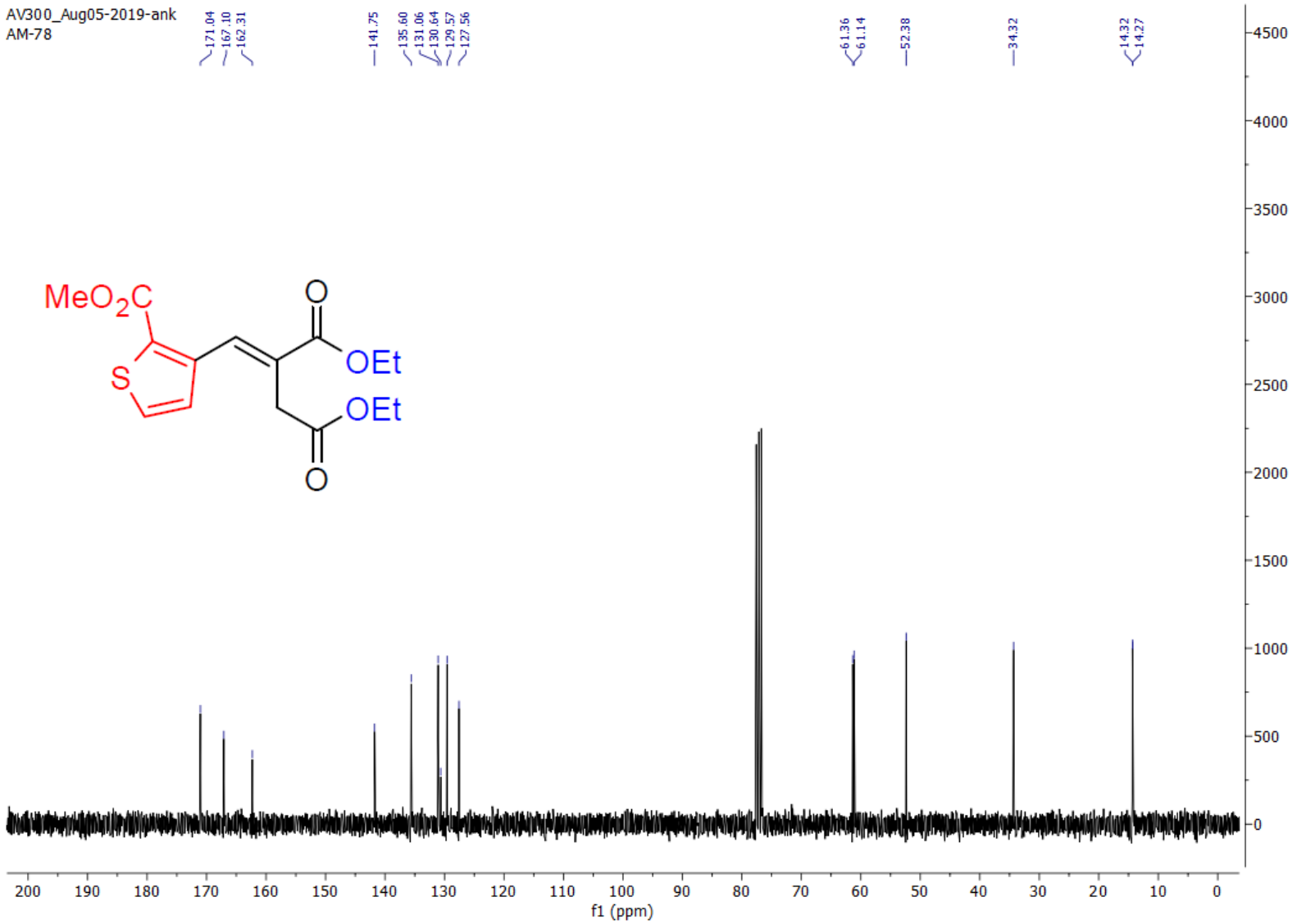

^{1}H NMR (300 MHz, $CDCl_3$) of **5bg**

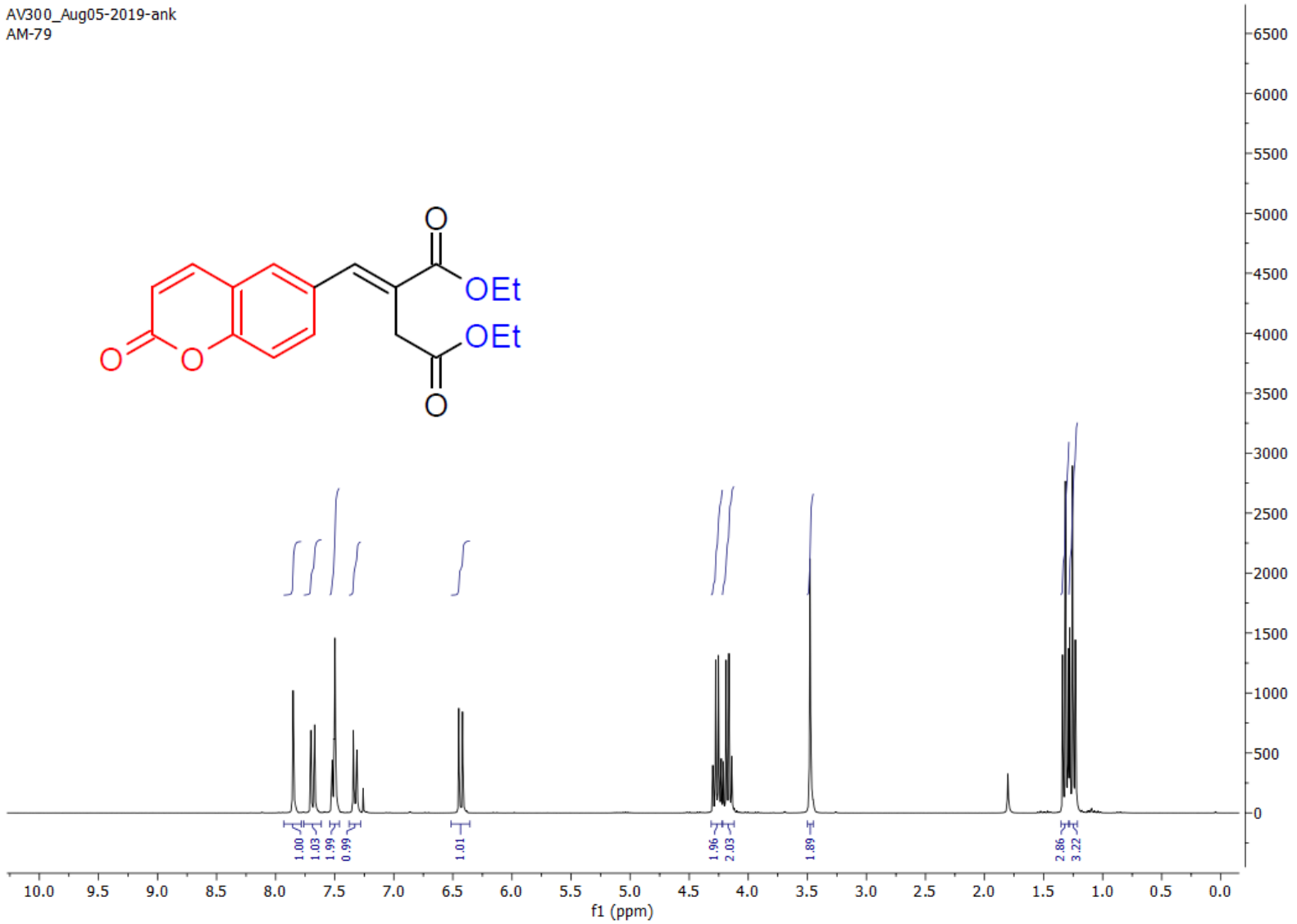

$^{13}C\{^{1}H\}$ NMR (75 MHz, $CDCl_3$) of **5bg**

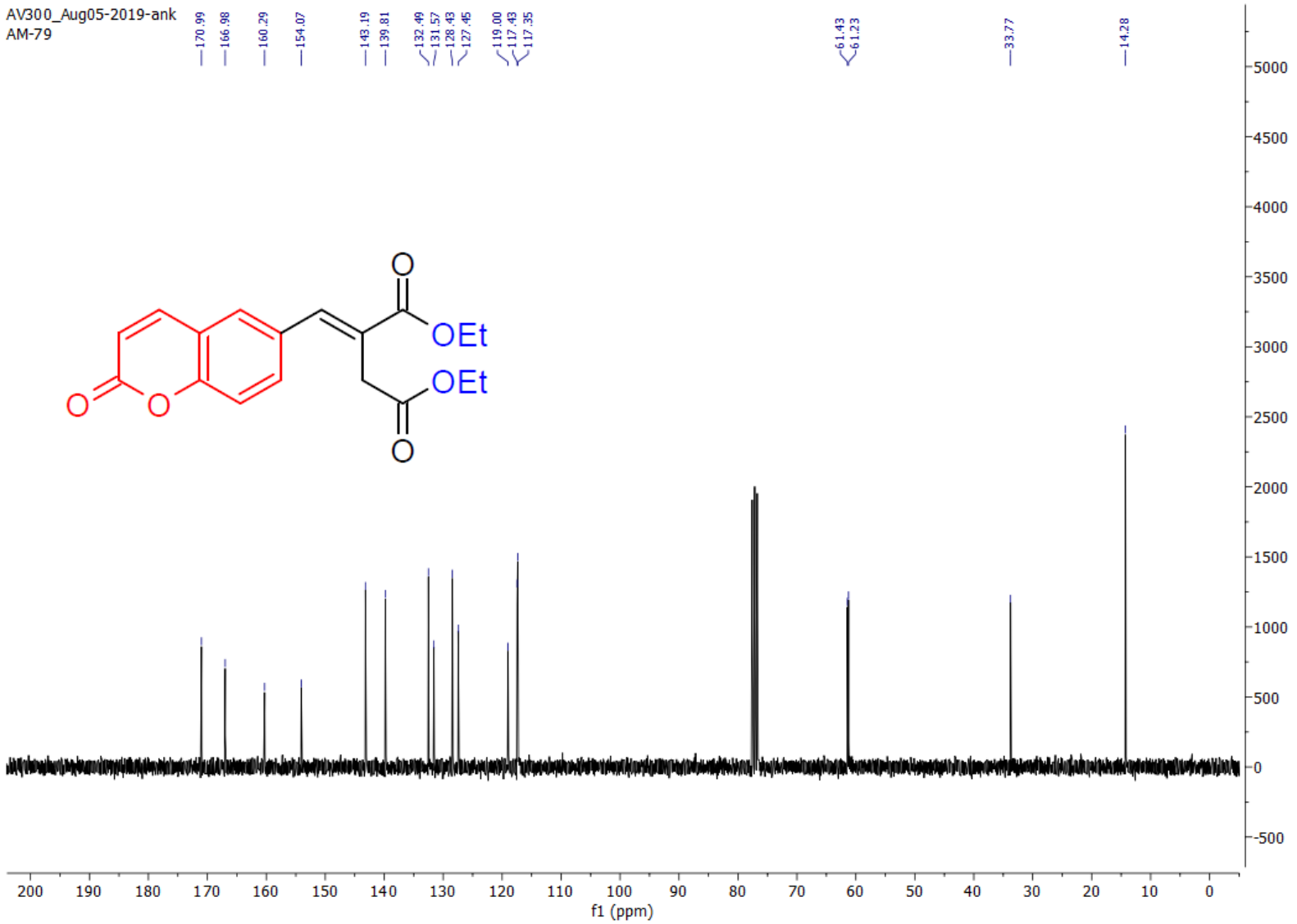

^{1}H NMR (300 MHz, $CDCl_3$) of **5bi**

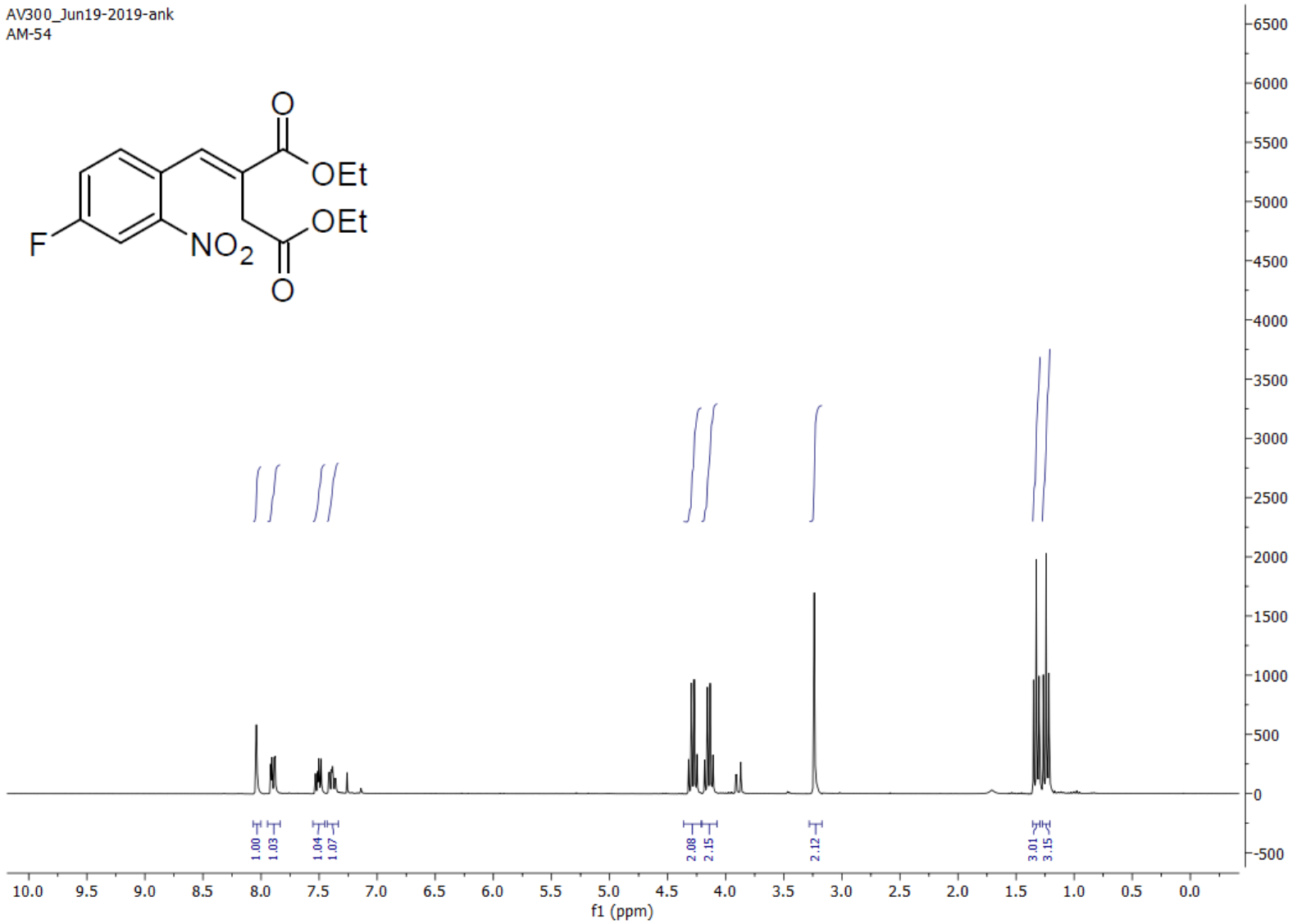

$^{13}C\{^{1}H\}$ NMR (75 MHz, $CDCl_3$) of **5bi**

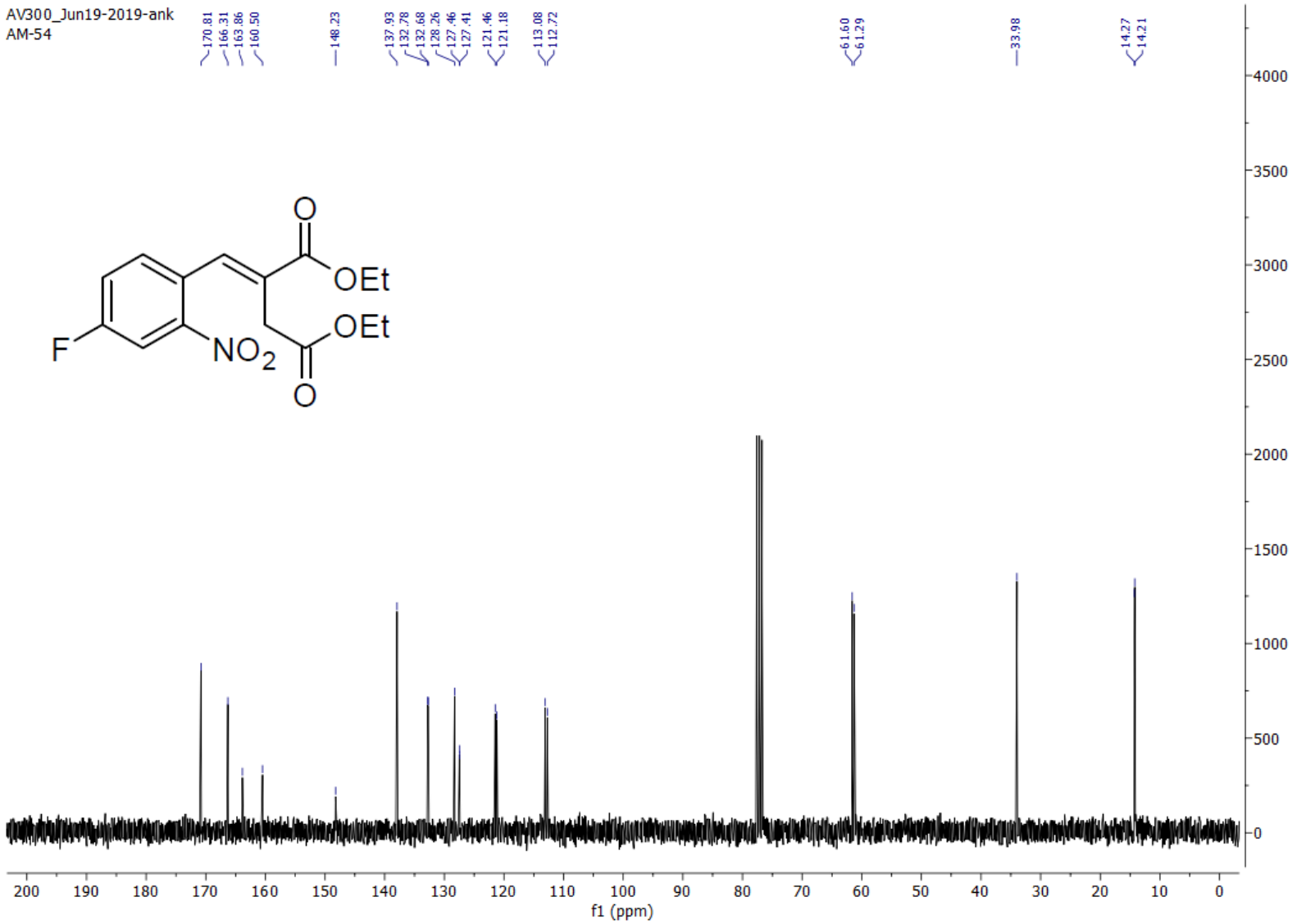

^{1}H NMR (300 MHz, $CDCl_3$) of **5bq**

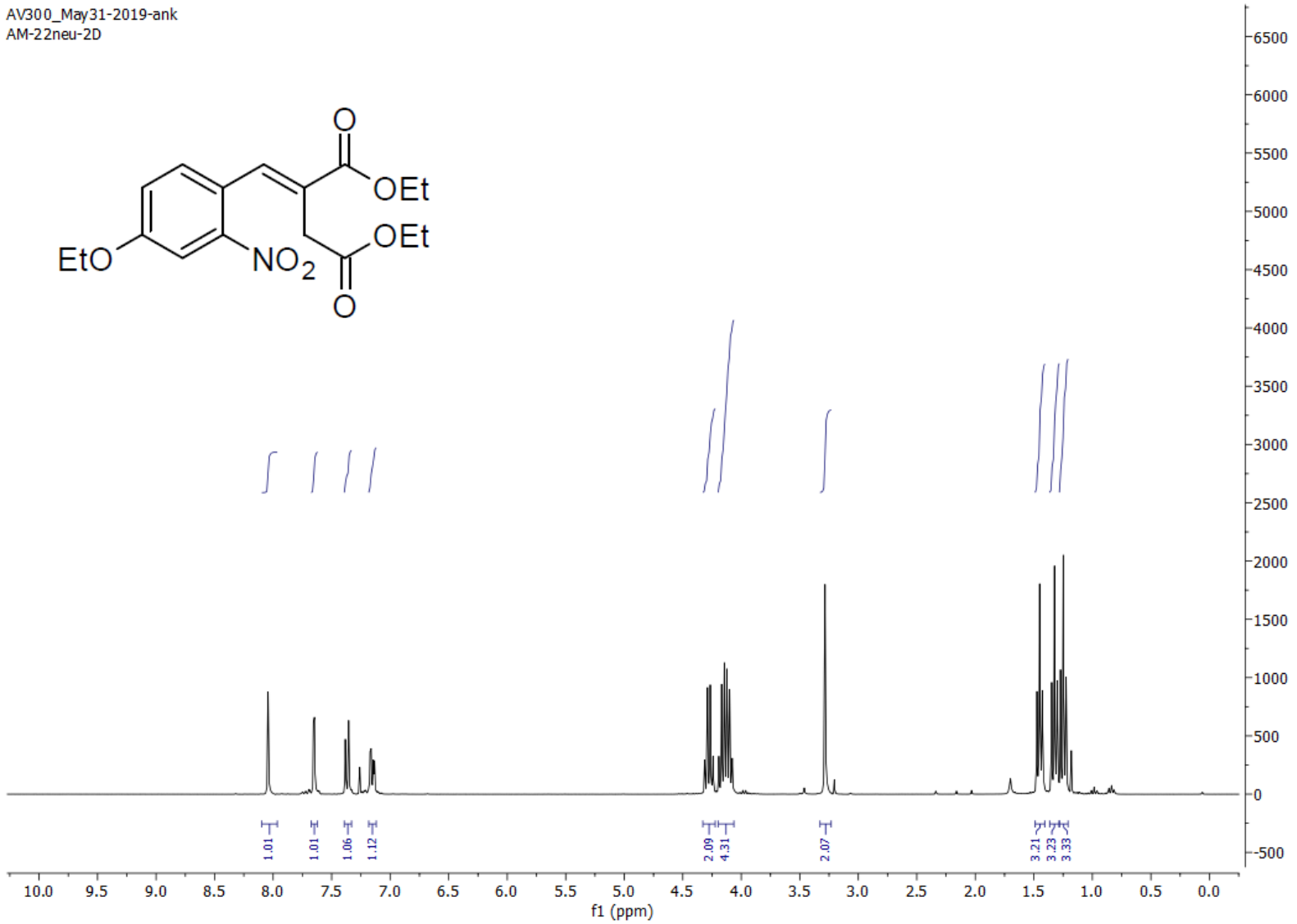

$^{13}C\{^{1}H\}$ NMR (75 MHz, $CDCl_3$) of **5bq**

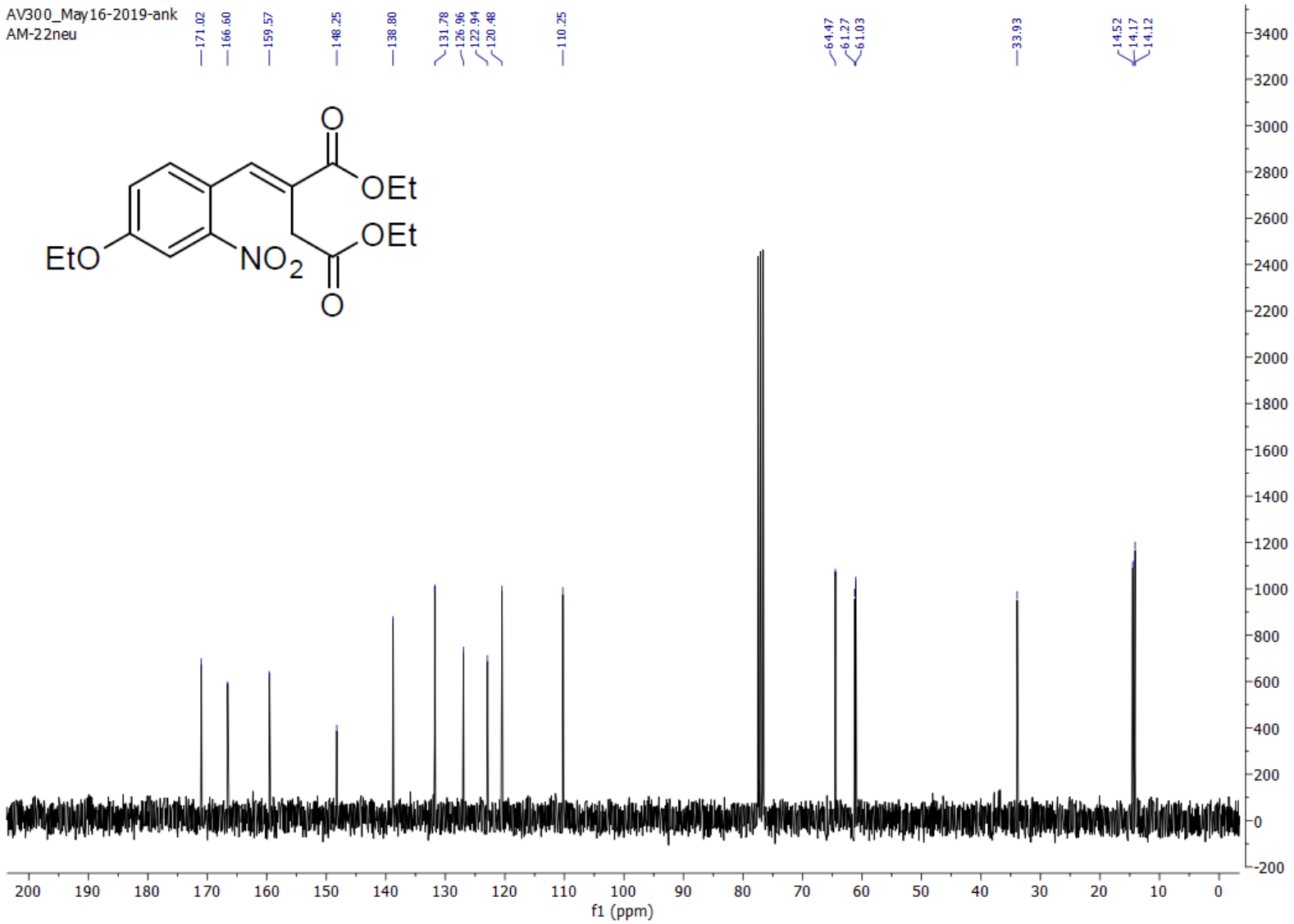

^{1}H NMR (400 MHz, $CDCl_3$) of **5bo**

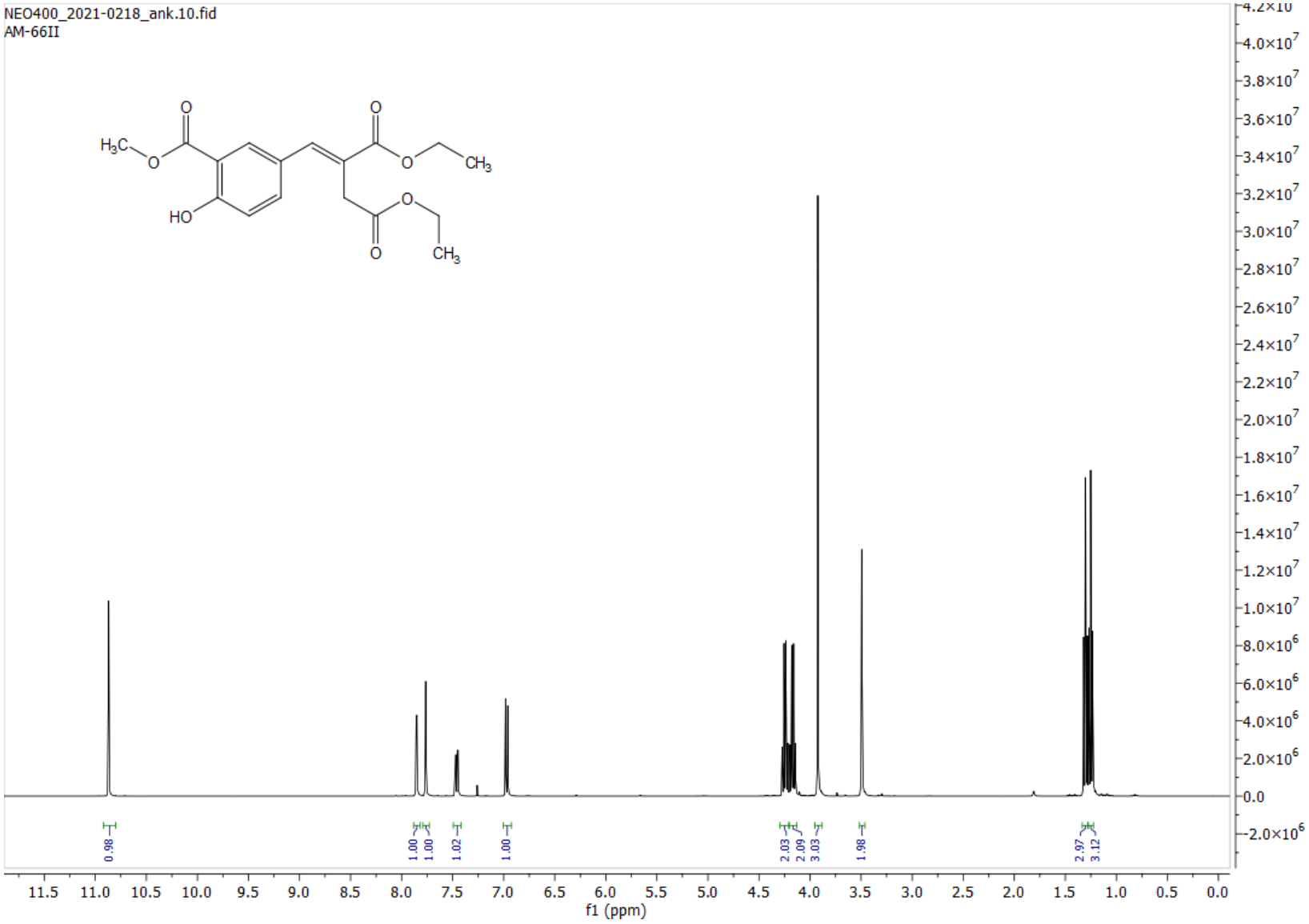

$^{13}C\{^{1}H\}$ NMR (101 MHz, $CDCl_3$) of **5bo**

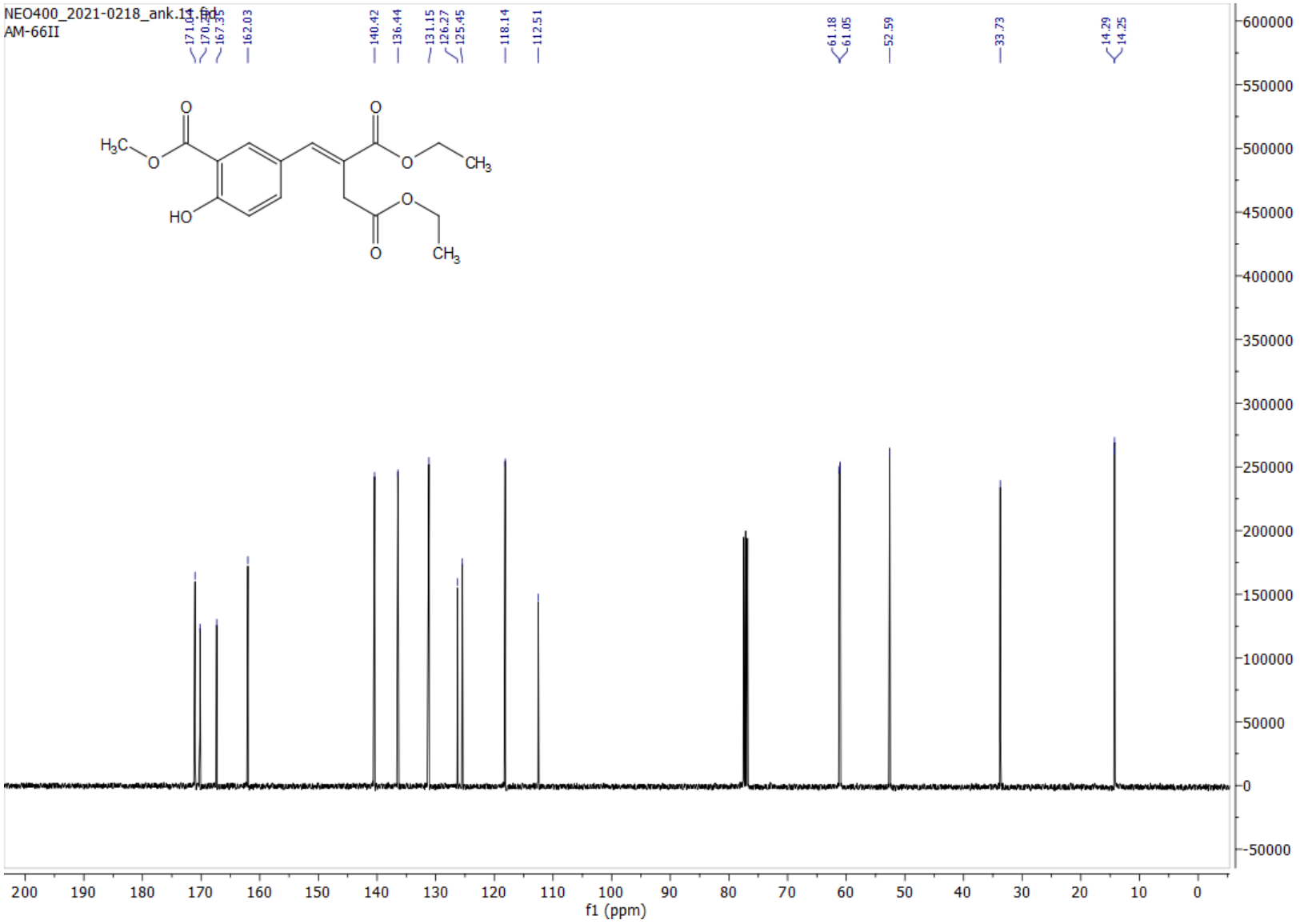

^{1}H NMR (300 MHz, DMSO-d_6) of **6bc**

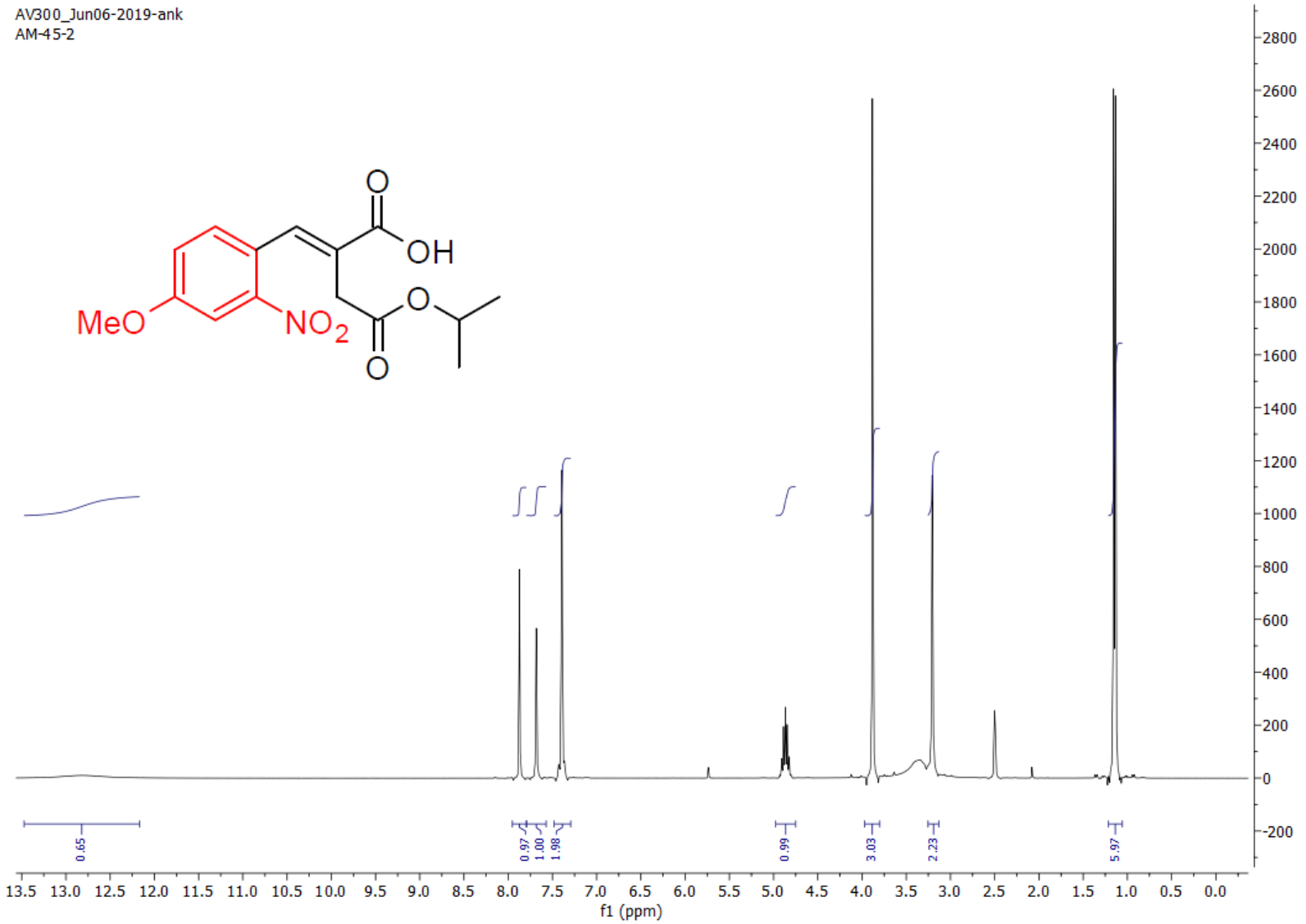

$^{13}C\{^{1}H\}$ NMR (75 MHz, DMSO-d_6) of **6bc**

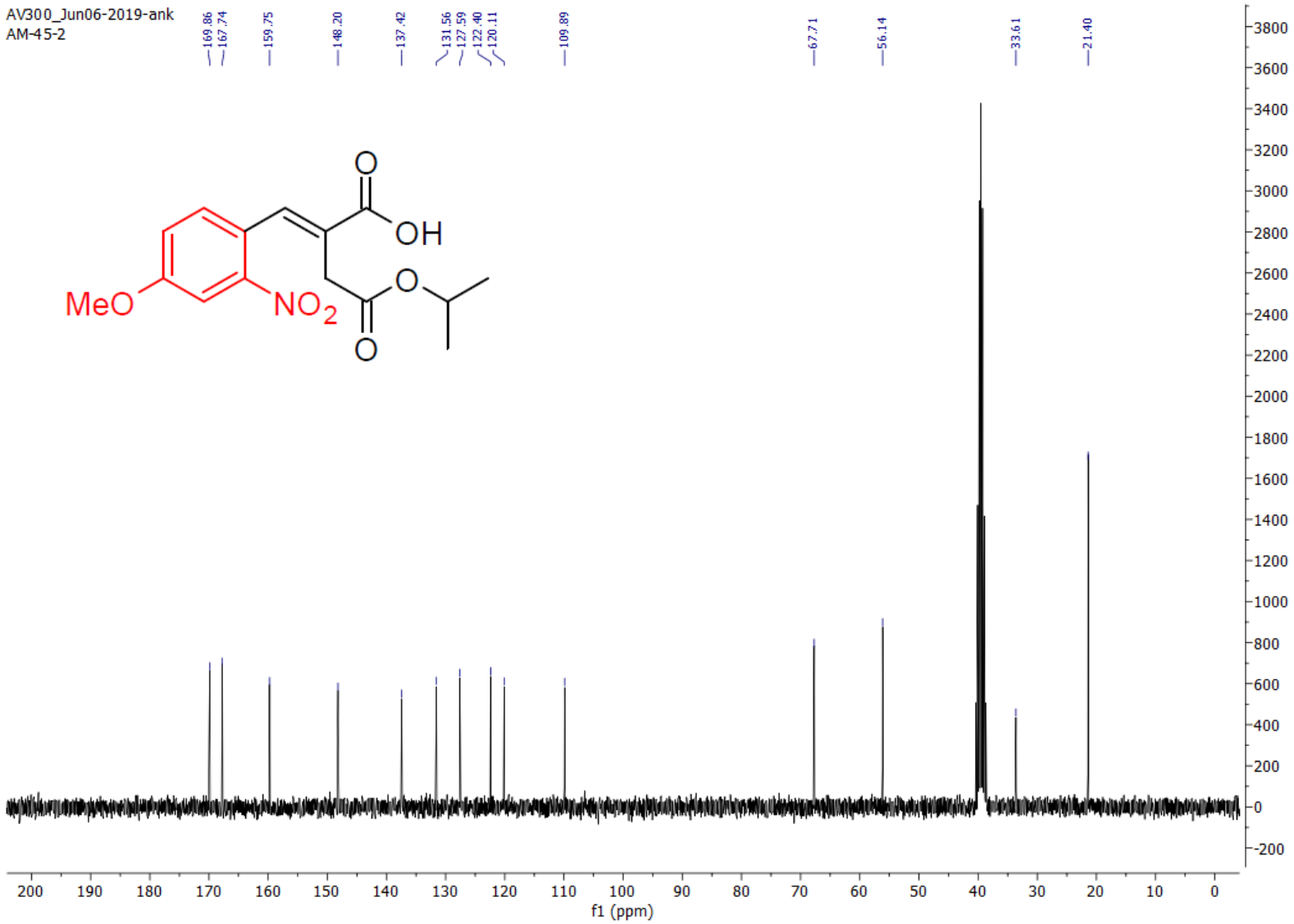

^{1}H NMR (300 MHz, $CDCl_3$) of **6bd**

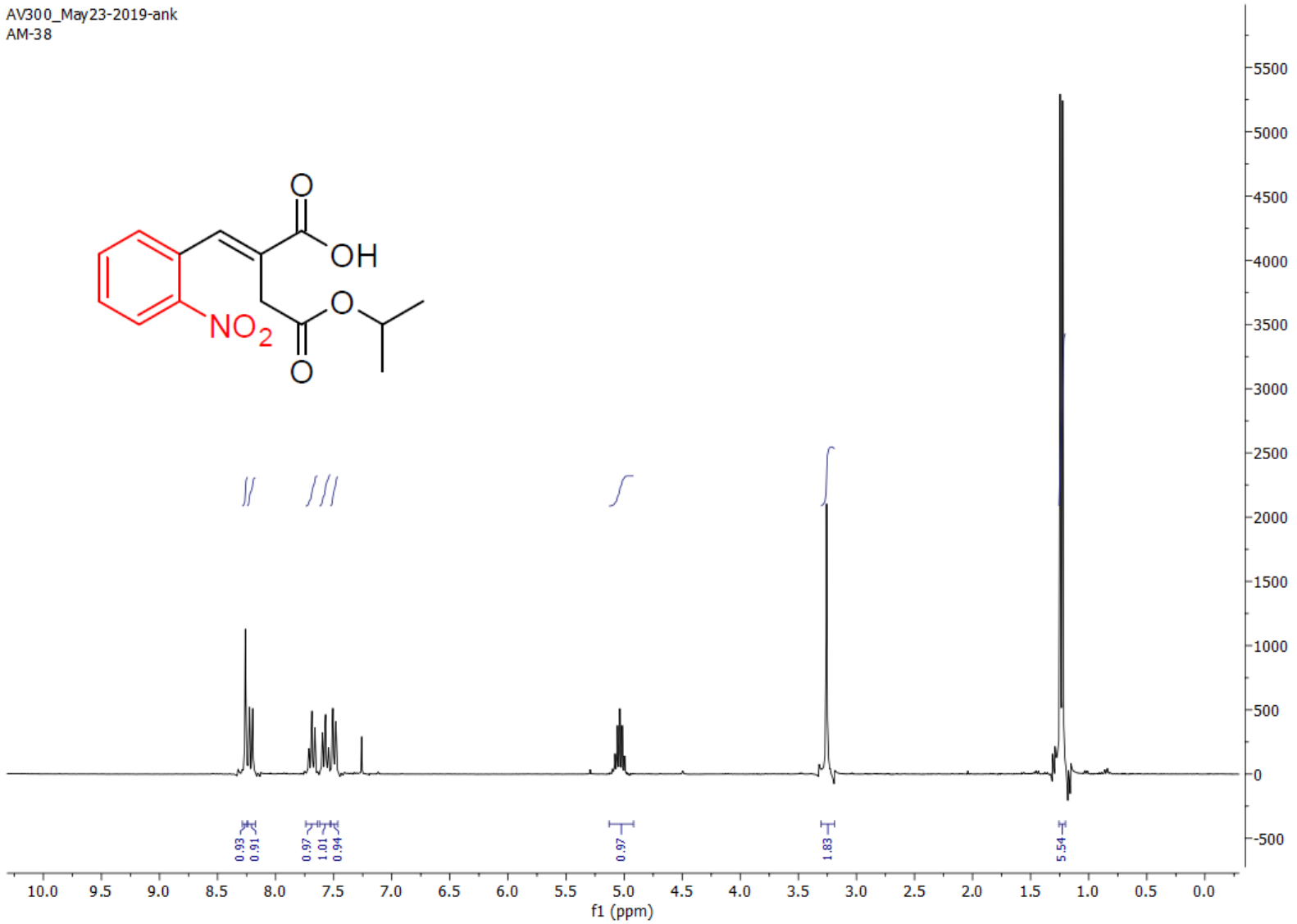

$^{13}C\{^{1}H\}$ NMR (75 MHz, $CDCl_3$) of **6bd**

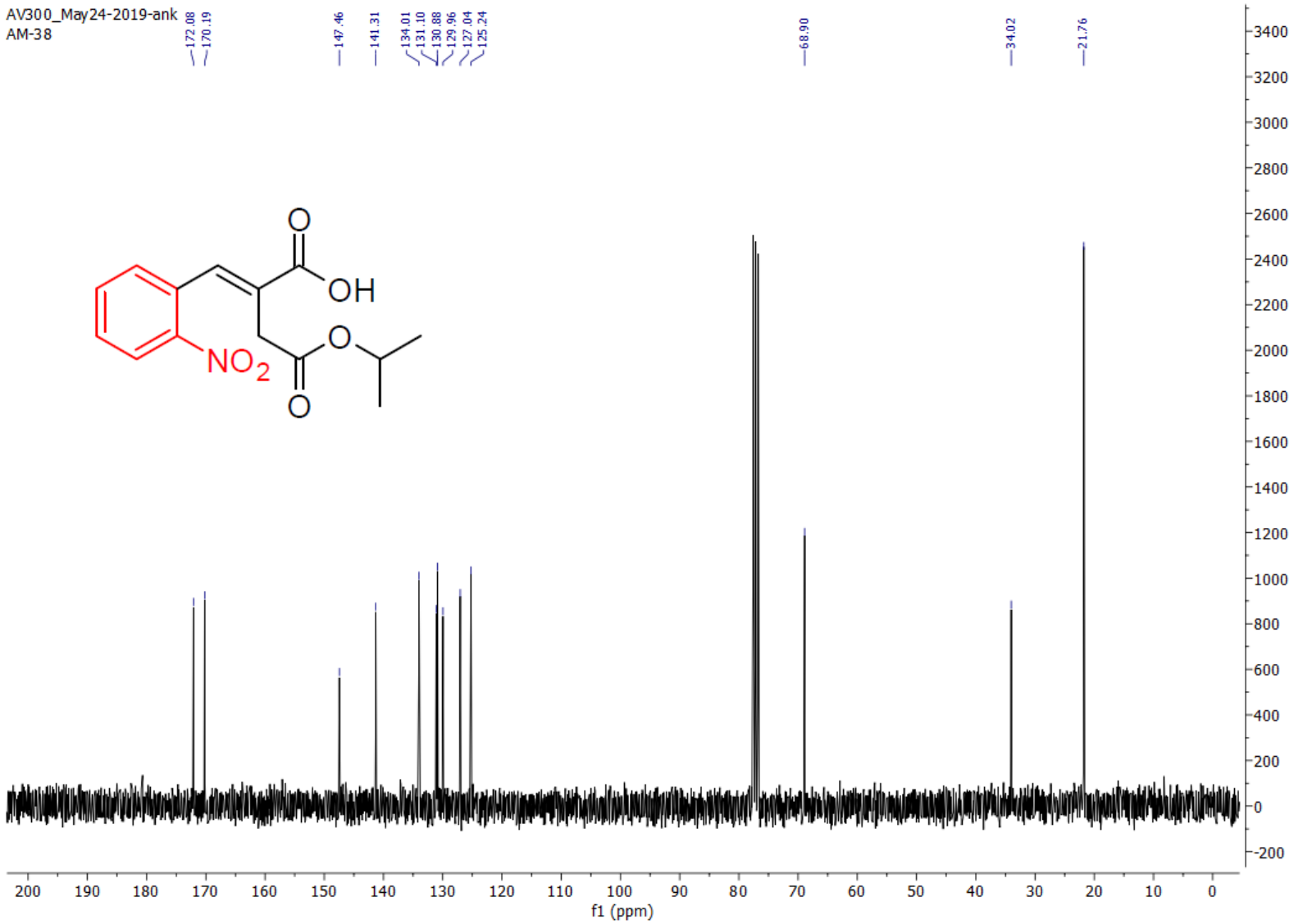

^{1}H NMR (400 MHz, $CDCl_3$) of **6bj**

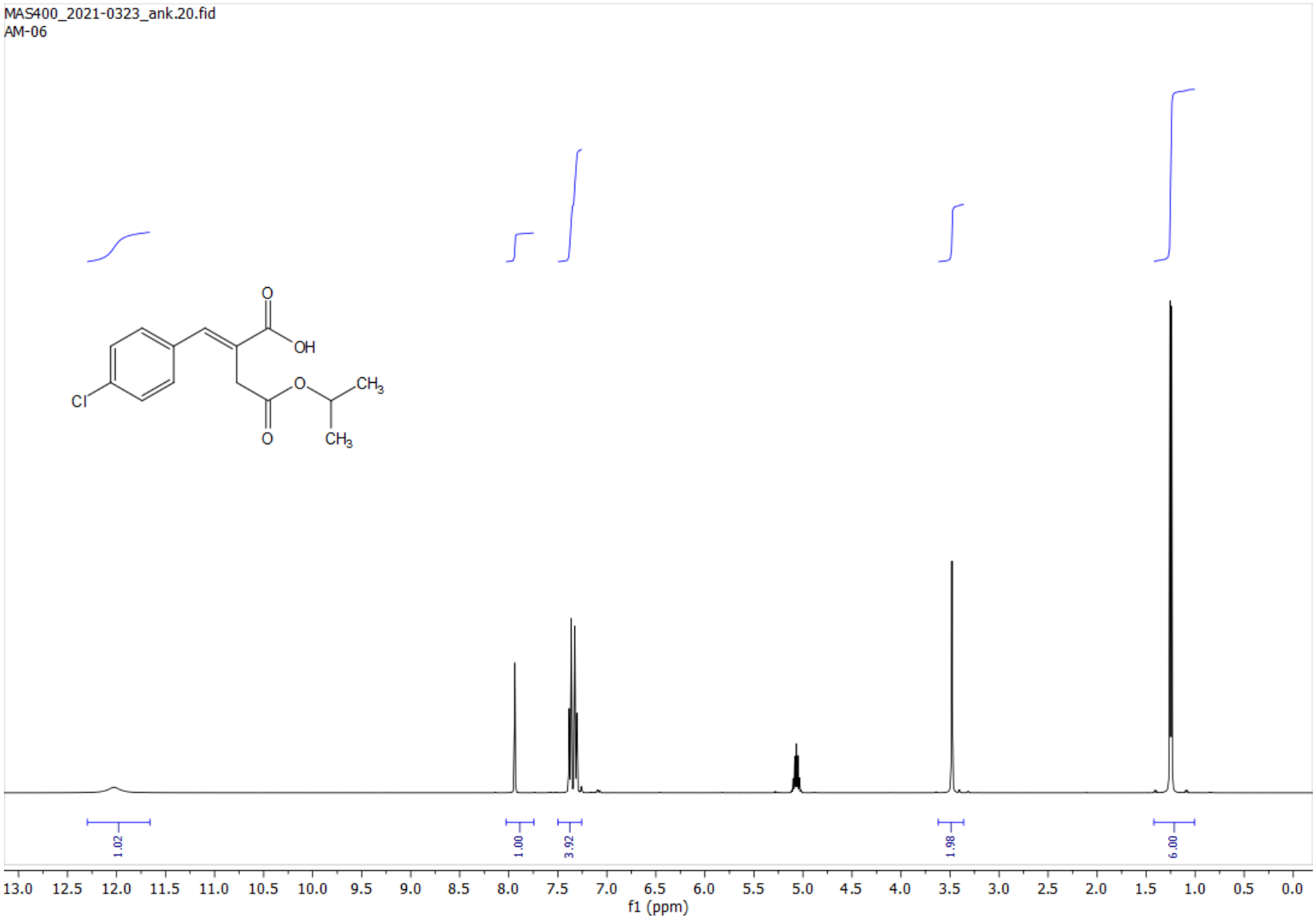

$^{13}C\{^{1}H\}$ NMR (101 MHz, $CDCl_3$) of **6bj**

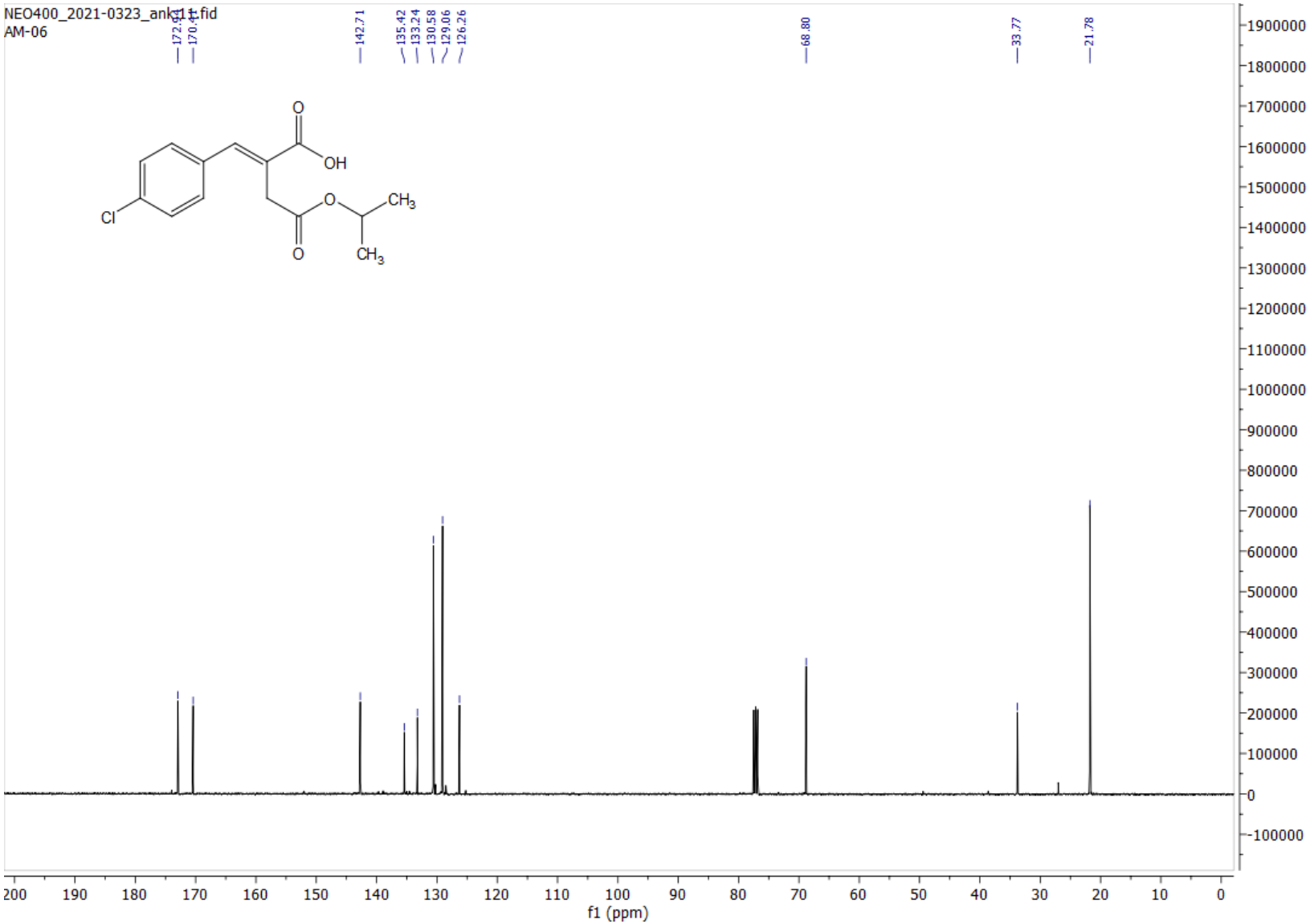

^{1}H NMR (400 MHz, $CDCl_3$) of **6bk**

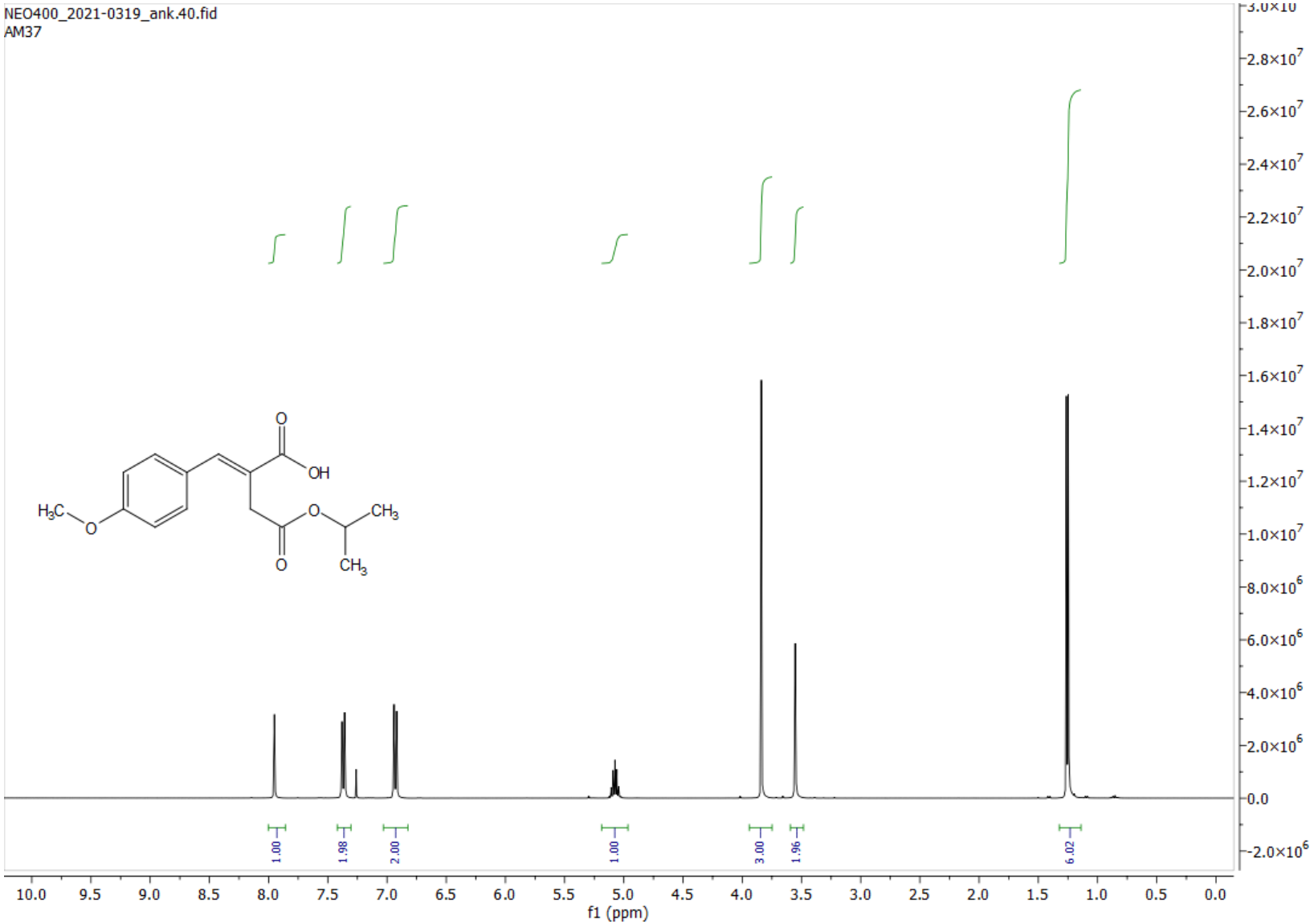

$^{13}C\{^{1}H\}$ NMR (101 MHz, $CDCl_3$) of **6bk**

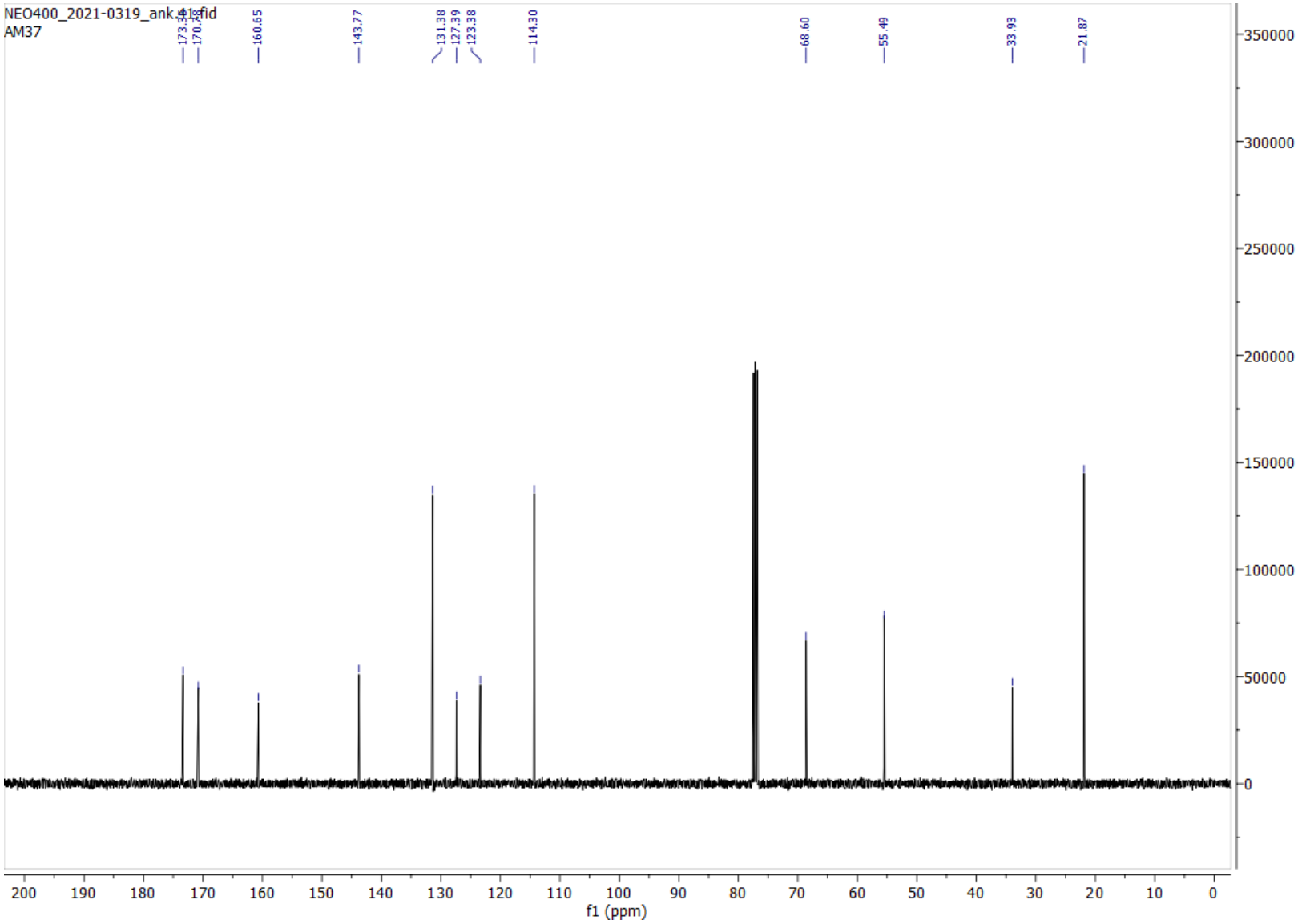

^{1}H NMR (300 MHz, $CDCl_3$) of **6bl**

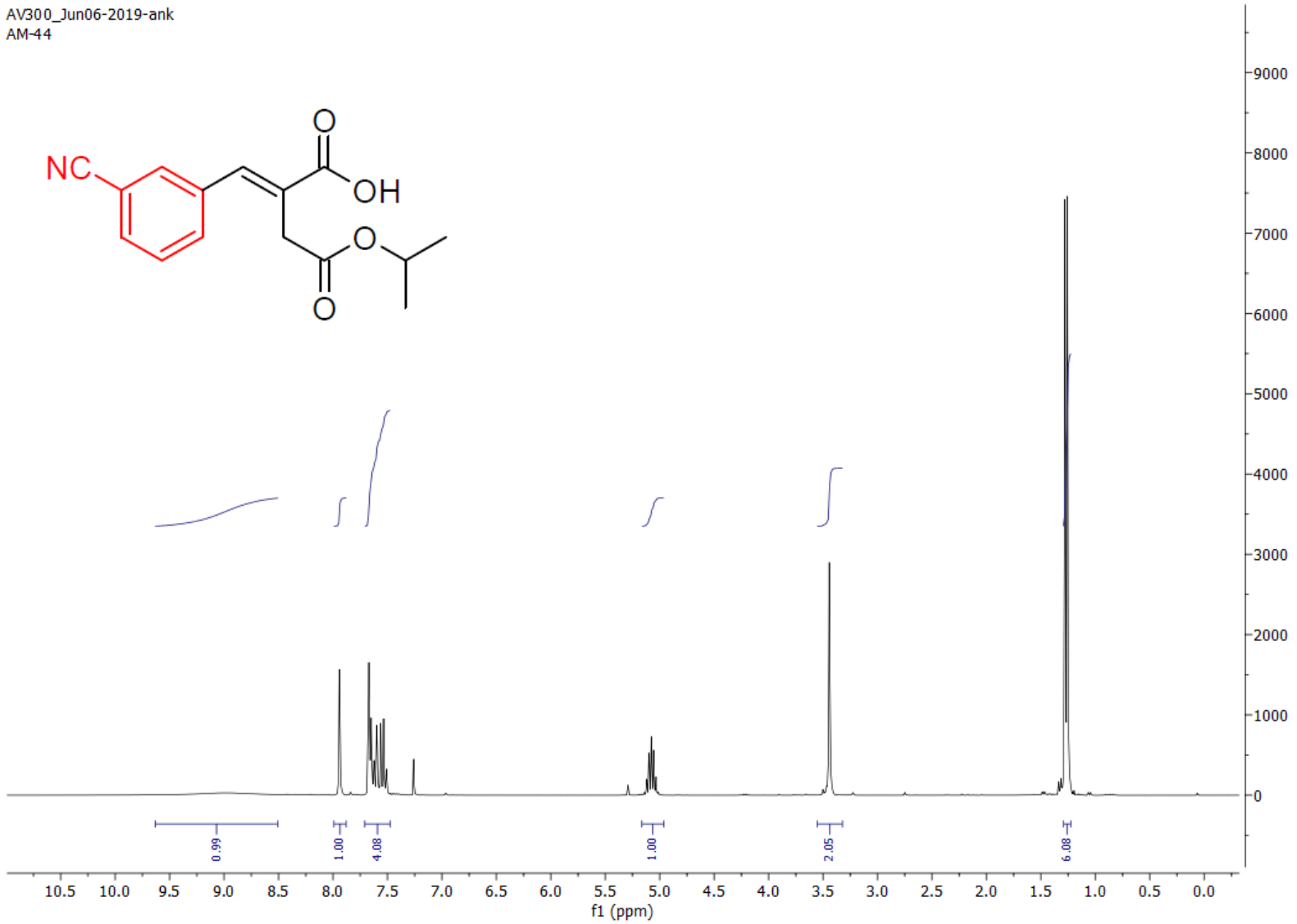

$^{13}C\{^{1}H\}$ NMR (75 MHz, $CDCl_3$) of **6bl**

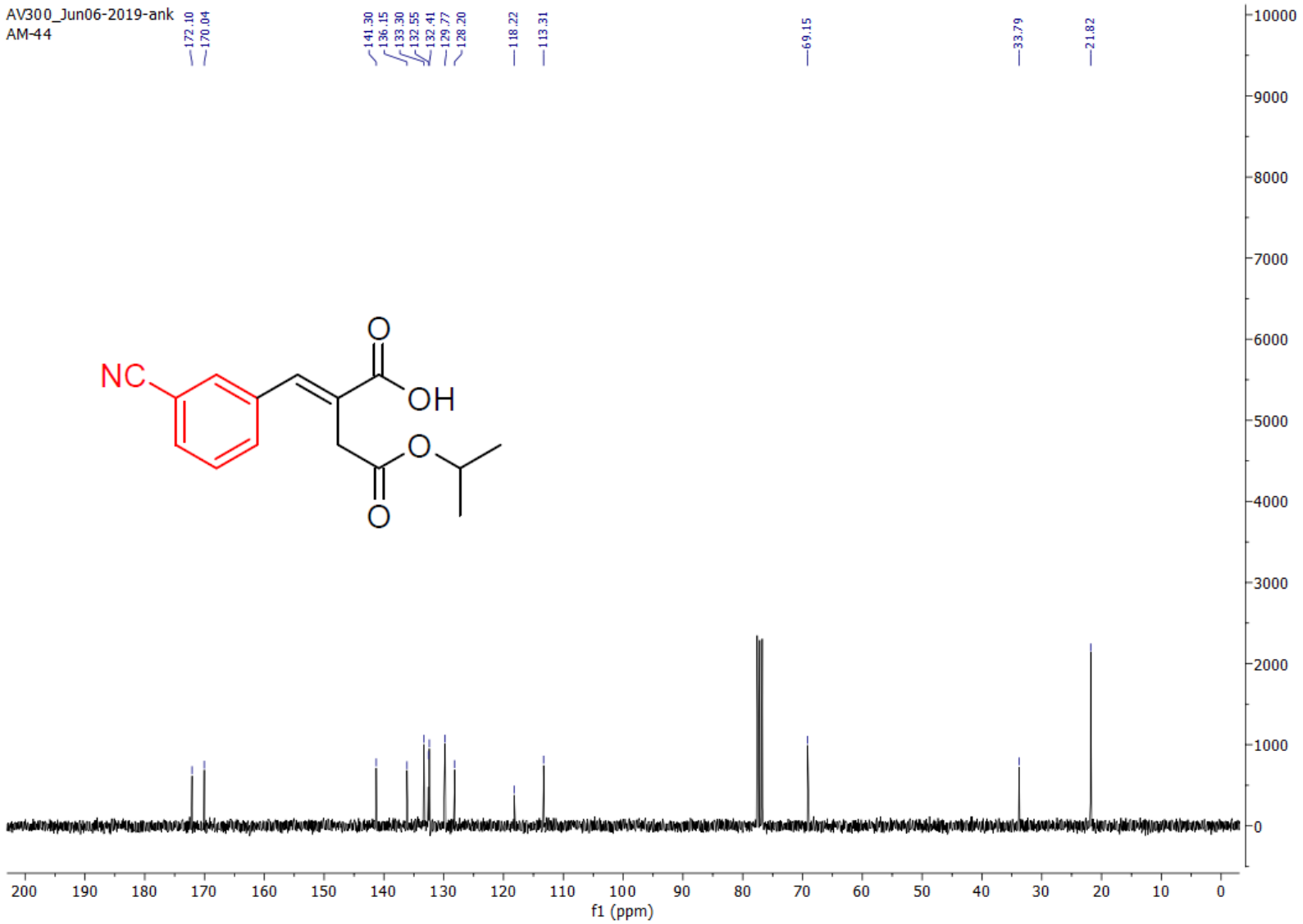

^{1}H NMR (300 MHz, $CDCl_3$) of **6bm**

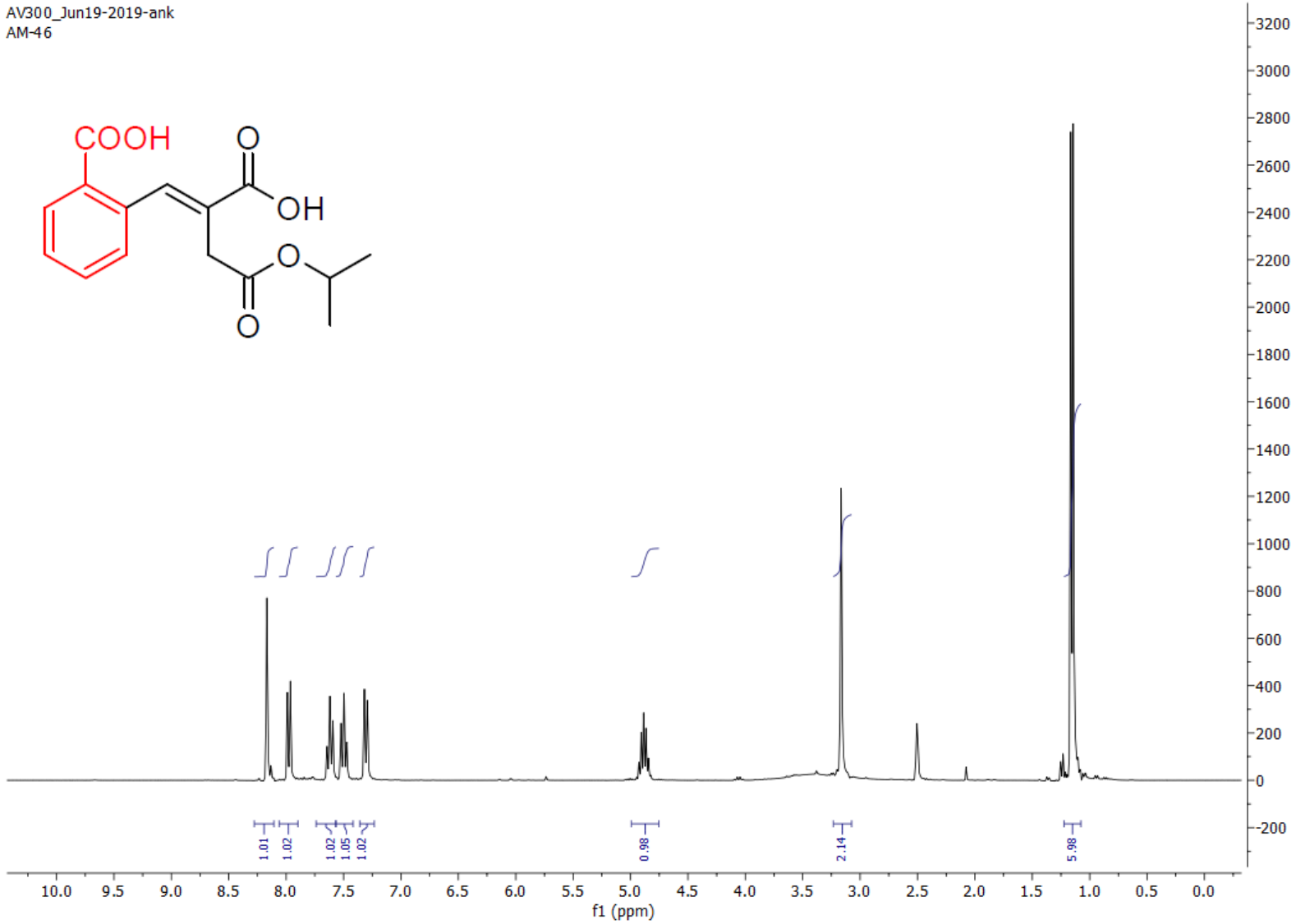

$^{13}C\{^{1}H\}$ NMR (75 MHz, $CDCl_3$) of **6bm**

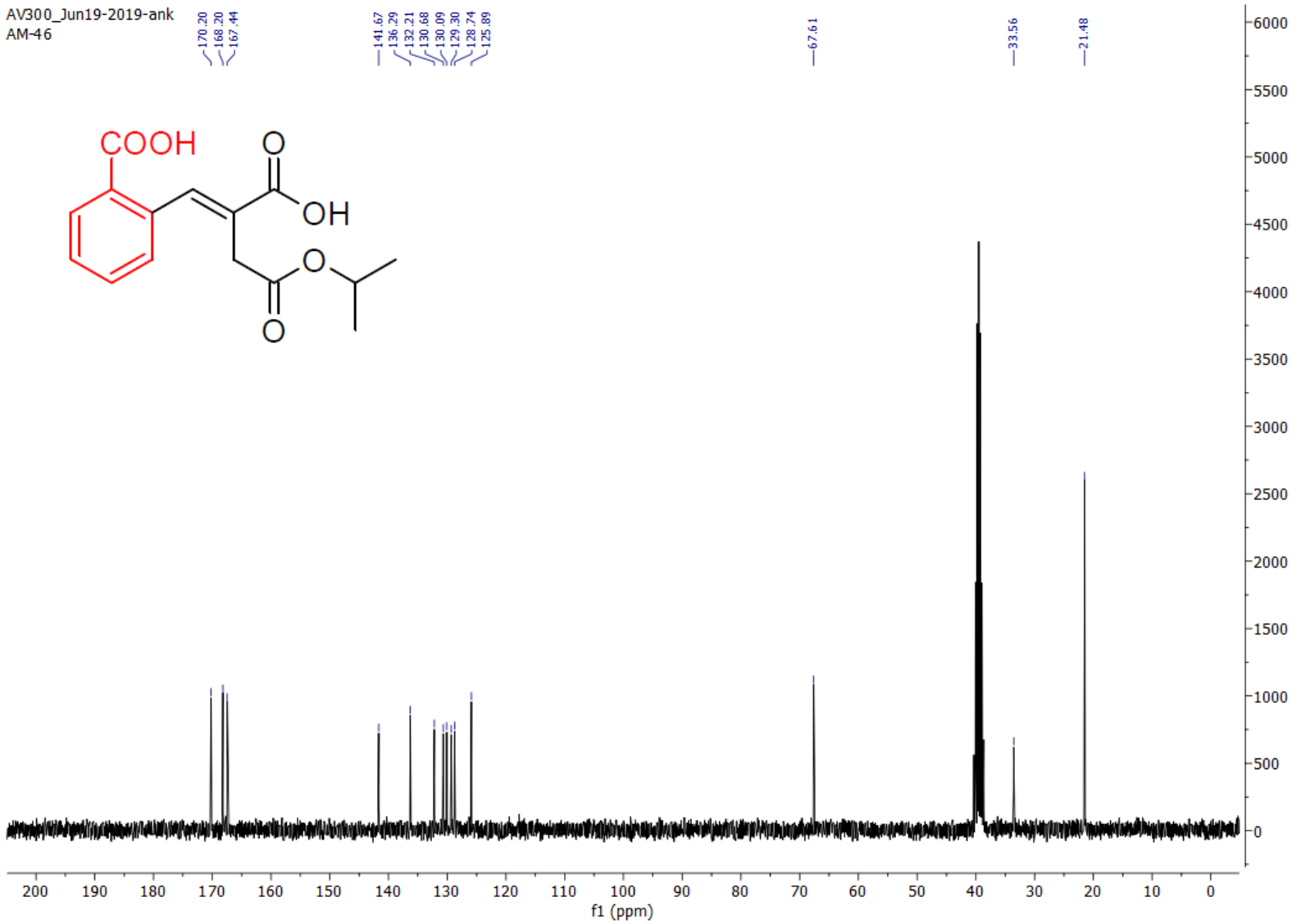

^{1}H NMR (300 MHz, $CDCl_3$) of **6bn**

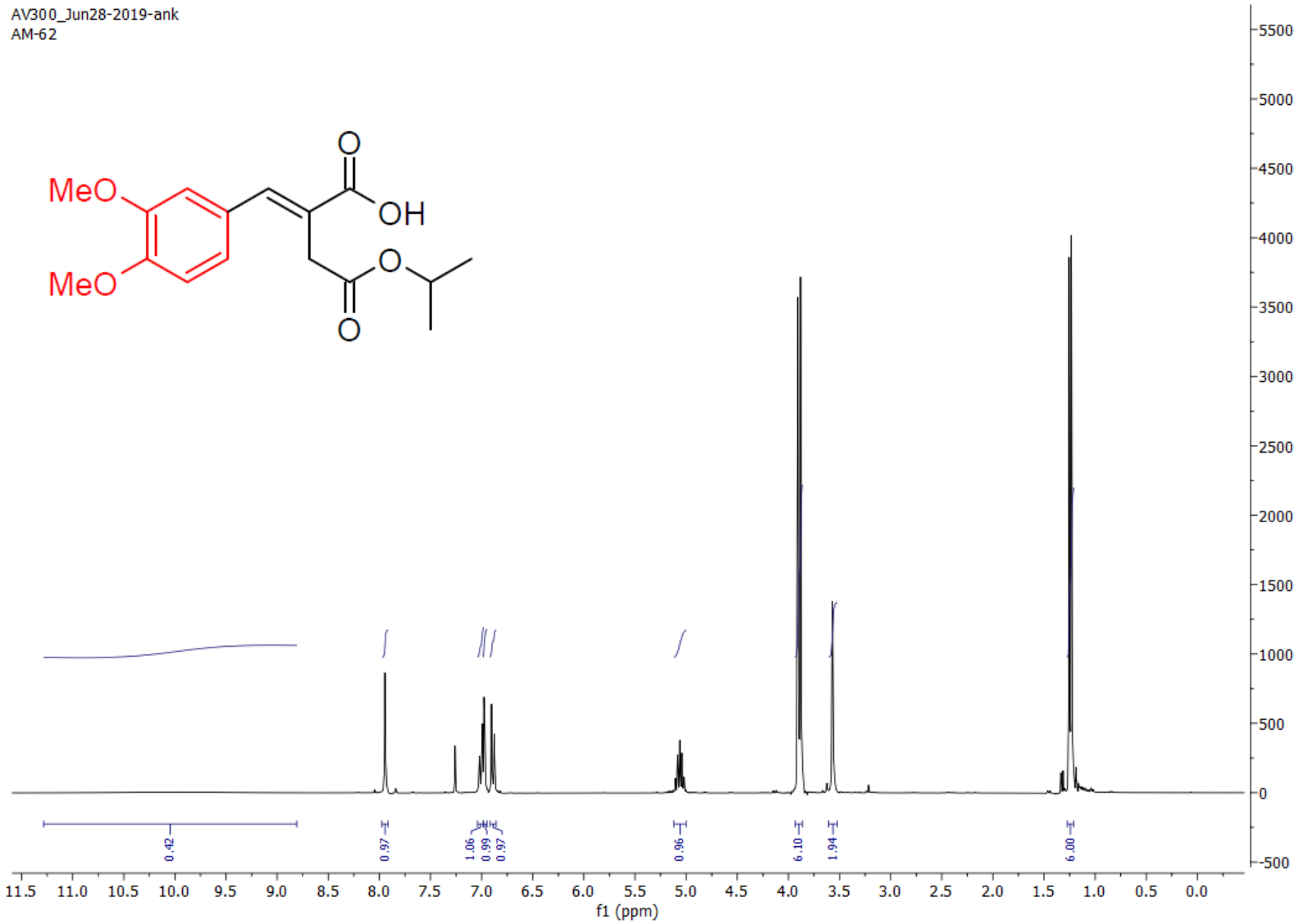

$^{13}C\{^{1}H\}$ NMR (75 MHz, $CDCl_3$) of **6bn**

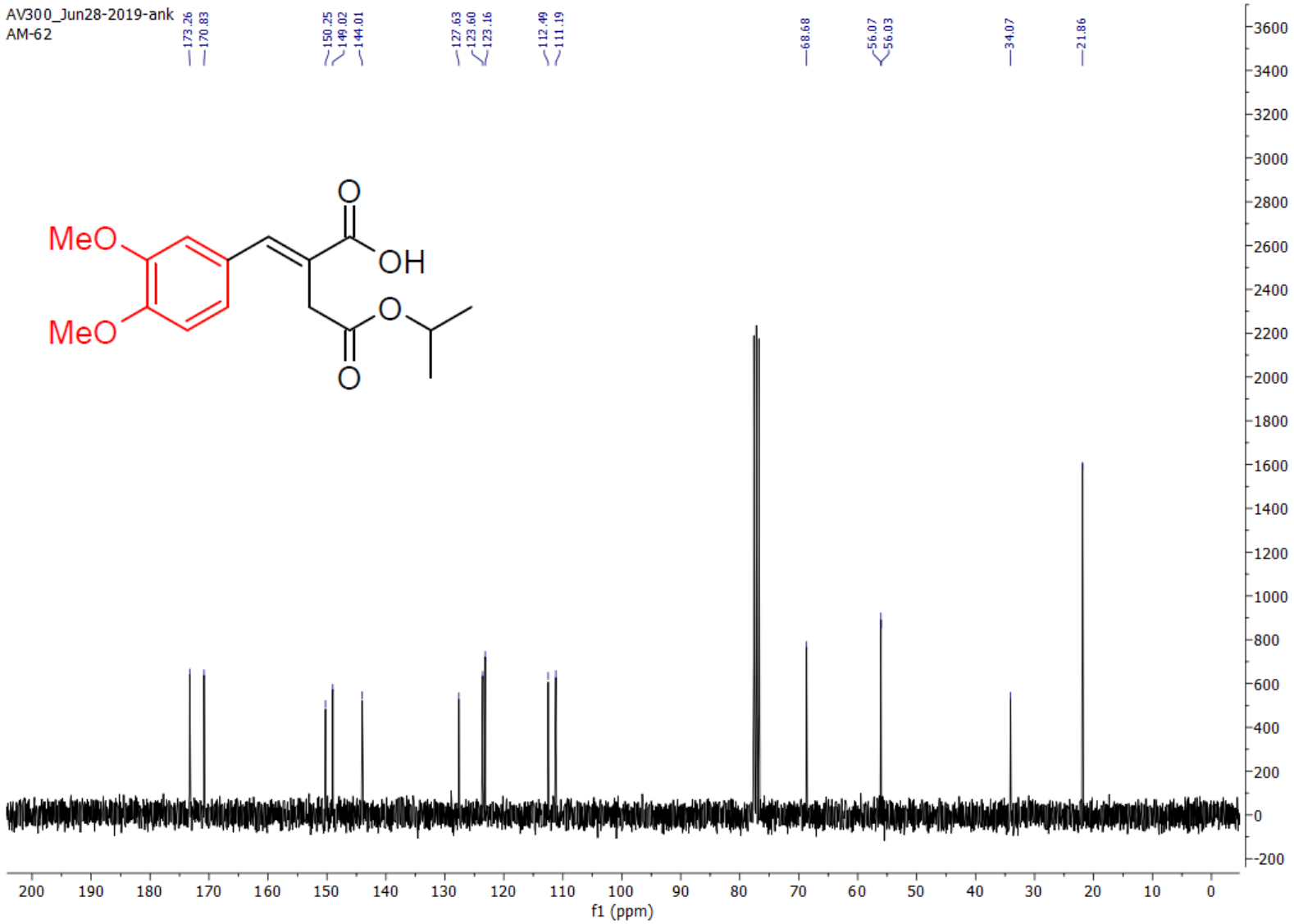

^{1}H NMR (300 MHz, acetone-d_6) of **6cn**

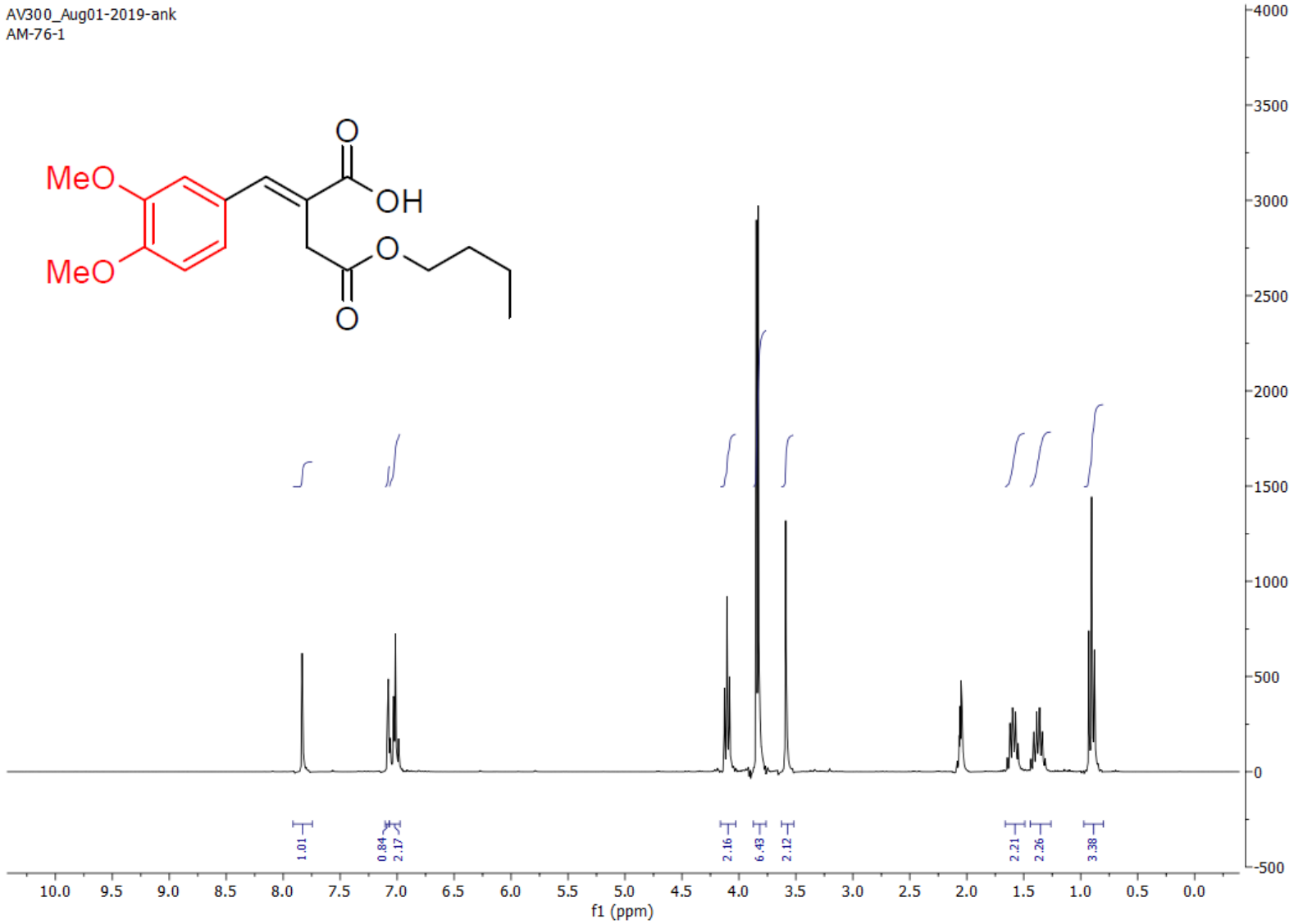

$^{13}C\{^{1}H\}$ NMR (75 MHz, acetone-d_6) of **6cn**

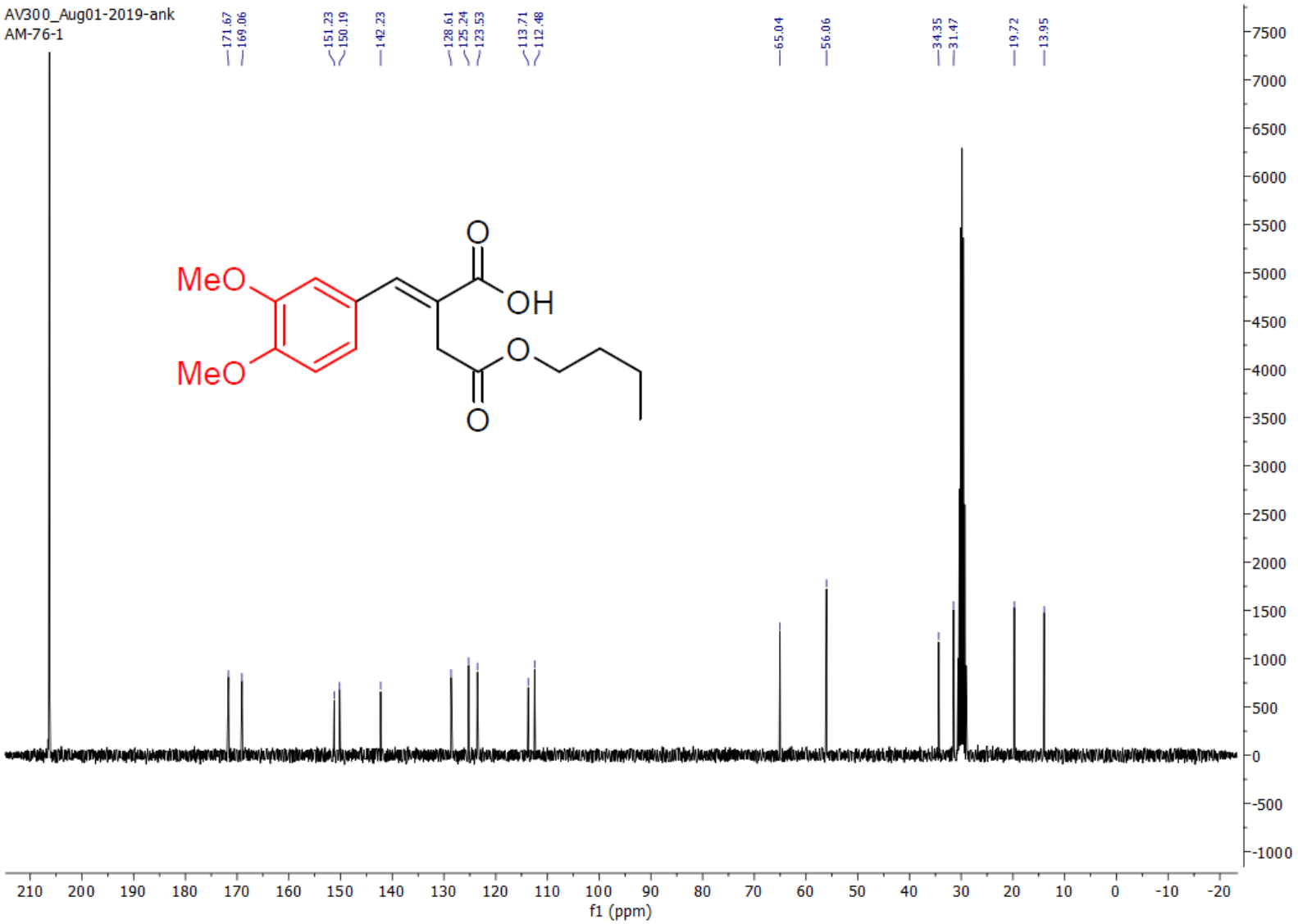

^{1}H NMR (400 MHz, $CDCl_3$) of **6ap**

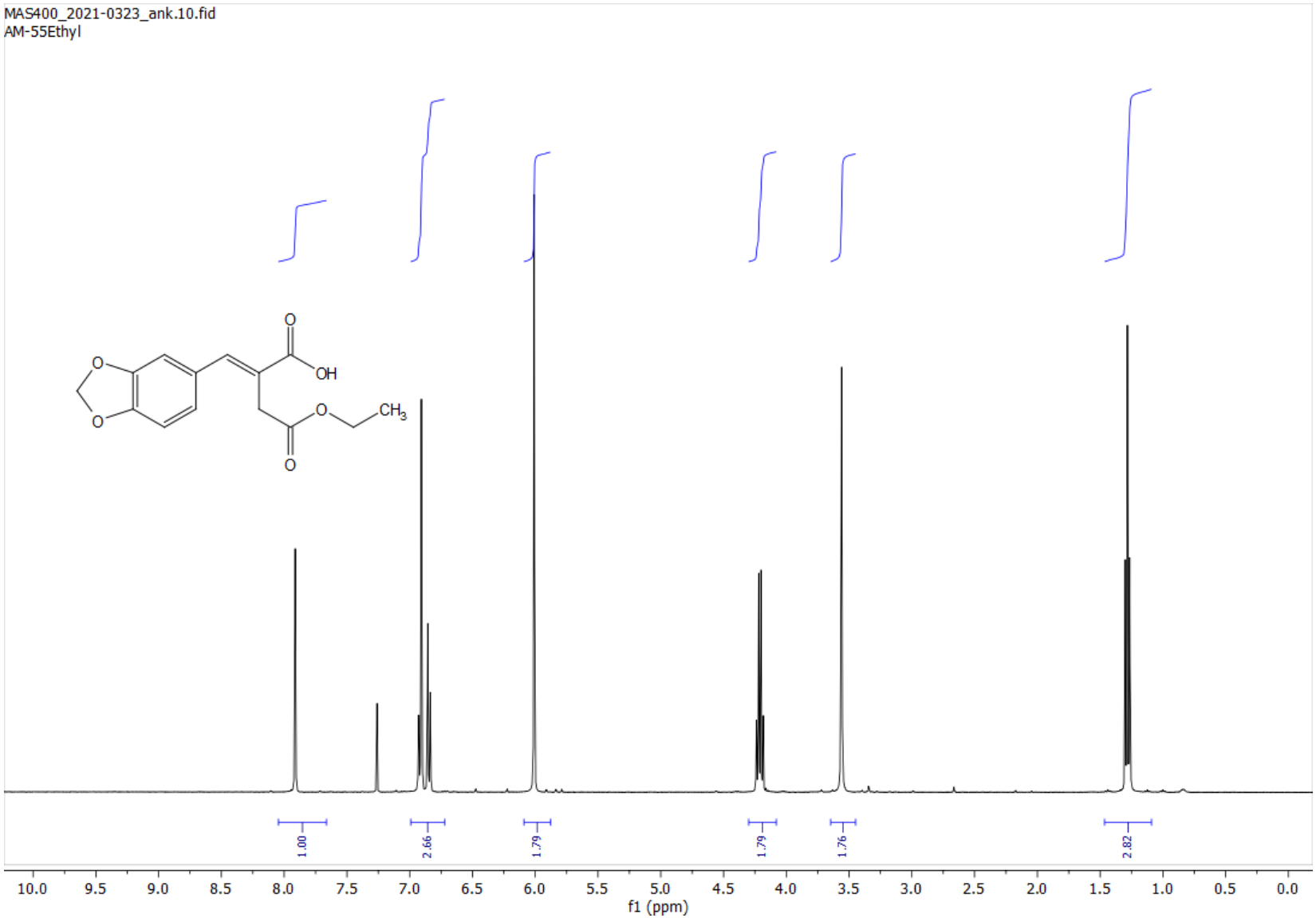

$^{13}C\{^{1}H\}$ NMR (101 MHz, $CDCl_3$) of **6ap**

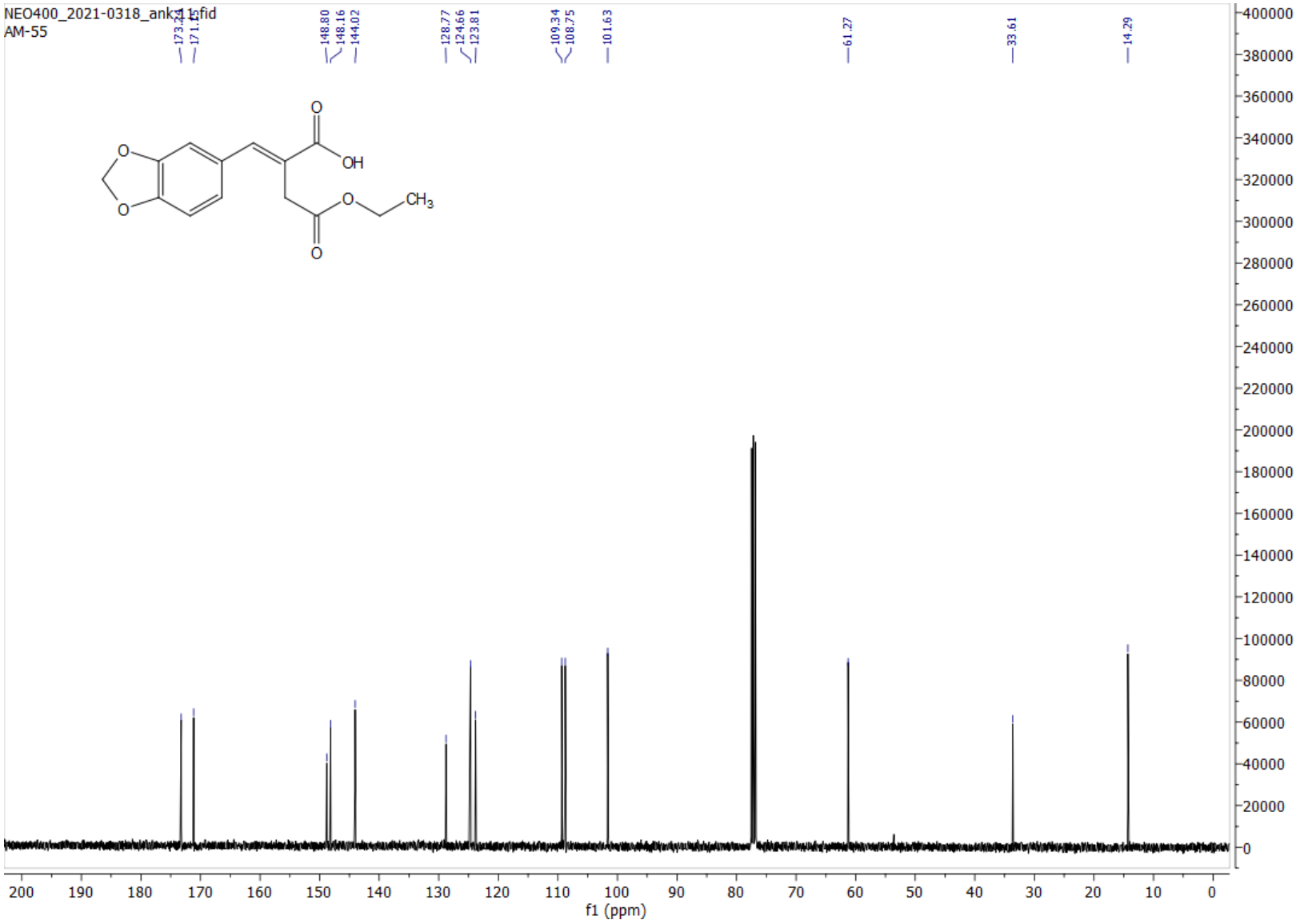

^{1}H NMR (400 MHz, $CDCl_3$) of **6bp**

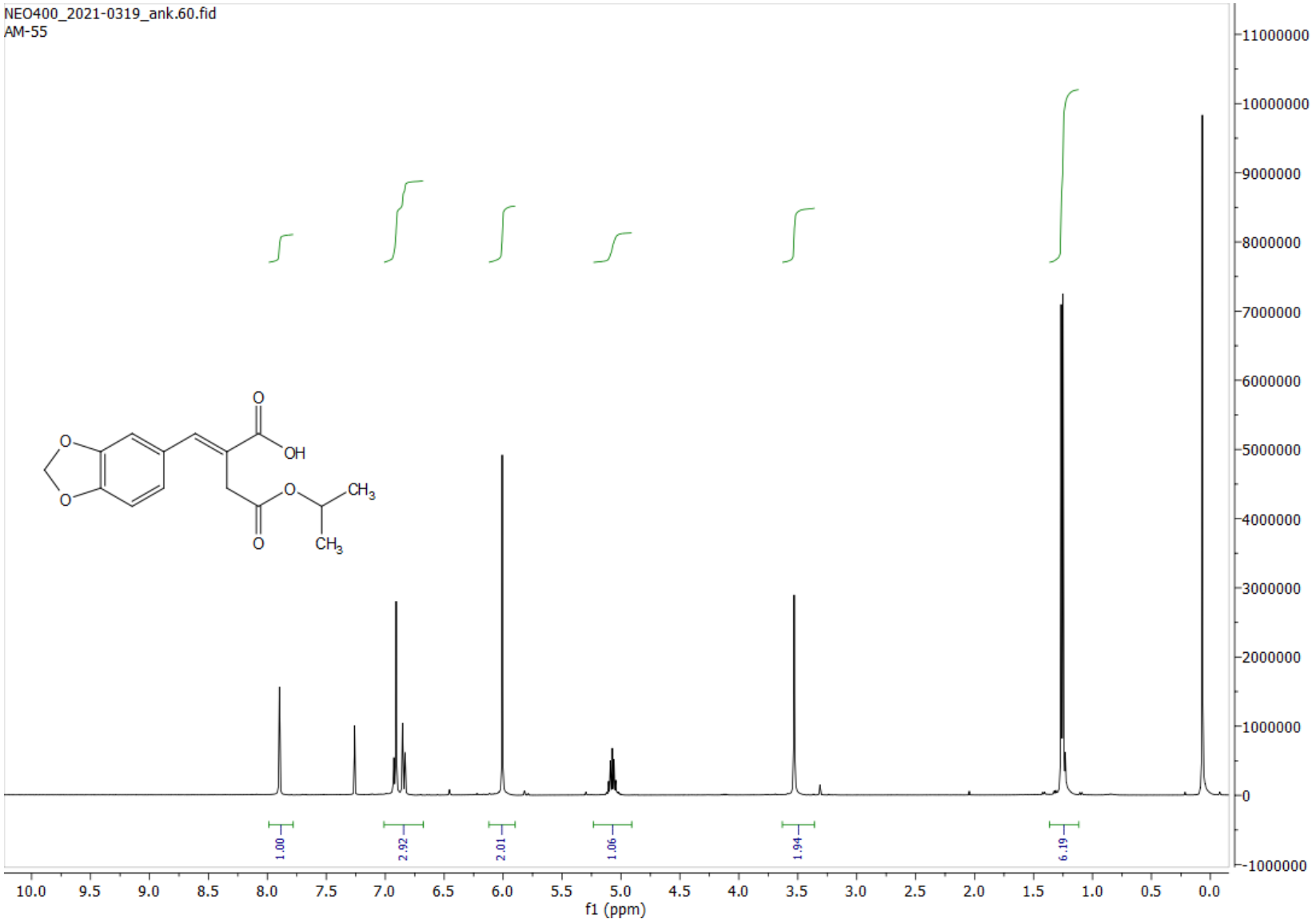

$^{13}C\{^{1}H\}$ NMR (101 MHz, $CDCl_3$) of **6bp**

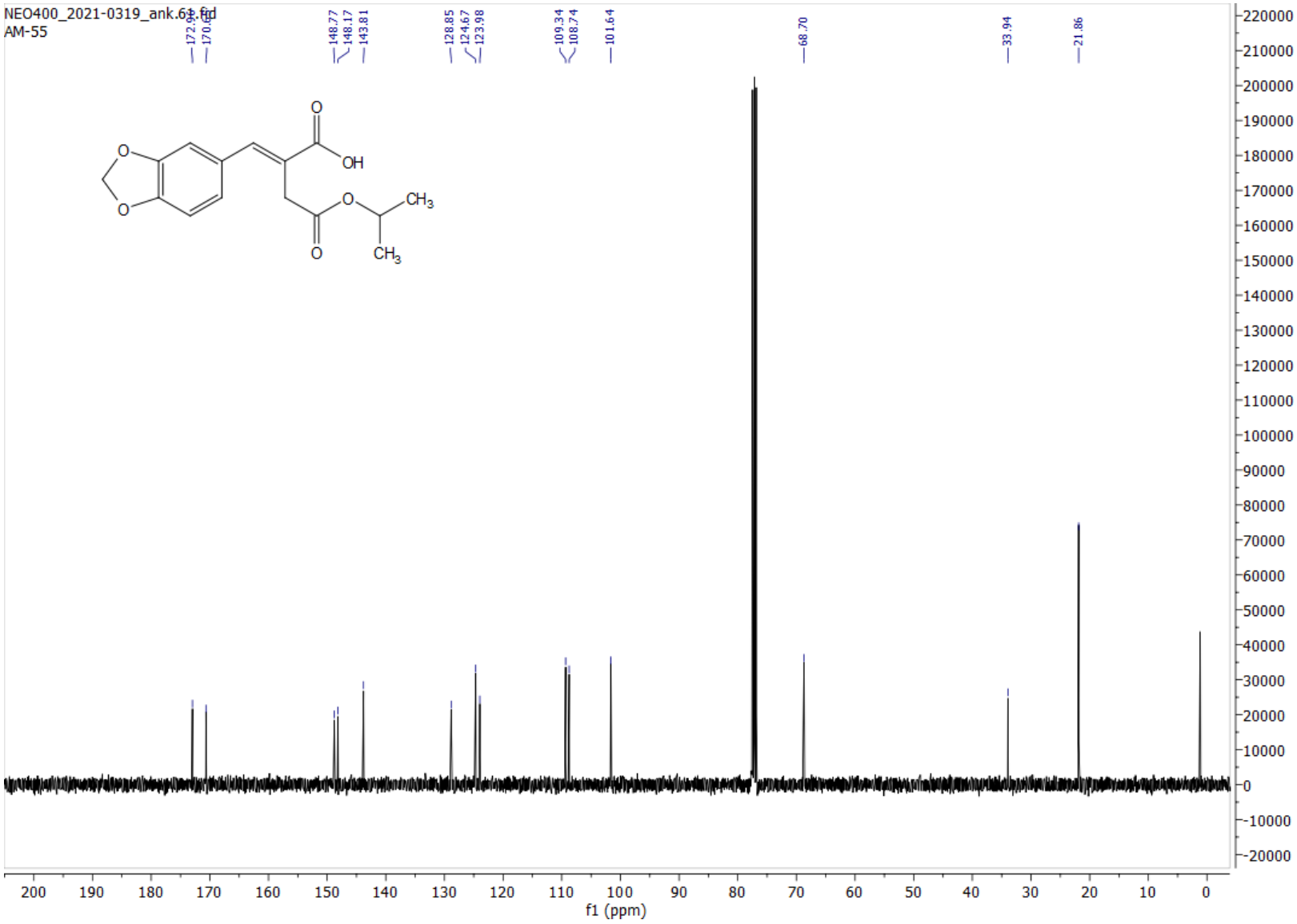

^{1}H NMR (400 MHz, DMSO-d_6) of **9aa**

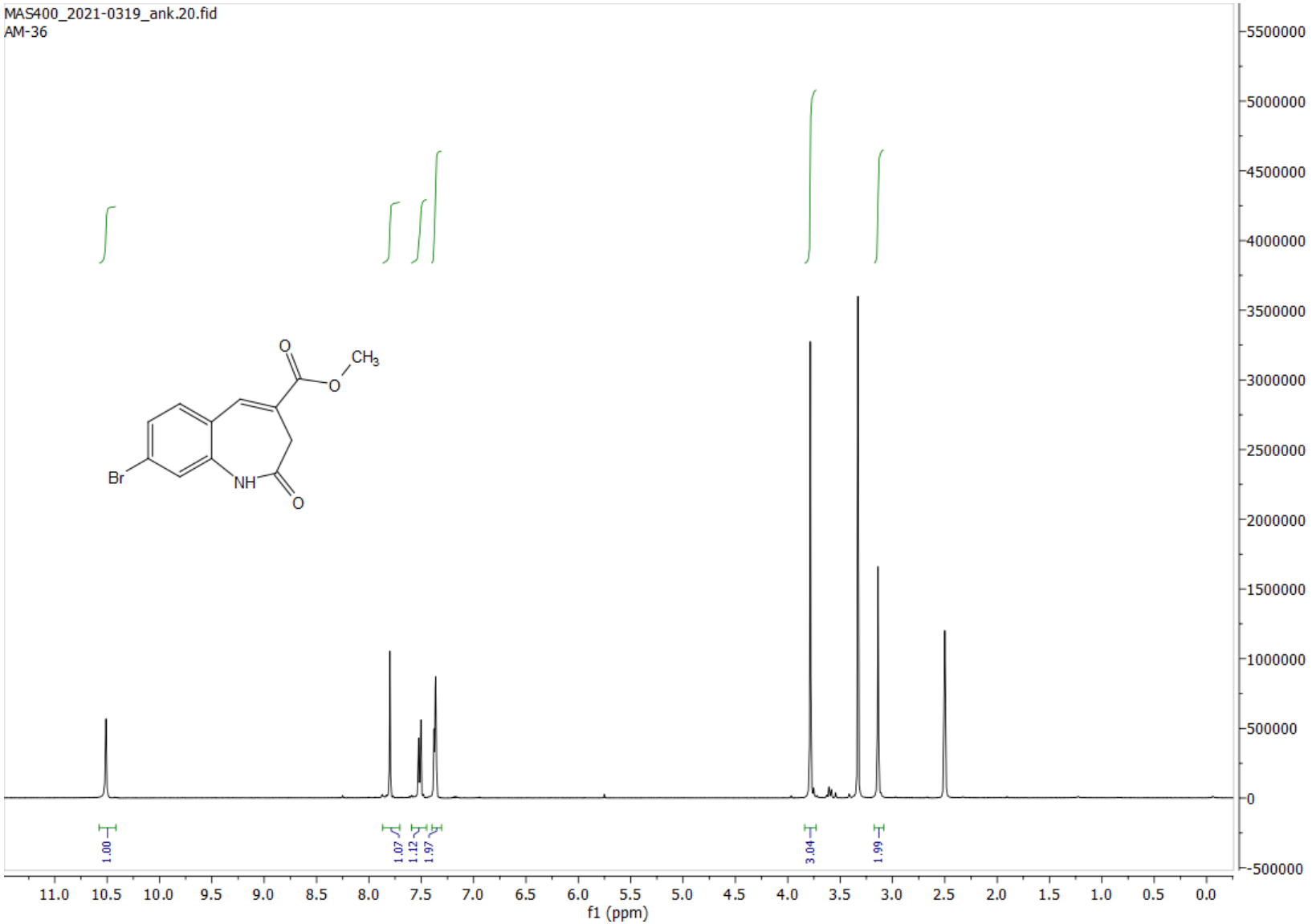

$^{13}C\{^{1}H\}$ NMR (101 MHz, DMSO-d_6) of **9aa**

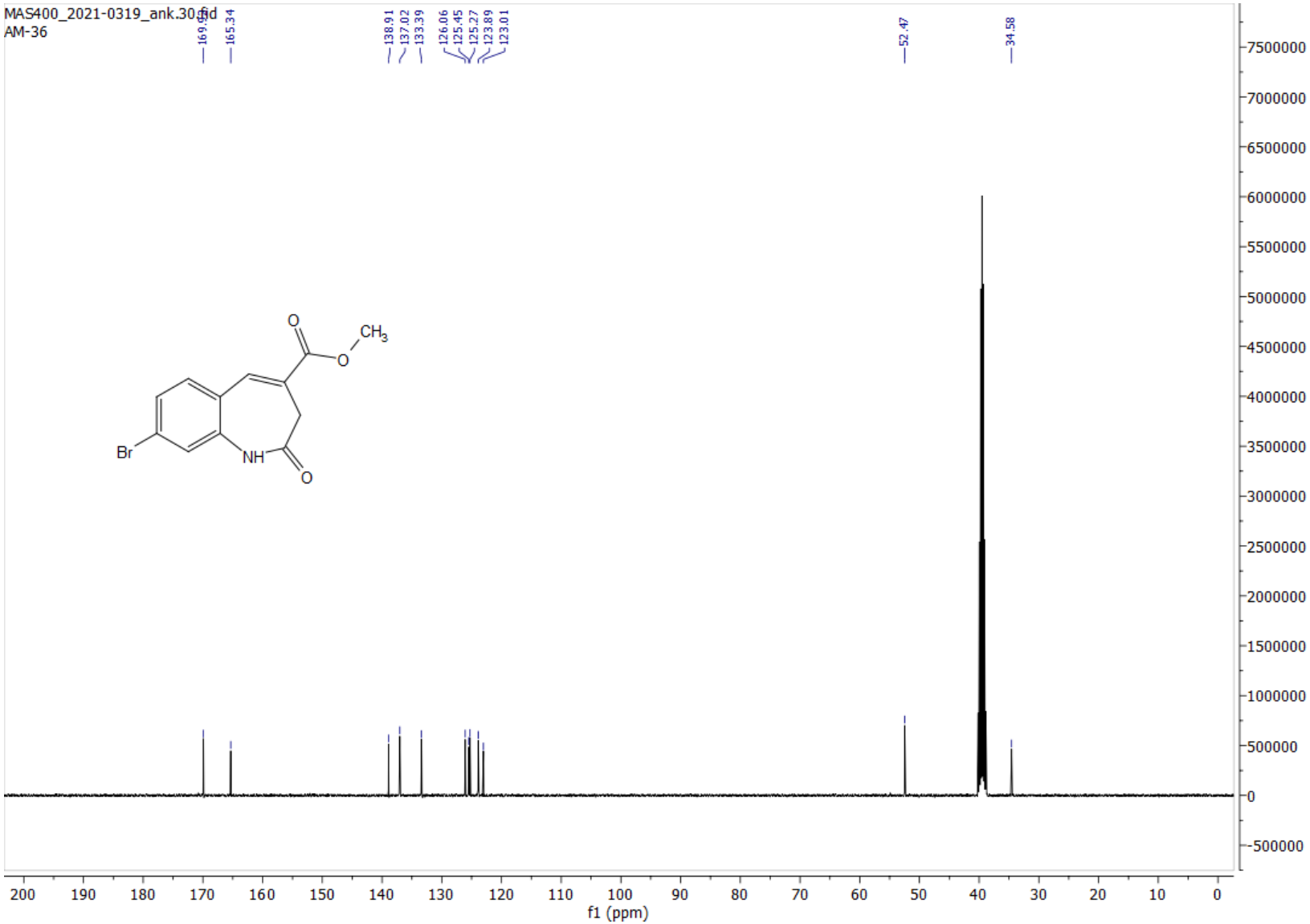

^{1}H NMR (300 MHz, DMSO-d_6) of **9ba**

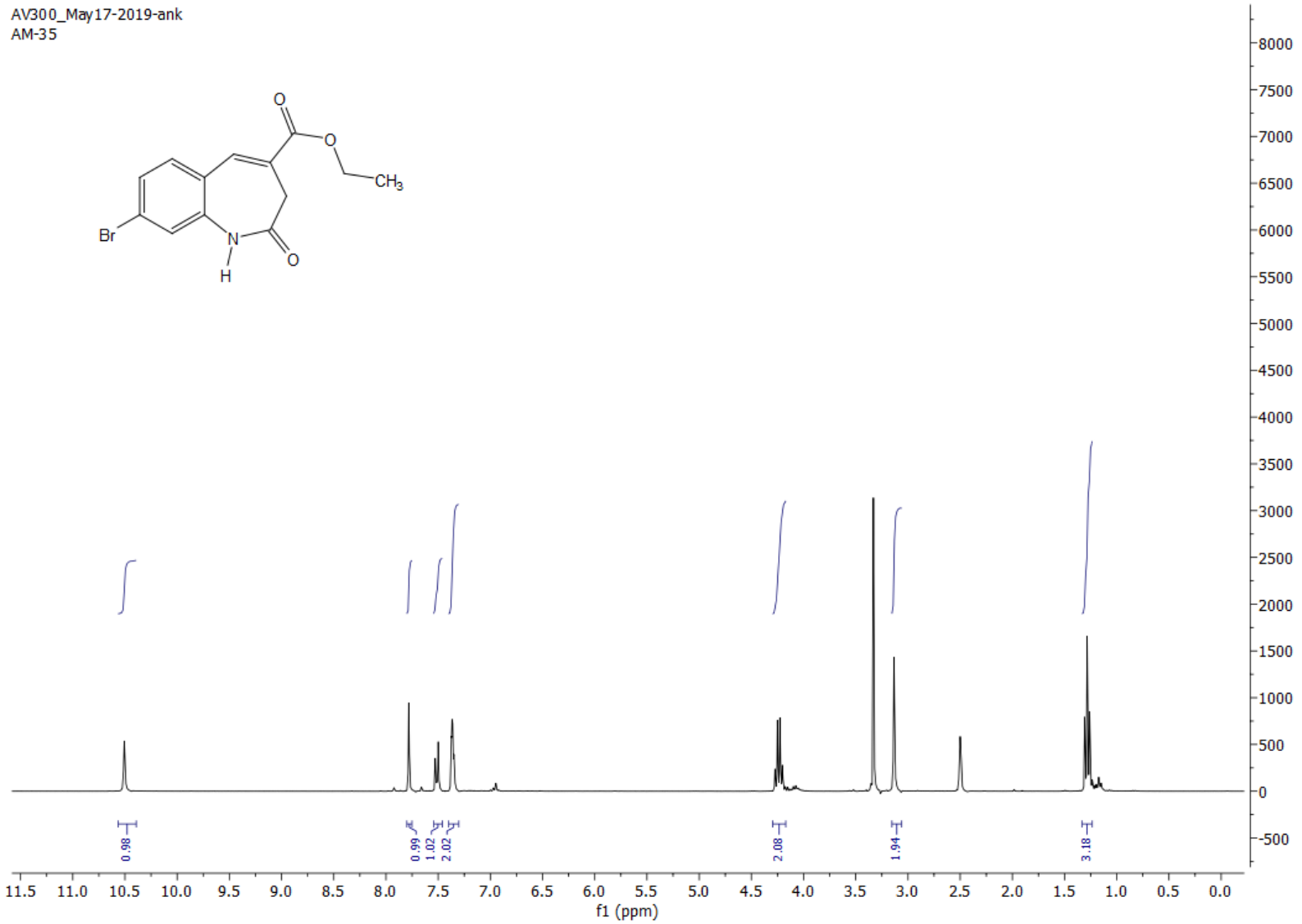

$^{13}C\{^{1}H\}$ NMR (75 MHz, DMSO-d_6) of **9ba**

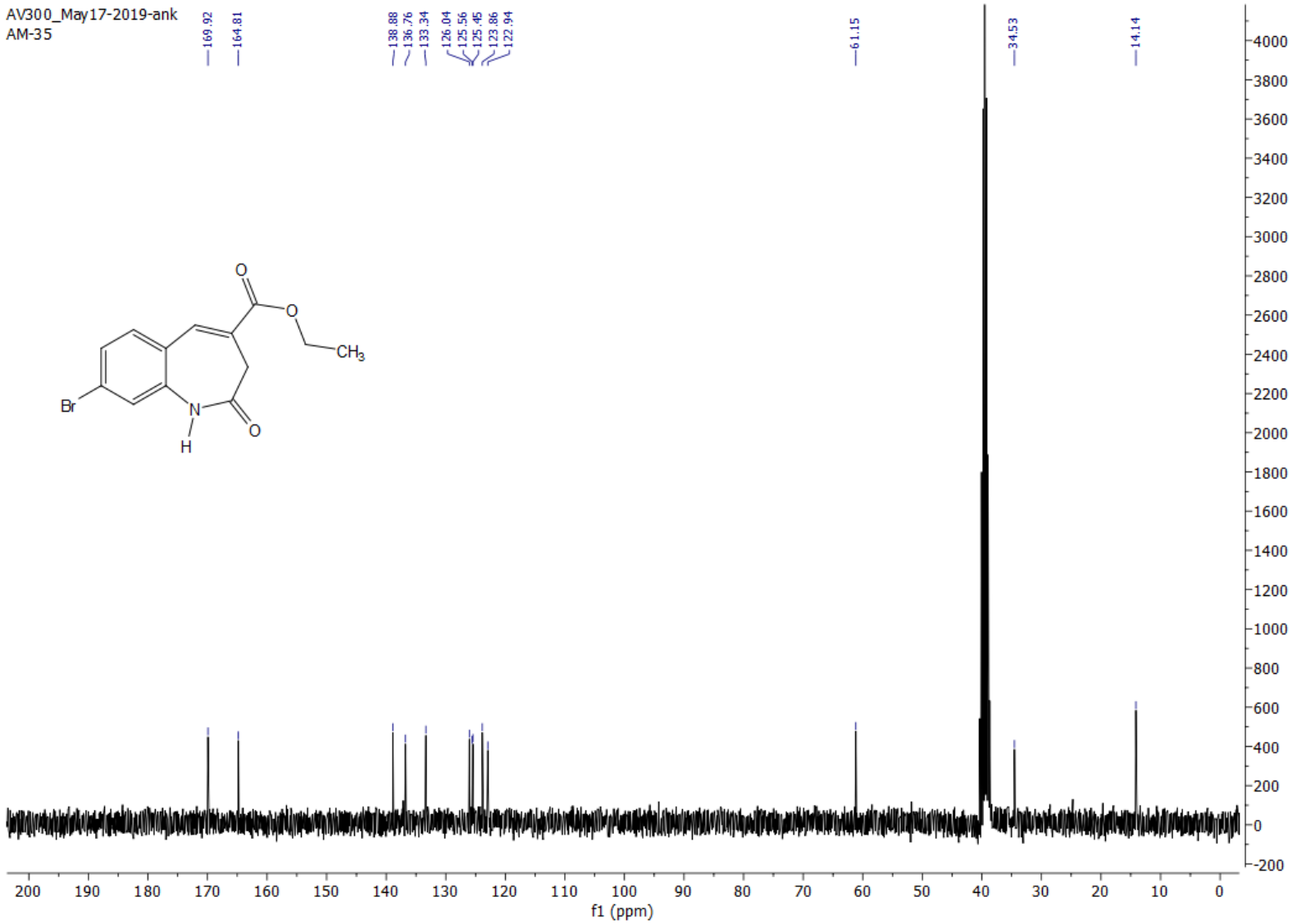

^{1}H NMR (400 MHz, DMSO-d_6) of **9ab**

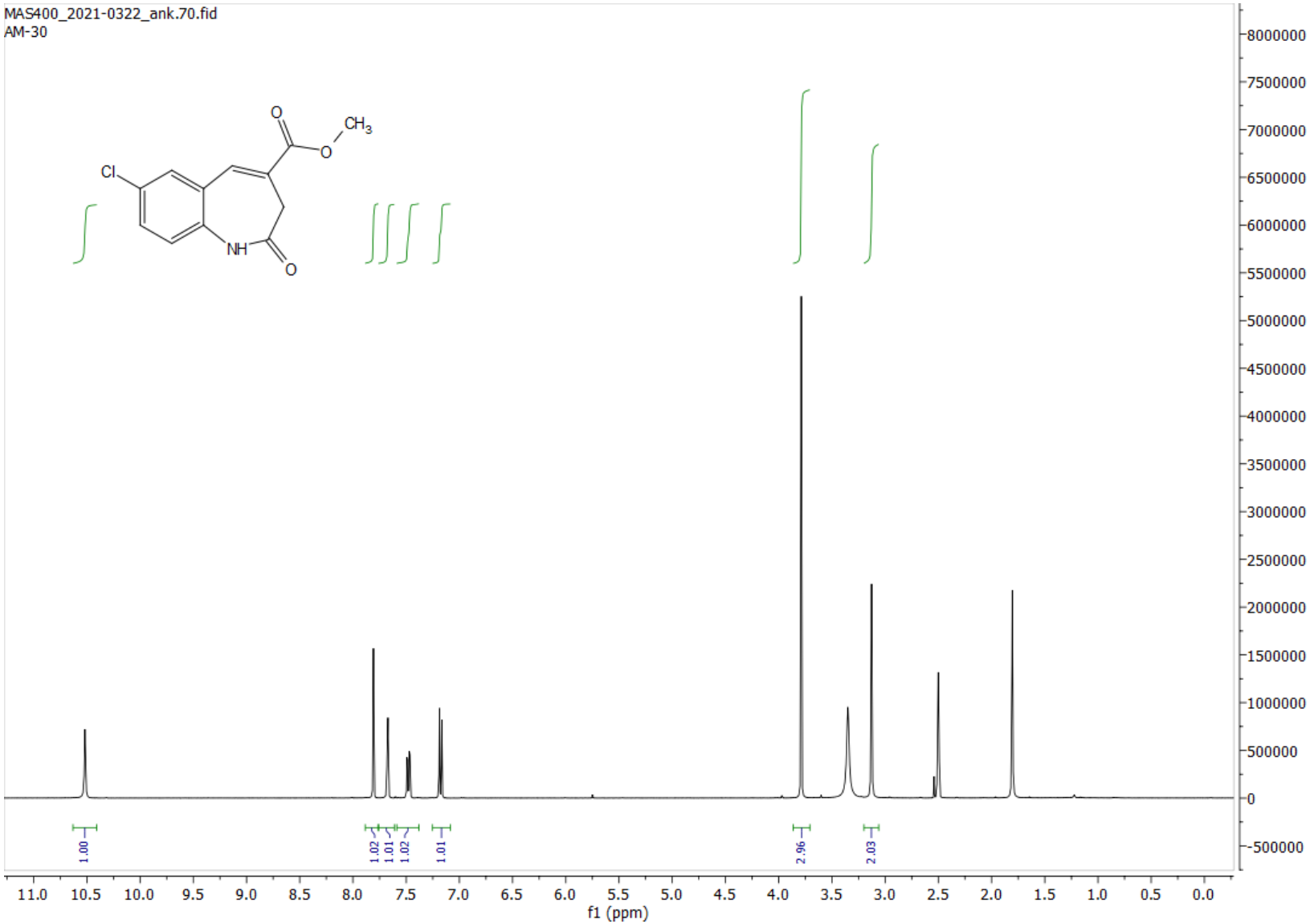

$^{13}C\{^{1}H\}$ NMR (101 MHz, DMSO-d_6) of **9ab**

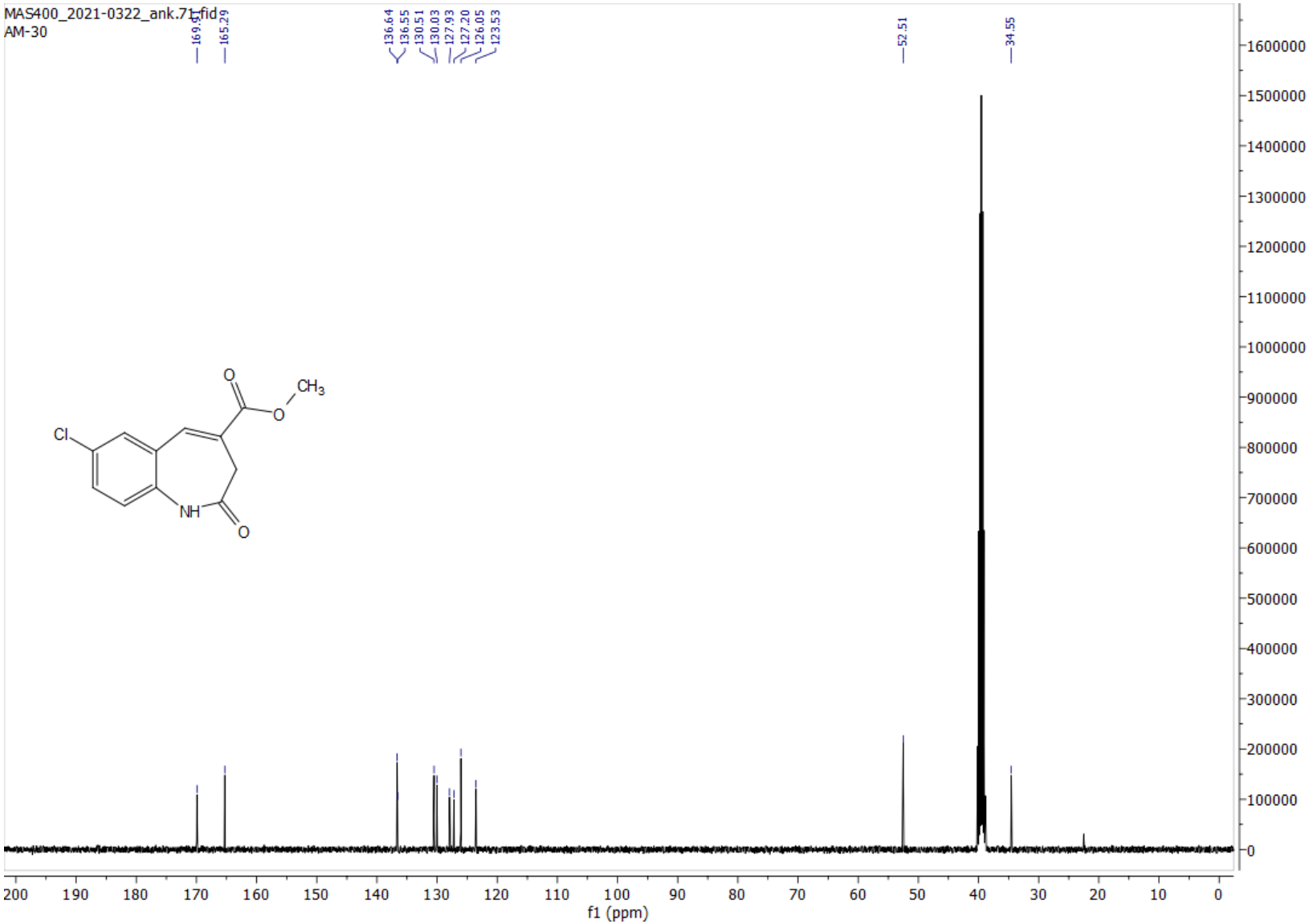

^{1}H NMR (300 MHz, DMSO-d_6) of **9bd**

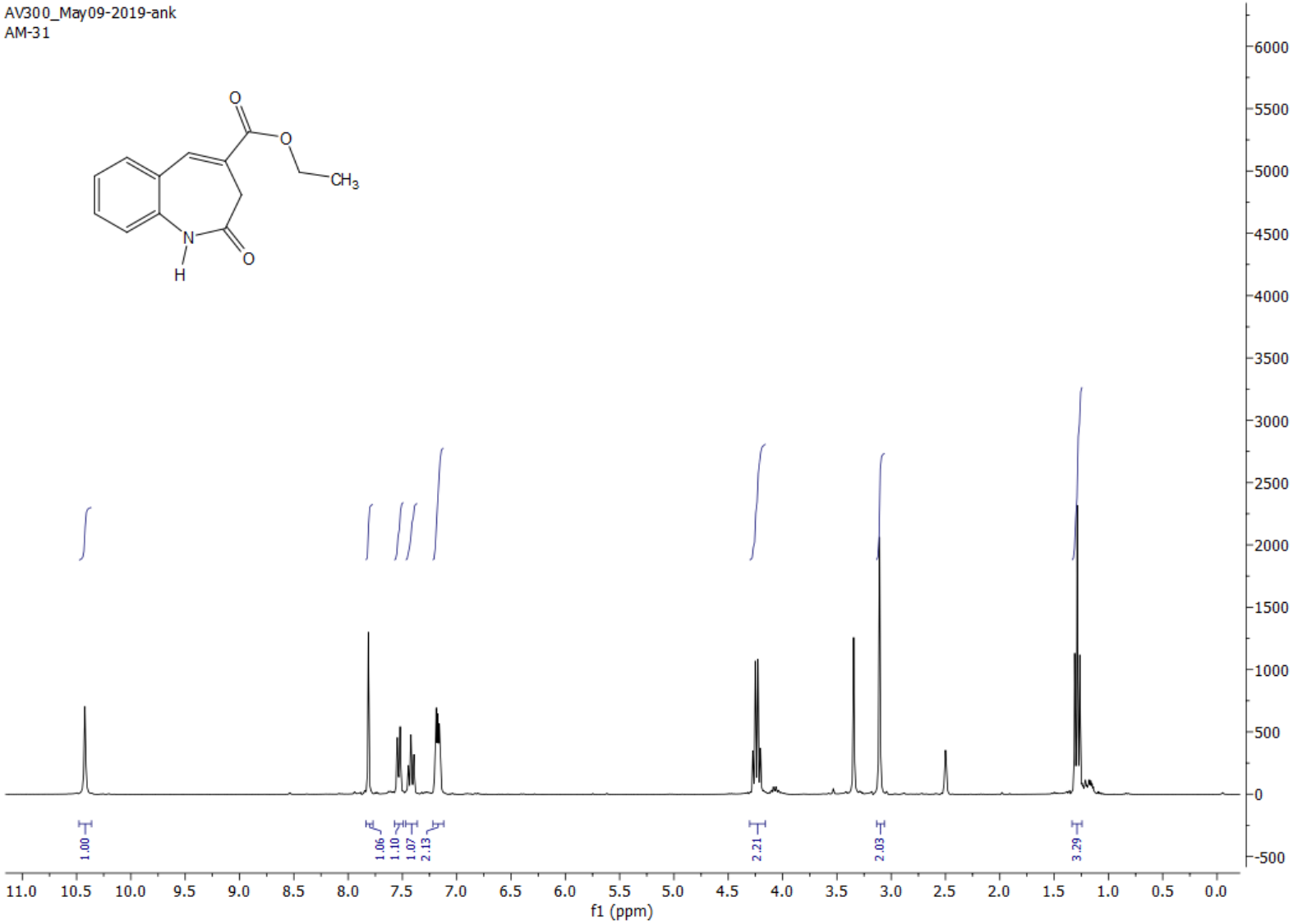

$^{13}C\{^{1}H\}$ NMR (75 MHz, DMSO-d_6) of **9bd**

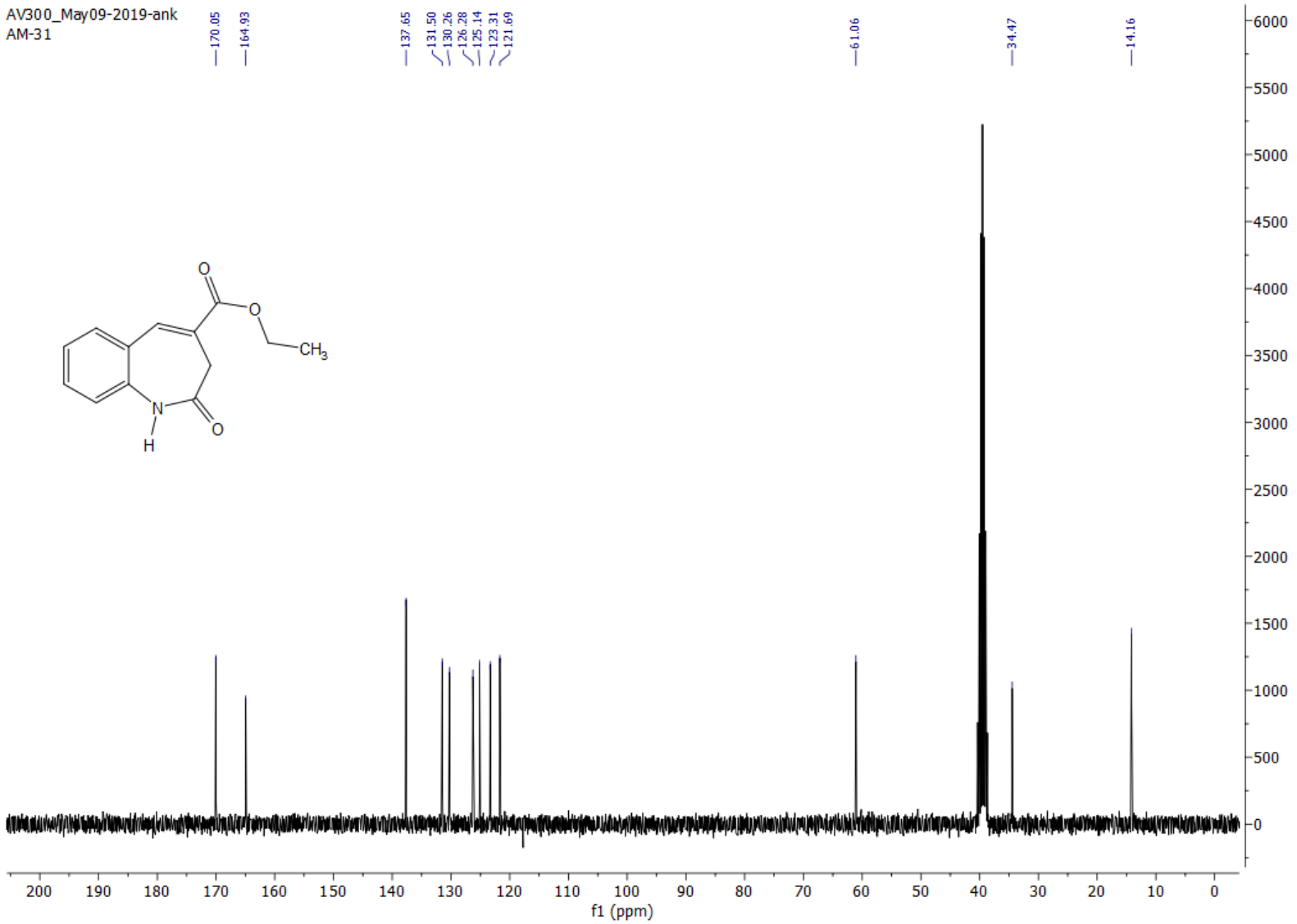

^{1}H NMR (300 MHz, DMSO-d_6) of **9ac**

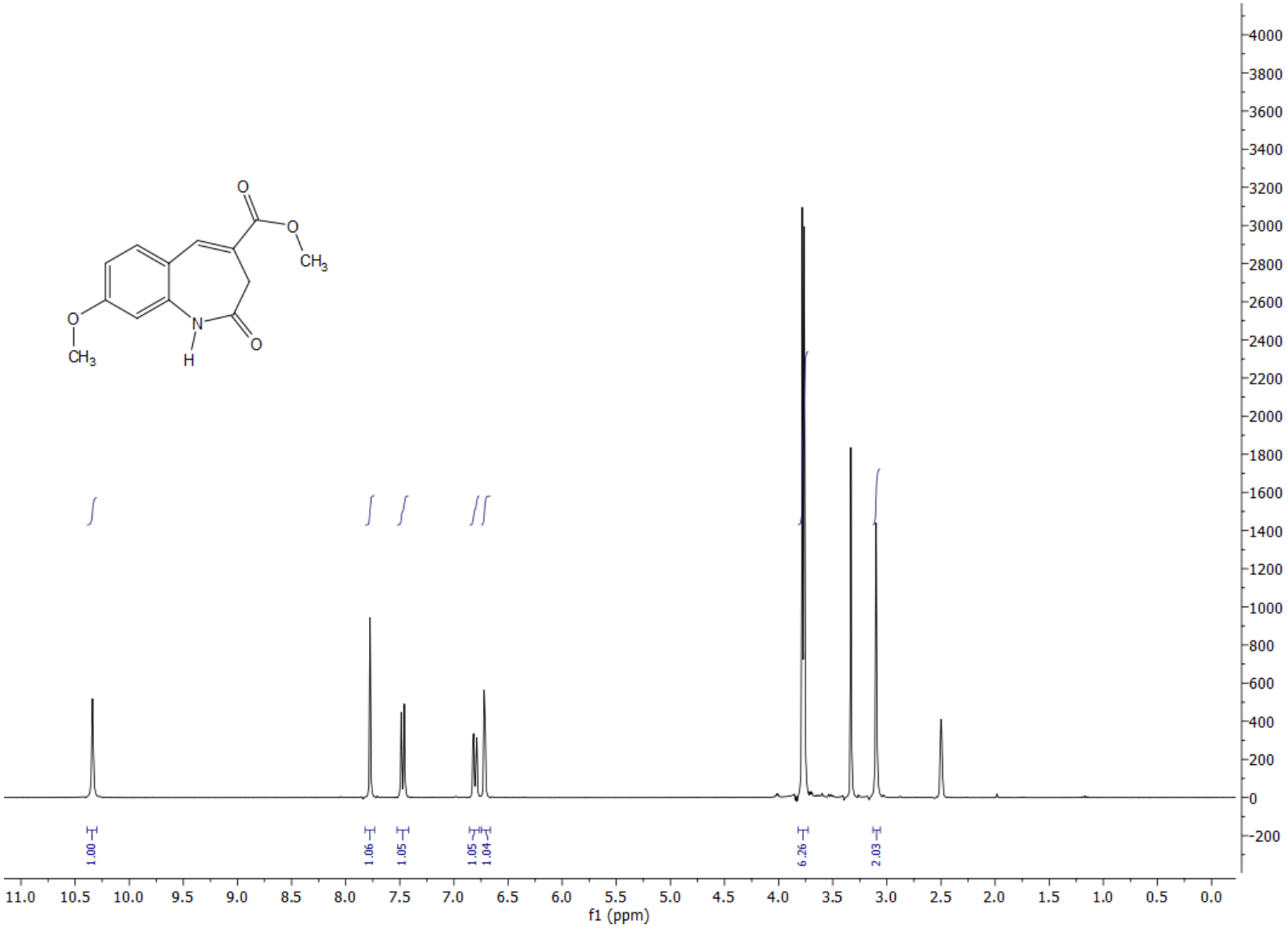

$^{13}C\{^{1}H\}$ NMR (75 MHz, DMSO-d_6) of **9ac**

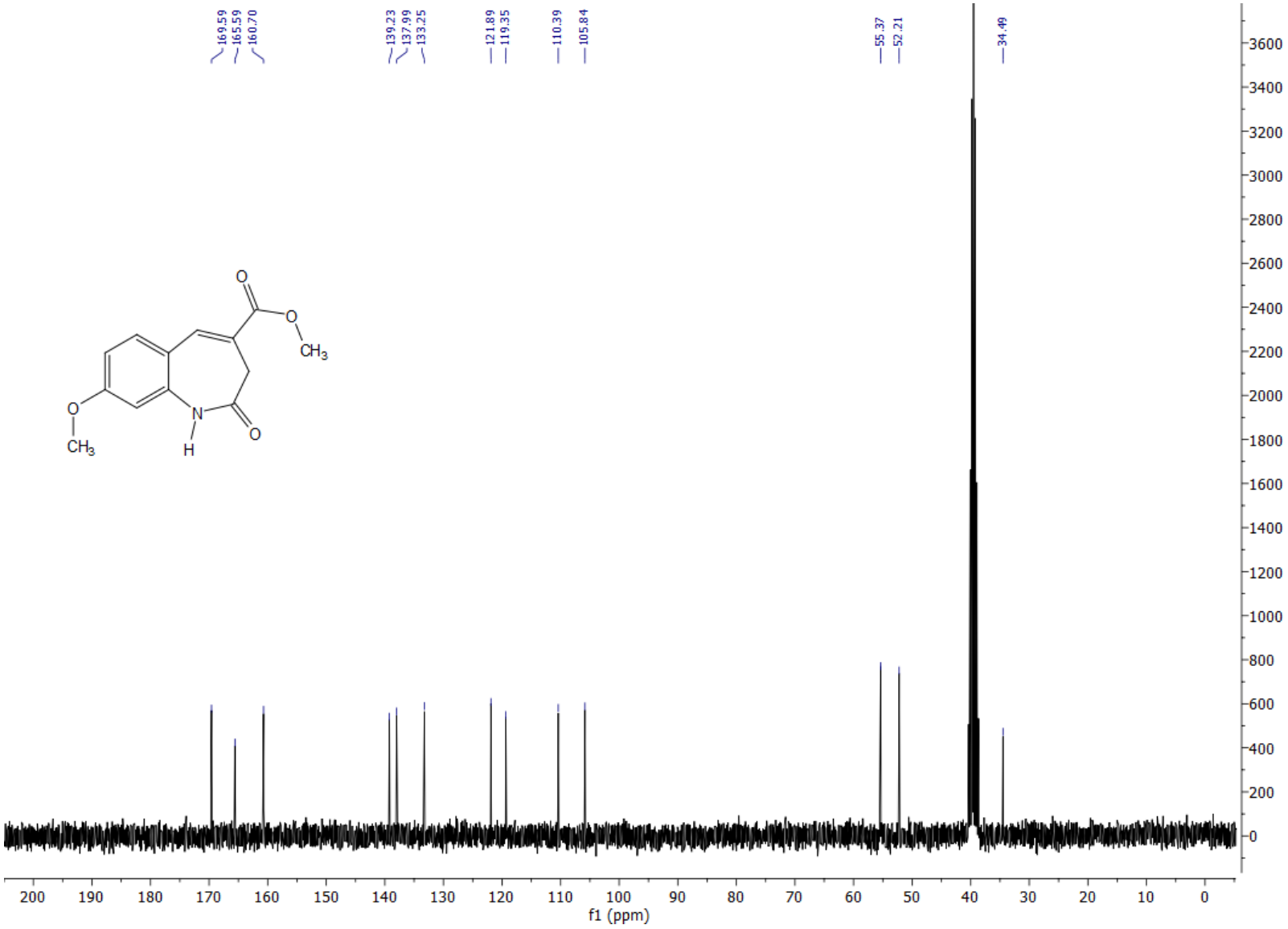

^{1}H NMR (400 MHz, $CDCl_3$) of **9ac**

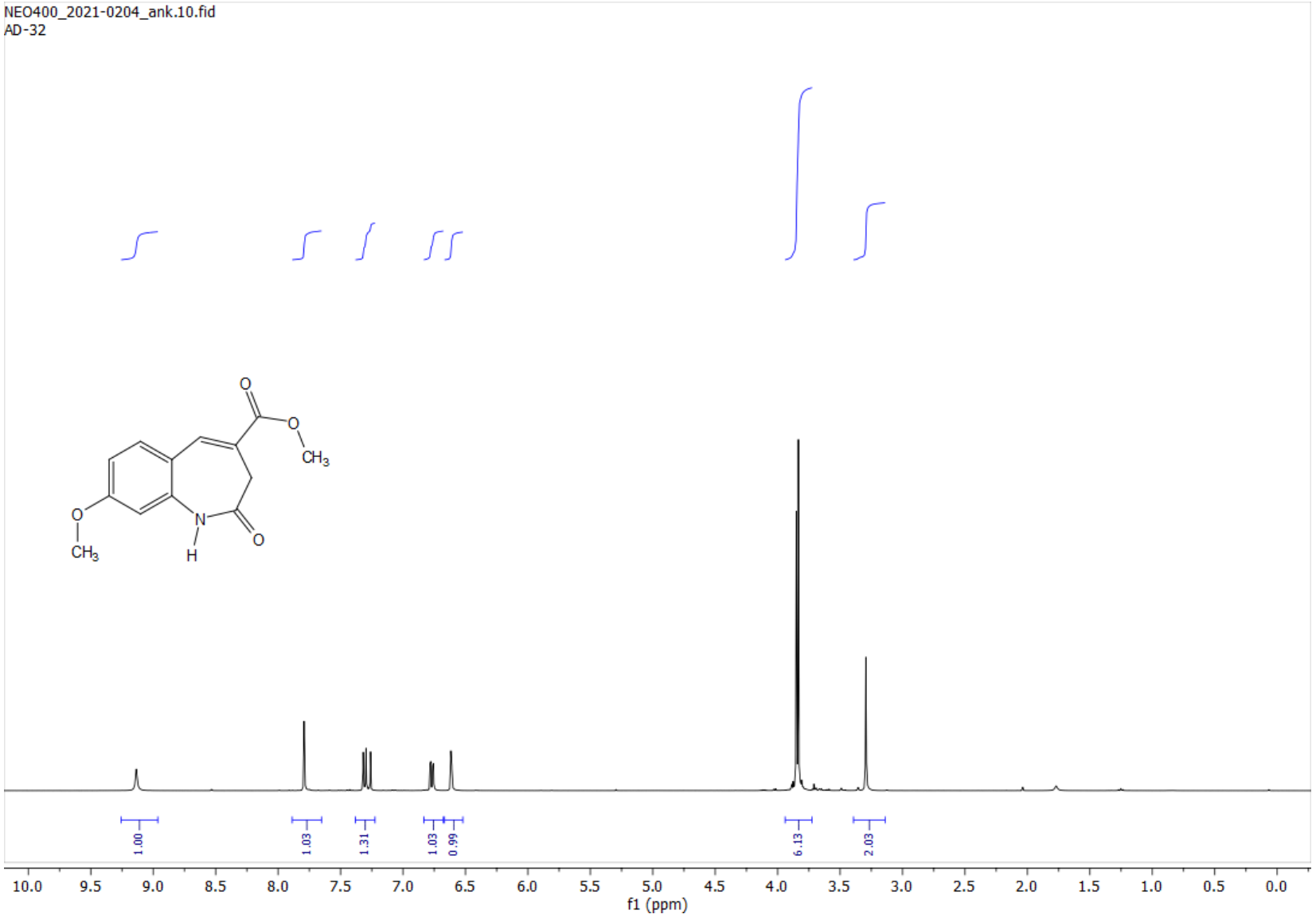

$^{13}C\{^{1}H\}$ NMR (101 MHz, $CDCl_3$) of **9ac**

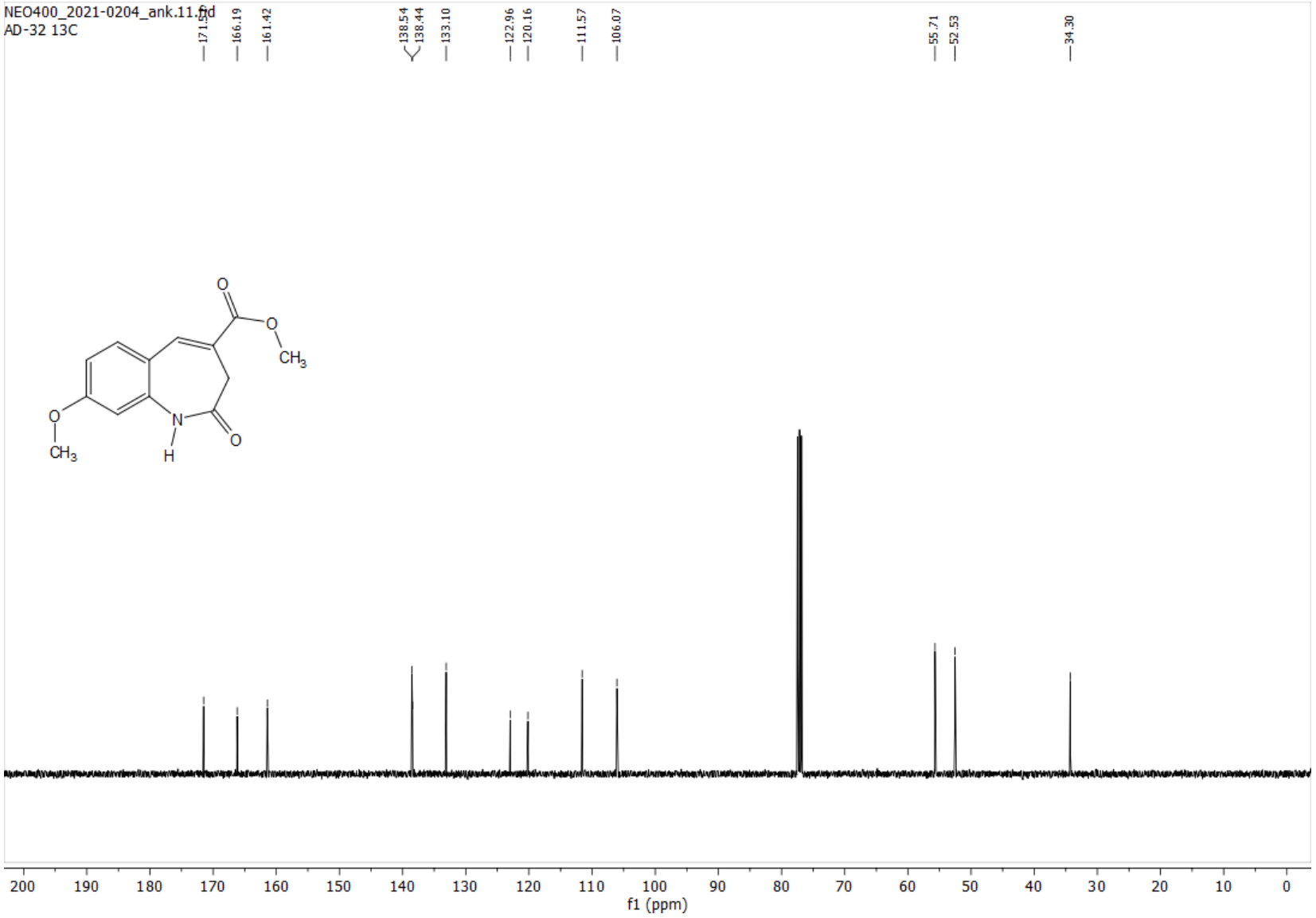

H,H-COSY (400 MHz, $CDCl_3$) of **9ac**

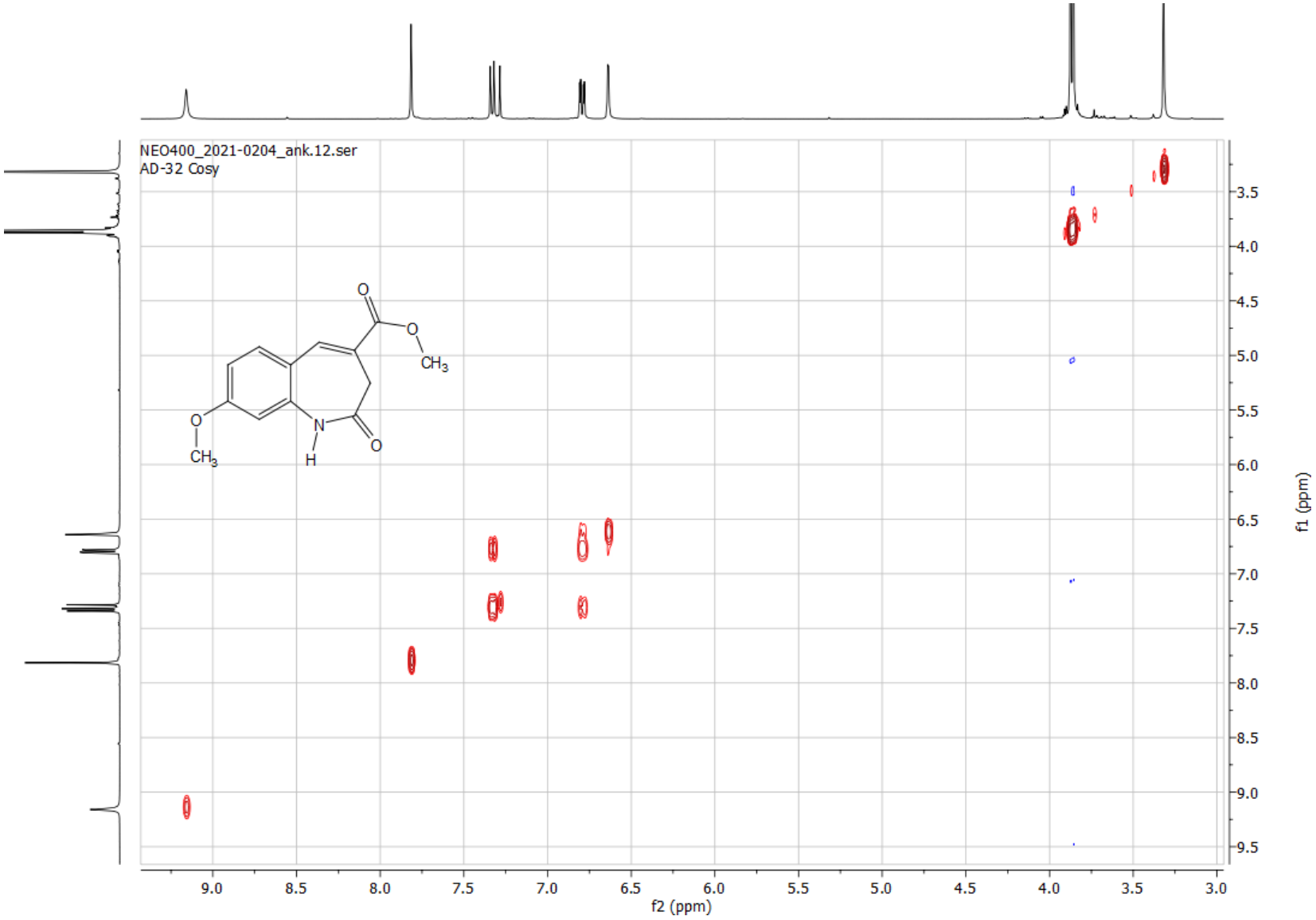

NOESY (400 MHz, $CDCl_3$) of **9ac**

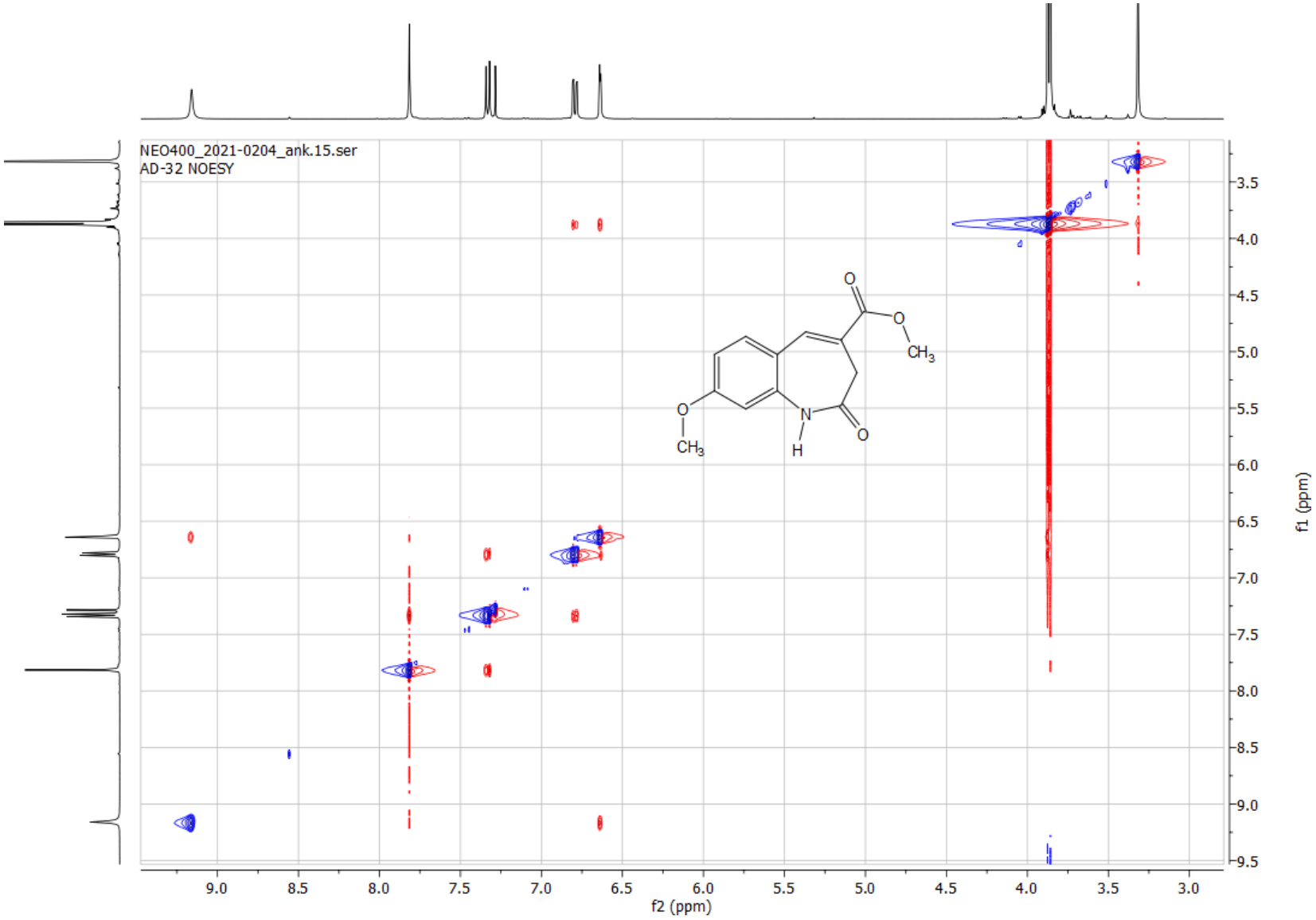

HSQC (400/101 MHz, $CDCl_3$) of **9ac**

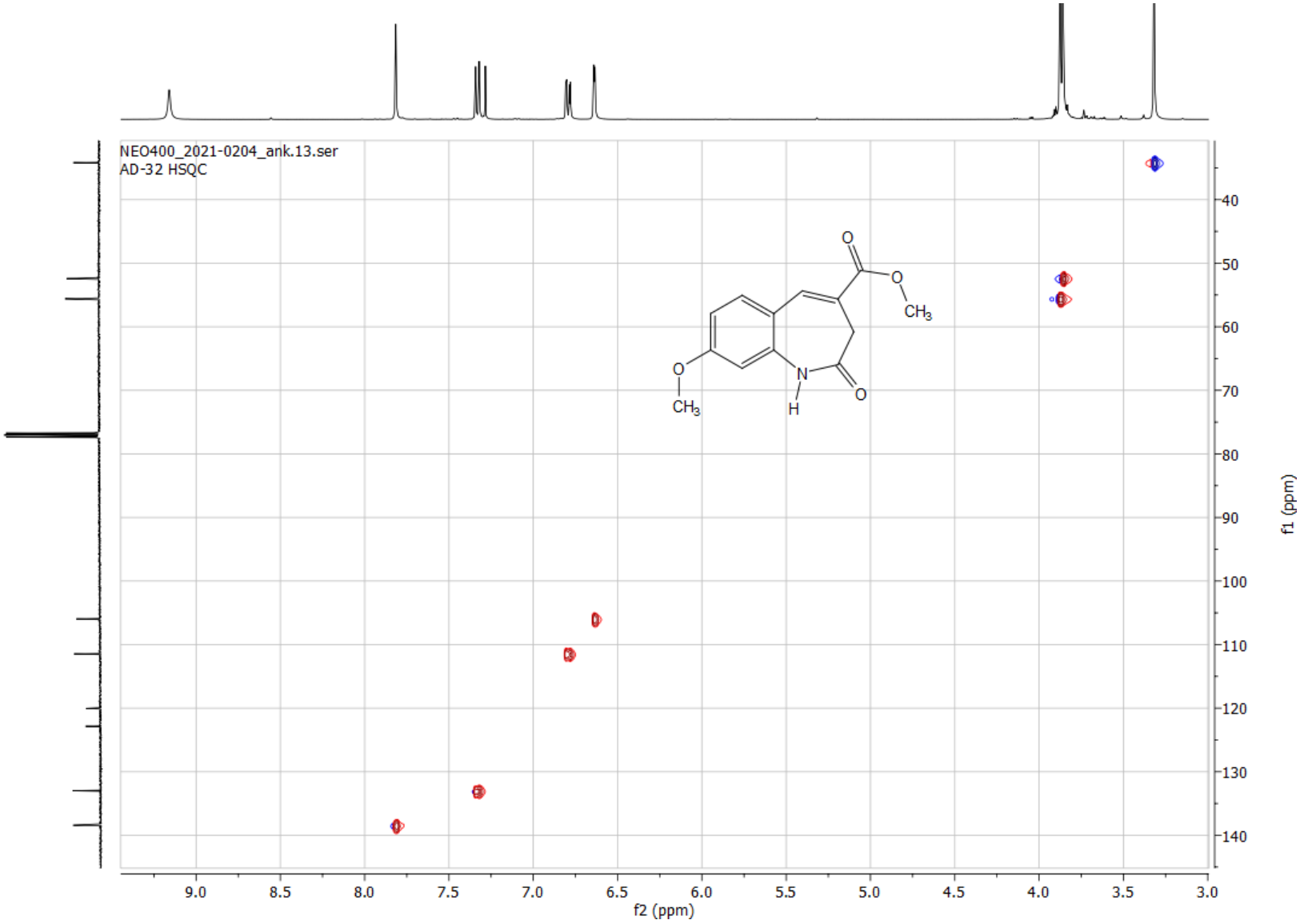

HMBC (400/101 MHz, $CDCl_3$) of **9ac**

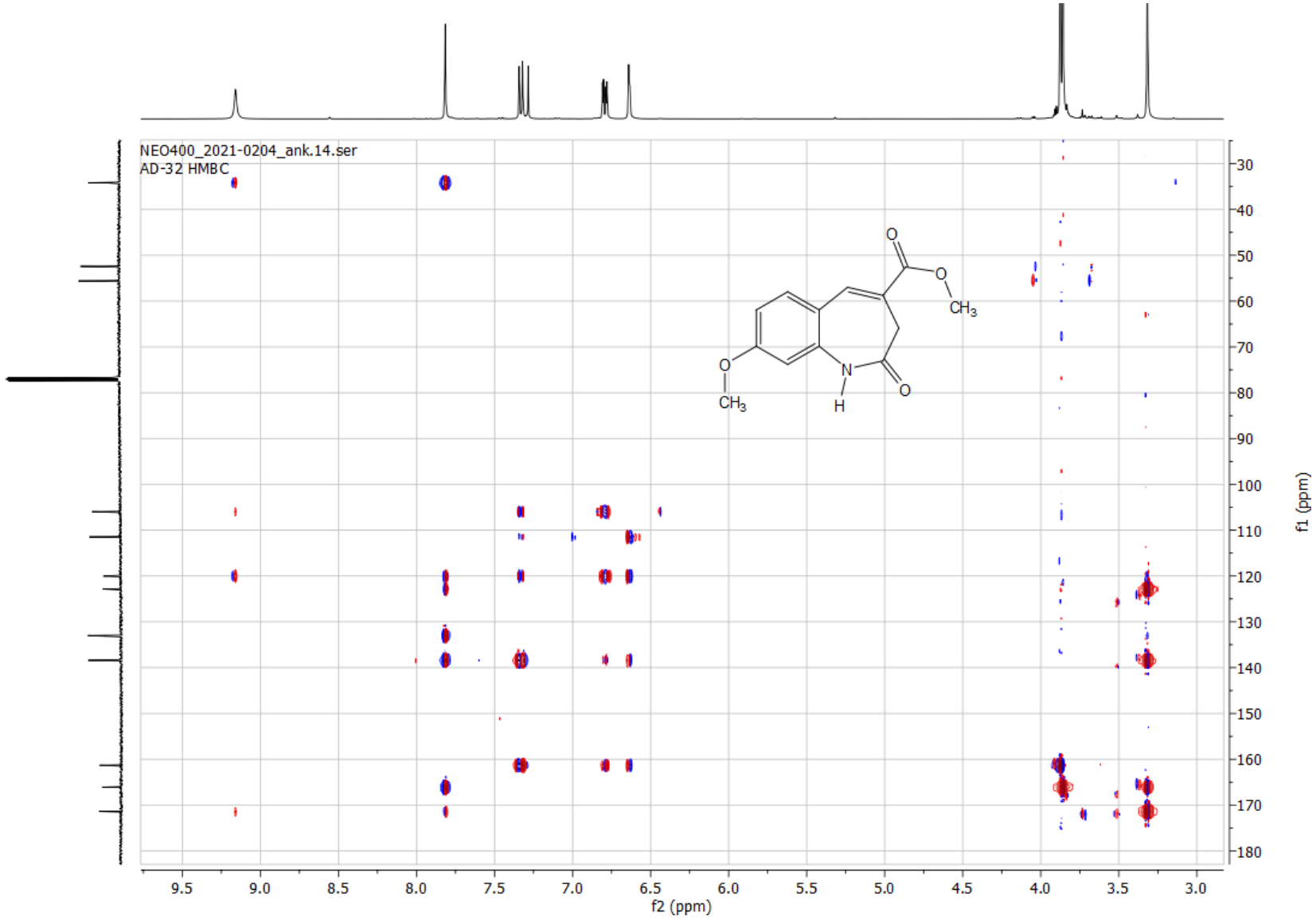

^{1}H NMR (300 MHz, $CDCl_3$) of **10bc**

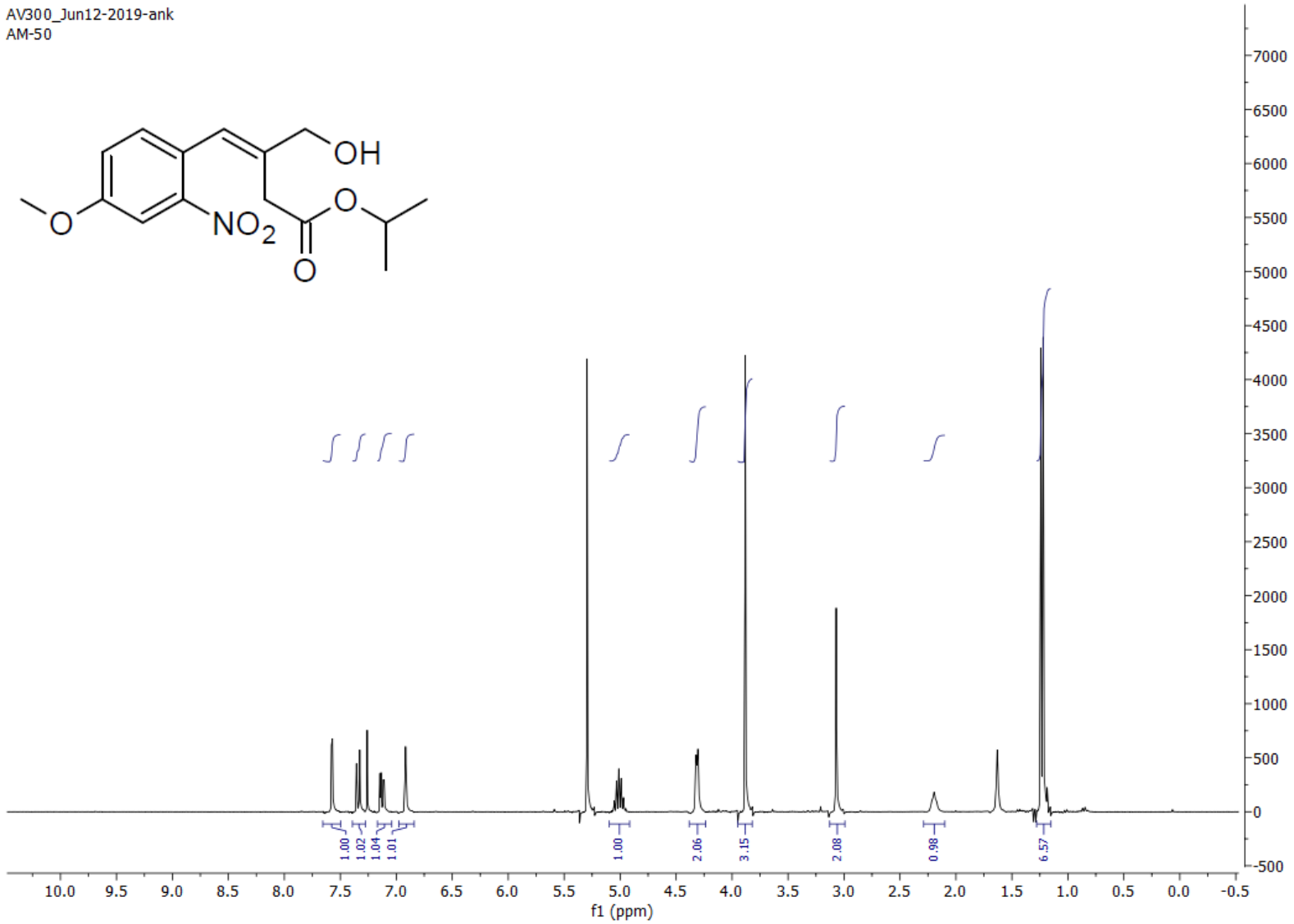

$^{13}C\{^{1}H\}$ NMR (75 MHz, $CDCl_3$) of **10bc**

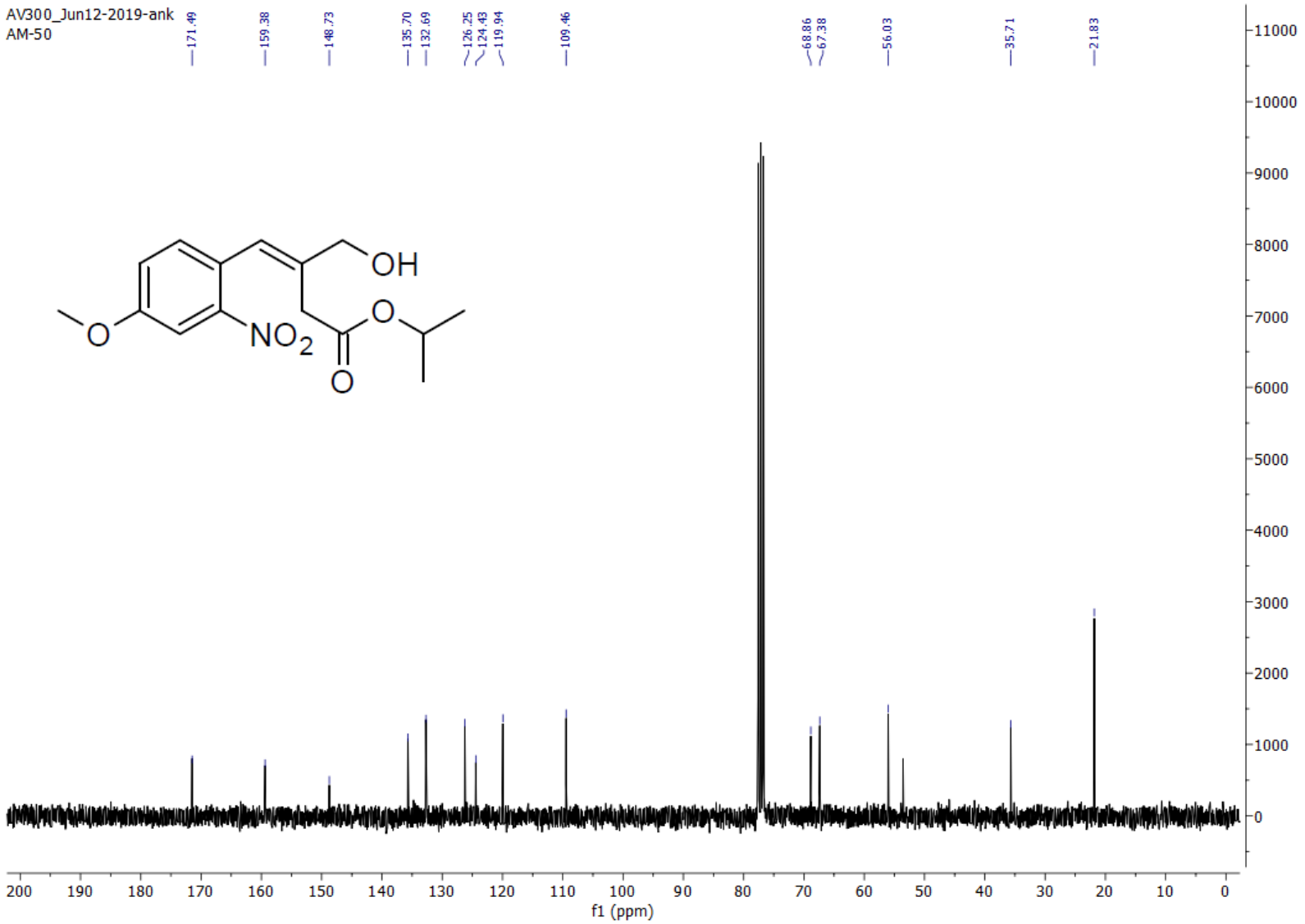

^{1}H NMR (400 MHz, $CDCl_3$) of **10bd**

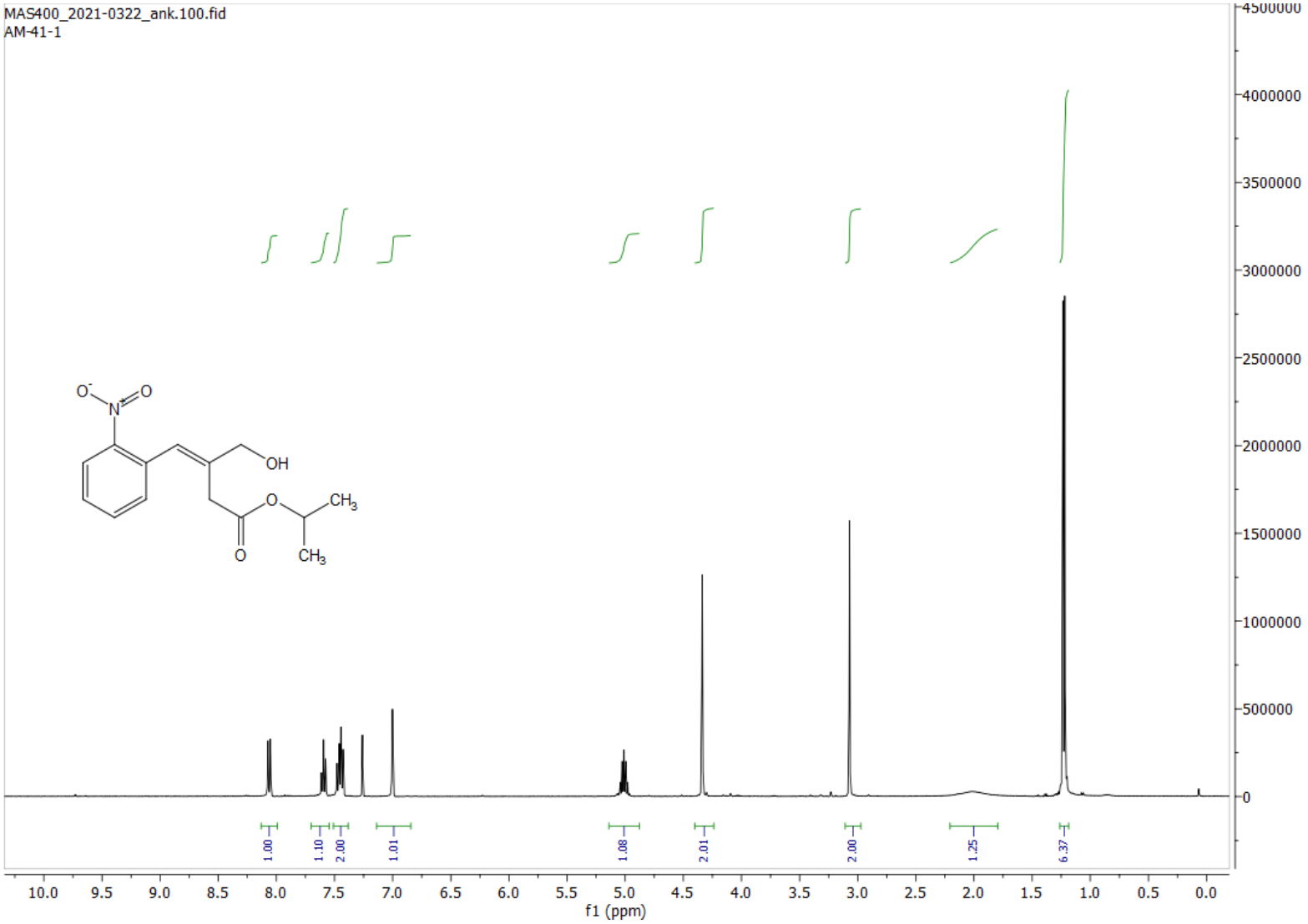

$^{13}C\{^{1}H\}$ NMR (101 MHz, $CDCl_3$) of **10bd**

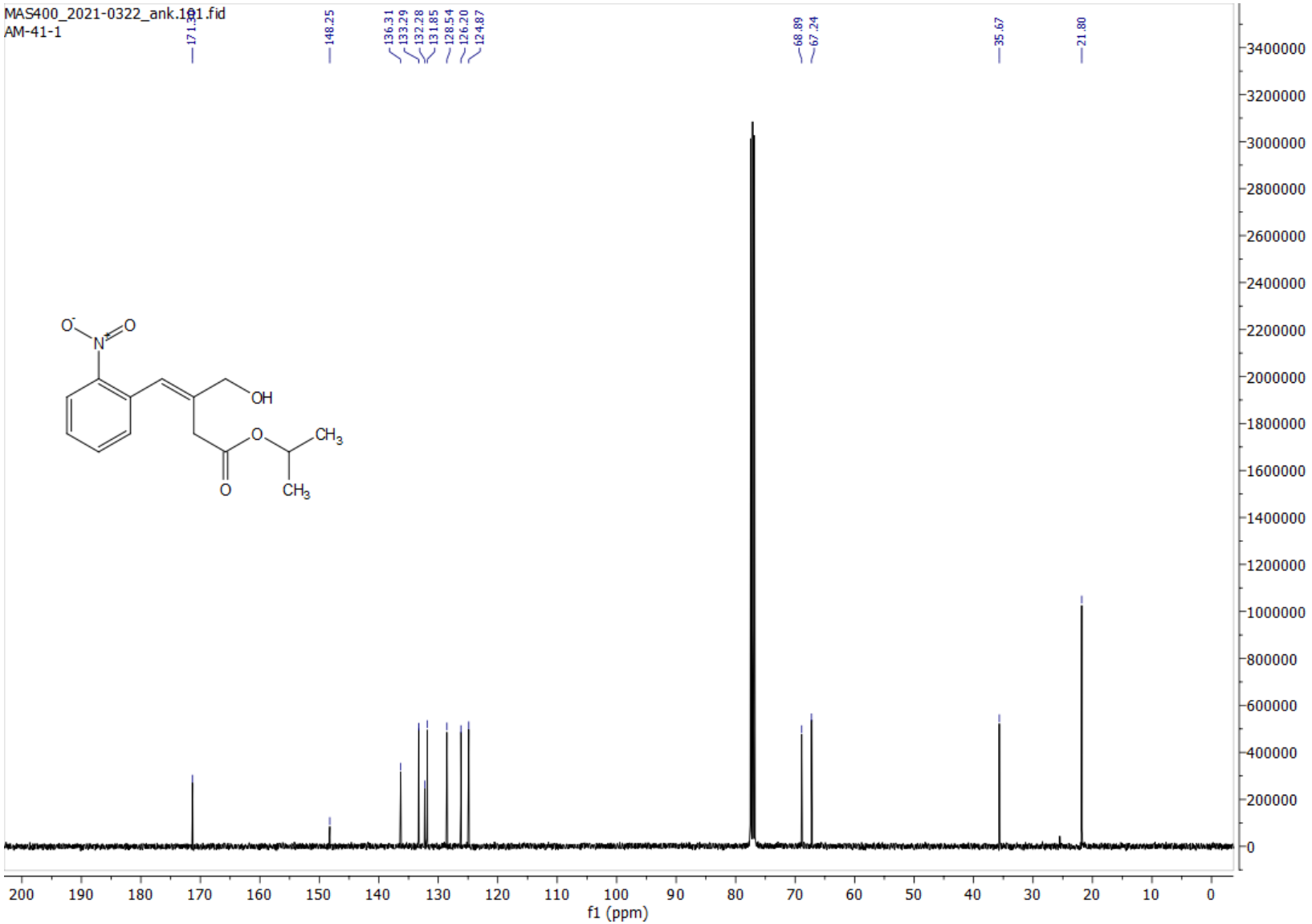

^{1}H NMR (300 MHz, DMSO-d_6) of **11bc**

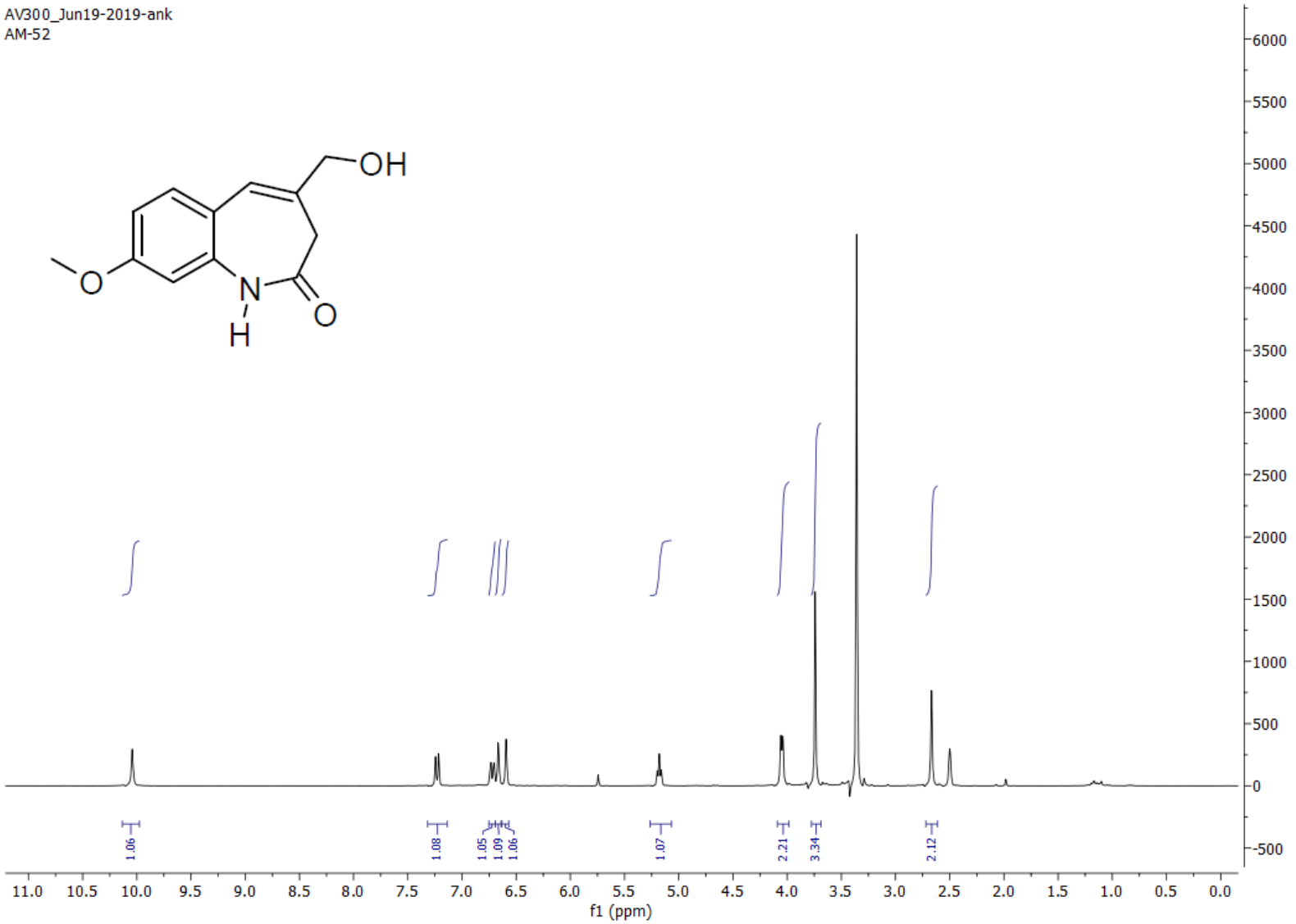

$^{13}C\{^{1}H\}$ NMR (75 MHz, DMSO-d_6) of **11bc**

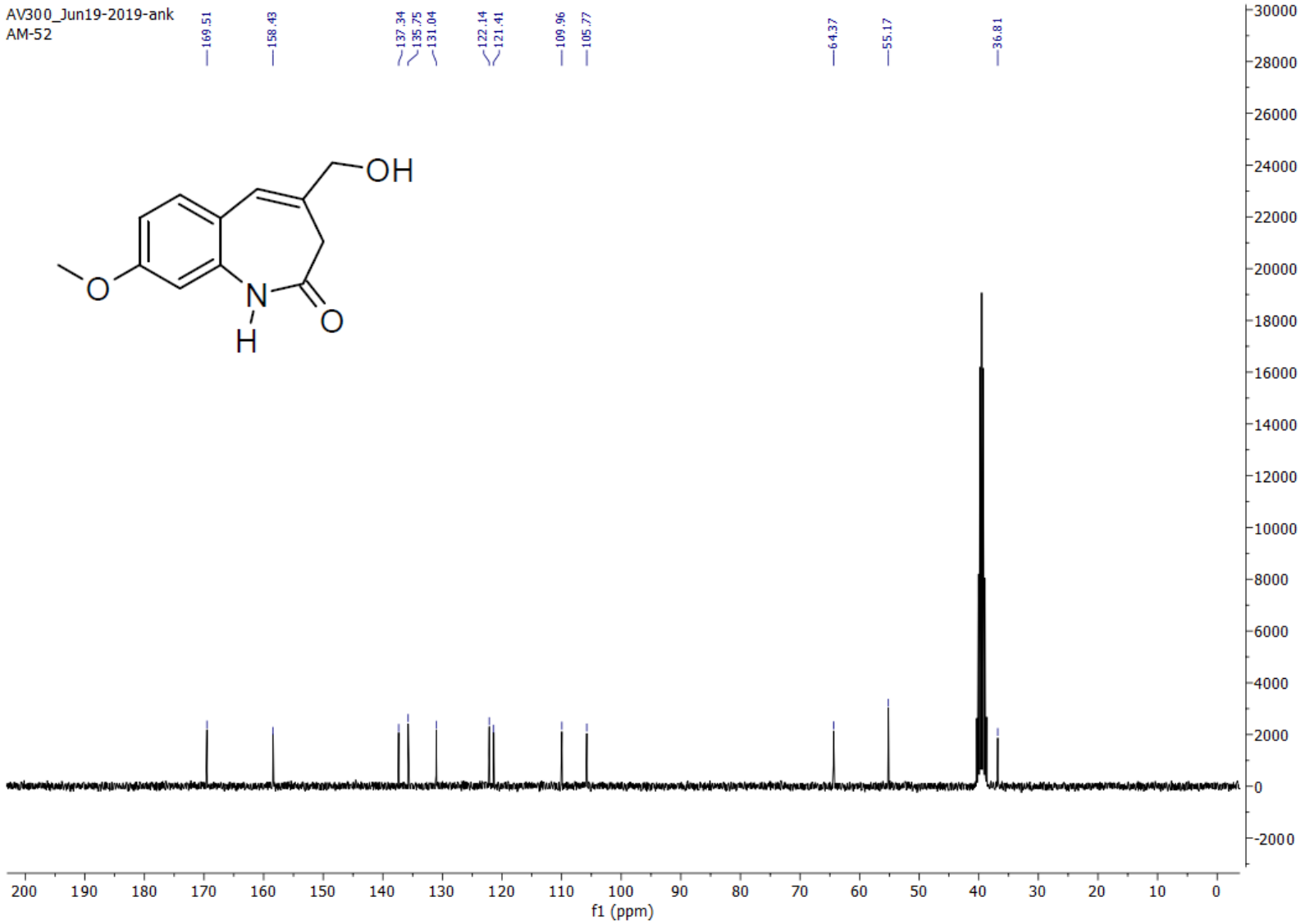

^{1}H NMR (300 MHz, DMSO-d_6) of **11bd**

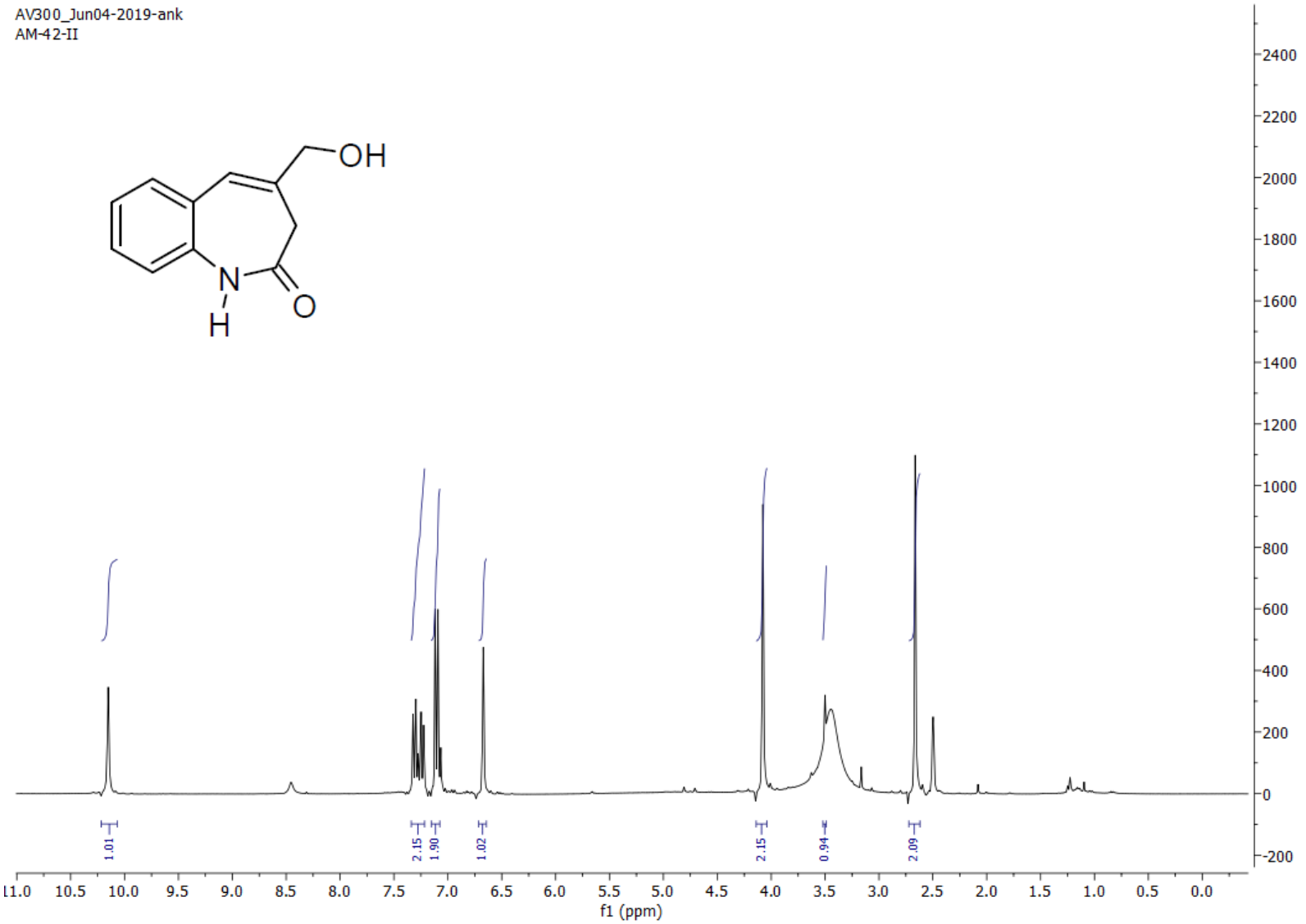

$^{13}C\{^{1}H\}$ NMR (75 MHz, DMSO-d_6) of **11bd**